

UNIVERSITY OF OKLAHOMA

GRADUATE COLLEGE

EXPERIMENTAL AND NUMERICAL EVALUATION OF SHAPE MEMORY
POLYMER FOR LOST CIRCULATION TREATMENT IN GEOTHERMAL WELLS

A DISSERTATION

SUBMITTED TO THE GRADUATE FACULTY

in partial fulfillment of the requirements for the

Degree of

DOCTOR OF PHILOSOPHY

By

ABDELMJEED KAMAL ABDELRAHMAN MOHAMED

Norman, Oklahoma

2022

EXPERIMENTAL AND NUMERICAL EVALUATION OF SHAPE MEMORY
POLYMER FOR LOST CIRCULATION TREATMENT IN GEOTHERMAL WELLS

A DISSERTATION APPROVED FOR THE
MEWBOURNE SCHOOL OF PETROLEUM AND GEOLOGICAL ENGINEERING

BY THE COMMITTEE CONSISTING OF

Dr. Saeed Salehi, Chair

Dr. Ramadan Ahmed, Co-Chair

Dr. Hamidreza Karami

Dr. Ramkumar Parthasarathy

© Copyright by ABDELMJEED KAMAL ABDELRAHMAN MOHAMED 2022
All Rights Reserved.

Dedication

This Ph.D. dissertation is dedicated to the special woman in my life, Afaf Mohamed, my teacher, caregiver, and dearest mother.

Acknowledgment

I would like to express my deepest gratitude to my advisor, Dr. Saeed Salehi, for the technical guidance during my entire Ph.D. studies. He has always been there to motivate, support, and resolve any challenge I encounter. Dr. Salehi has constantly encouraged and pushed me to publish my research in high-ranked journals and technical conferences and attend workshops, training, and technical presentations to enrich my knowledge. In addition to academics, Dr. Salehi had a significant impact on developing my leadership skills. He always encouraged me to join technical organizations and voluntary work. Dr. Salehi has been a mentor and advisor who greatly impacted my professional life. I will be forever grateful for his endless support.

I would also like to thank all my committee members for devoting their time and effort. They were very generous with their time and advice, and their valuable feedback and guidance significantly improved my research plan and achievements. Special thanks to Dr. Ramadan Ahmed for his great experience and input into the experimental setup design and construction. His valuable inputs and suggestions on the design, experimental plan, and scientific papers significantly improved my research quality.

I would also like to acknowledge the U.S. Department of Energy Office of Energy Efficiency and Renewable Energy (EERE) under the Geothermal Program Office Award Number DE-EE0008602 for funding this research. I am also very thankful to the Mewbourne School of Petroleum and Geological Engineering and the Well Construction Technology Center at the University of Oklahoma for providing resources and support throughout my Ph.D. studies. I want to acknowledge Haliburton Company for providing the drilling fluid additives used in this study.

My deepest gratitude to Mr. Jeff McCaskill for his great help in the experimental setup construction and technical consultations while running the experiments. With his vast experience,

he was always there to resolve any technical issue. I would also like to thank Dr. Shawgi Ahmed and Dr. Musaab Magzoub for their assistance in building the experimental setup. Dr. Ahmed put incredible efforts from the early time of setup construction. Thanks to Mr. Abdelrahman Awad for his technical help in the CFD modeling part.

I would like to express my sincere gratitude to my research colleagues at the Well Construction Technology Center for their cooperation and continuous support throughout my research work. Last but not least, I am immensely grateful to my beloved family, friends, and host family in Norman (Henry Marshal and Lois Cox-Marshal) for their boundless emotional support, prayers, and wishes that helped me achieve this great milestone in my educational and professional journey.

Table of Contents

Dedication.....	iv
Acknowledgment.....	v
Table of Contents	vii
List of Tables.....	xii
List of Figures.....	xiii
Abstract.....	xviii
Chapter 1: Introduction.....	1
1.1 Overview of Lost Circulation Problem in Geothermal Formations	1
1.2 Problem Statement and Motivation.....	3
1.3 Research Objectives	4
1.4 Research Hypotheses.....	5
1.5 Research Scope and Methodology	6
Chapter 2: Literature Review	9
2.1 Overview of Geothermal Energy.....	9
2.2 Geothermal Drilling and Associated Challenges	11
2.3 Lost Circulation Problem	15
2.4 Mechanisms of Mud Filtration and Relevant Factors	16
2.4.1 Filtration Mechanisms in Fractured and Non-Fractured Formations	17
2.4.2 Filtration Mechanisms in Aqueous and Non-aqueous Drilling Fluids Systems.	20
2.5 Factors Affecting Mud Losses.....	21
2.5.1 Chemical and Geochemical Factors	22

2.5.2	<i>Geomechanical Factors, In-Situ Stresses, and Thermal Stresses</i>	24
2.5.3	<i>Impact of Fracture Size on Mud Losses</i>	27
2.5.4	<i>Impact of Rheology on Mud Losses</i>	27
2.5.5	<i>Impact of Temperature on Mud Losses</i>	29
2.5.6	<i>Impact of Pressure on Mud Losses</i>	30
2.5.7	<i>Effect of Rotational Speed, Mud Rate, and Wellbore Geometry on Mud Losses</i>	31
2.6	Statistical Assessment of Mud Losses in Different Formations.....	32
Chapter 3: Lost Circulation Treatment Methods and Applied Solutions		37
3.1	Overview of Field Practices	37
3.2	Conventional LCMs	39
3.3	Unconventional LCMs	41
3.3.1	<i>Nanoparticles (NPs)</i>	41
3.3.2	<i>Polymeric Gel</i>	42
3.3.3	<i>Shape Memory Polymer (SMP)</i>	45
3.4	Temperature Constraints	49
3.5	Recommended Particle Size Distribution.....	50
3.6	<i>Advanced Field Technologies</i>	52
3.7	Current Research Gap.....	55
Chapter 4: Laboratory Experimental Methods		57
4.1	Design of Experiments (DoE)	57
4.2	Experimental Setup Description.....	59
4.2.1	<i>Mud Preparation and Circulation System</i>	61
4.2.2	<i>Heating System</i>	61

4.2.3	<i>Rheology Measurement System</i>	62
4.2.4	<i>Main Test Section</i>	63
4.2.5	<i>Data Acquisition and Control System</i>	65
4.3	Testing and Calibrating the Flow Loop Setup.....	66
4.3.1	<i>Heating and Pressure Testing</i>	66
4.3.2	<i>Setup Calibration</i>	67
4.4	Experimental Methods and Procedures	68
4.4.1	<i>Material Selection, Preparation, and Characterization</i>	68
4.4.2	<i>Rheological Screening of the Base Fluid</i>	71
4.4.3	<i>LCM Mud Preparation</i>	73
4.4.4	<i>Rheology Experiments and Wellbore Hydraulics Analyses</i>	74
4.4.5	<i>SMP Activation and LCM Transportation</i>	76
4.4.6	<i>Fracture Sealing Experiments</i>	78
Chapter 5: Experimental Results and Discussions		80
5.1	Base Fluid Selection and Rheological Screening	80
5.1.1	<i>Effect of Temperature</i>	81
5.1.2	<i>Effect of Additives Concentration</i>	85
5.1.3	<i>Effect of Shear Rate</i>	89
5.1.4	<i>Effect of Time</i>	90
5.2	Shape Memory Polymer Activation	91
5.3	Rheology Experiments and Wellbore Hydraulics Analyses	93
5.3.1	<i>Effect of Temperature on the Base Fluid Rheology</i>	93
5.3.2	<i>Effect of Lost Circulation Materials (LCMs) on Fluid Rheology</i>	95

5.3.3	<i>Effect of Lost Circulation Materials (LCMs) on Wellbore Hydraulics</i>	96
5.4	Settling Behavior of Lost Circulation Materials	98
5.4.1	<i>Effect of LCM Concentration and Annular Velocity</i>	98
5.4.2	<i>Effect of Pipe Rotational Speed</i>	100
5.4.3	<i>Effect of Inclination Angel</i>	102
5.5	Fracture Sealing Experiments.....	104
5.5.1	<i>Calcium Carbonate</i>	104
5.5.2	<i>Walnut</i>	106
5.5.3	<i>Cedar Fiber</i>	107
5.5.4	<i>Shape Memory Polymer</i>	108
5.5.5	<i>Blend of Shape Memory Polymer and Cedar Fiber</i>	110
Chapter 6:	Computational Fluid Dynamics (CFD) Simulation Study.....	112
6.1	Model Development and Assumptions	112
6.2	Geometry and Mesh Independence Study.....	115
6.3	Model Performance and Accuracy	116
Chapter 7:	Environmental and Economic Feasibility Analyses of Different LCM	124
7.1	Environmental Analysis	124
7.1.1	<i>Calcium Carbonate (CaCO₃)</i>	125
7.1.2	<i>Cedar Fiber</i>	126
7.1.3	<i>Walnut</i>	127
7.1.4	<i>Shape Memory Polymer (SMP)</i>	127
7.2	Economic Feasibility Analysis	130
Chapter 8:	Summary, Conclusions, and Recommendations	133

8.1	Summary.....	133
8.2	Conclusions	133
8.3	Recommendations	136
	Nomenclature	139
	References	142

List of Tables

Table 3.1: Common LCMs used in drilling operations (Mohamed et al., 2021a)	40
Table 3.2: Summary of polymeric gel systems used in lost circulation application (Hamza et al., 2019).....	44
Table 4.1: Experimental phases and methodology.....	58
Table 4.2: Range of experimental parameters of the flow loop setup.....	66
Table 4.3: Properties of used lost circulation materials	70
Table 4.4: Properties of the tested additives.....	72
Table 4.5: The experimental parameters of the rheology screening	73
Table 4.6: The experimental parameters of LCM transportation experiments	77
Table 4.7: The experimental parameters of fracture sealing experiments.....	79
Table 6.1: Specifications of the different mesh sizes tested in this study	116
Table 7.1: Price and recommended concentrations of different LCMs for severe mud losses...	131

List of Figures

Figure 1.1: Workflow of the research methodology.	6
Figure 2.1: Common applications of geothermal energy (U.S. Department of Energy, 2019)..	11
Figure 2.2: Cost allocation for a 50 MW geothermal plant (Mohamed et al., 2021a).	14
Figure 2.3: Main challenges in geothermal drilling operations (Mohamed et al., 2021a).	15
Figure 2.4: Schematic of the wellbore in mud filtration process (Magzoub et al., 2021).	18
Figure 2.5: Mud loss profile in a) permeable formation, b) fractured formation, and b) caverns and vugs (Chilingarian and Vorabutr, 1983).	20
Figure 2.6: Effect of drilled cuttings on a) filter cake thickness and b) filter cake porosity and permeability (Bageri et al., 2019).	24
Figure 2.7: Cooling effect on a) tangential stresses and b) breakdown pressure (Zhang, 2019).	26
Figure 2.8: Complications of accumulated cuttings or solids sag phenomenon (Mohamed et al., 2021a).	29
Figure 2.9: NPT percentages for offshore gas wells: a) deep wells and b) shallow wells (Modified after Rohani, 2012).	34
Figure 2.10: Cost allocation for a 50-MW geothermal power plant (Modified from Cole et al., 2017).	35
Figure 2.11: Statistics of mud losses with a) formation type and b) depth (Modified from Rosenberg and Gala, 2012).	36
Figure 3.1: Effect of ferric oxide NPs on the filtration performance of drilling mud (Mahmoud et al., 2018).	42

Figure 3.2: Filtration performance of PAM/PEI gel (PBM-2.5) and reference mud (Magzoub et al., 2021).	44
Figure 3.3: Programming and activation cycle of shape memory polymers (Mohamed et al., 2021c).	46
Figure 3.4: Sealing performance of SMP and other LCMs in 1000-micron fracture: a) mud loss and b) sealing pressure (Magzoub et al., 2021a).	47
Figure 3.5: The change in cubic epoxy size soaked in 0.35 M TBD-EG at different times at 170°C (Kuang et al., 2018).	49
Figure 3.6: Illustration of the mud window in underbalanced, conventional, and managed pressure drilling (Huque et al., 2020).	53
Figure 3.7: Types of CwD systems (Patel et al., 2019).	54
Figure 4.1: The detailed plan of this study.	59
Figure 4.2: Schematic design and components of the high-temperature flow loop.	60
Figure 4.3: Schematic design of the modified main test section for fracture sealing experiments.	65
Figure 4.4: Calibration data for PAC-R solution at 120 °F: a) 0.8 wt.% and b) 1.5 wt.%.	68
Figure 4.5: Particle size distribution of used LCMs.	71
Figure 4.6: 3D fractured discs used in this study: a) complex fracture, b) 3000 microns, and c) 2000 microns.	79
Figure 5.1: Effect of temperature on the apparent viscosity of different viscosifiers.	83
Figure 5.2: Effect of temperature on the apparent viscosity of different fluid loss control additives.	84
Figure 5.3: Fluid samples before and after rheology experiments (3.0 lb/bbl).	85

Figure 5.4: Effect of viscosifier concentration on fluid viscosity with temperature: a) bentonite, b) Xanthan, c) HEC, and d) THERMA-VIS. 86

Figure 5.5: Gelled THERMA-VIS on the rheometer's bob (5.0 lb/bbl). 87

Figure 5.6: Effect of filtration control additives' concentration on fluid viscosity with temperature: a) PAC-L, b) PAC-R, c) POLYAC PLUS, and d) THERMA-CHEK. 89

Figure 5.7: Effect of shear rate on THERMA-VIS viscosity at different temperatures. 90

Figure 5.8: Thermal stability of THERMA-VIS with time. 91

Figure 5.9: Effect of temperature on SMP particles: a) 21°C, and b) 160°C. An apparent increase in particle size was seen at 160°C. 93

Figure 5. 10: Effect of temperature on the base fluid's performance: a) flow curve, and b) apparent viscosity. 95

Figure 5. 11: Effect of LCM concentration on the base fluid's flow curve at 160°C: a) 1.0 wt.%, and b) 3.0 wt.%. 96

Figure 5. 12: Effect of LCM concentration on the base fluid's viscosity at 160°C: a) 1.0 wt.%, and b) 3.0 wt.%. 96

Figure 5. 13: Raw data of ΔP and Q for LCM muds at 160°C: a) 1.0 wt.%, and b) 3.0 wt.%... 97

Figure 5. 14: Fanning friction factor data of LCM muds at 160°C: a) 1.0 wt.%, and b) 3.0 wt.%. 97

Figure 5. 15: Effect of annular velocity on LCM transportation at 160°C: a) 1.0 wt.%, and b) 3.0 wt.%. 100

Figure 5. 16: Effect of pipe rotational speed on LCM transportation at 160°C. 102

Figure 5. 17: Effect of inclination angel on LCM transportation at 160°C. 103

Figure 5. 18: Summary of the effect of the operational parameters on SMP transportation at 160°C.....	104
Figure 5.19: Sealing performance of calcium carbonate at different fracture sizes.	105
Figure 5.20: Fractured discs after the experiments with calcium carbonate.	105
Figure 5.21: Sealing performance of walnut at different fracture sizes.	106
Figure 5.22: Fractured discs after the experiments with walnut.	107
Figure 5.23: Sealing performance of cedar fiber at different fracture sizes.	108
Figure 5.24: Fractured discs after the experiments with cedar fiber.	108
Figure 5.25: Sealing performance of shape memory polymer at different fracture sizes.	109
Figure 5.26: Fractured discs after the experiments with shape memory polymer.....	109
Figure 5.27: Sealing performance of SMP-fiber blend at different fracture sizes.	110
Figure 5.28: Fractured discs after the experiments with SMP-fiber blend.....	111
Figure 6.1: Workflow of the CFD simulation study.....	114
Figure 6.2: Quadratic structural mesh used in this study (Average quality: 0.996).	115
Figure 6.3: Example of a) converged solution (residual $\leq 1e-05$), and b) diverged solution(residual $\gg 1e-05$).....	116
Figure 6.4: Modeling vs. experimental data at the viewport location under different: a) annular velocities, b) pipe rotational speeds and c) inclination angles.....	118
Figure 6.5: Effect of annular velocity on SMP transportation at 160°C (3.0 wt.%).	119
Figure 6.6: Effect of drill pipe rotation on SMP transportation at 160°C (3.0 wt.%).	120
Figure 6.7: Effect of inclination angle on SMP transportation at 160°C (3.0 wt.%).	121
Figure 6.8: Modeling data vs. extrapolated experimental data under different: a) annular velocities, b) pipe rotational speeds and c) inclination angles.....	123

Figure 7.1: Cost of shape memory polymer compared to conventional LCMs. 132

Abstract

Lost circulation presents formidable challenges to drilling operations, especially in high-temperature and fractured formations. Lost circulation events increase the nonproductive time (NPT) and the total cost of drilling operations. In some severe cases of complete or high losses, well control is jeopardized, leading to a loss in lives and resources. Besides the conventional lost circulation materials (LCMs), LCM pills, and cement squeeze, several innovative solutions have been introduced to mitigate and treat the lost circulation events, including wellbore strengthening, managed pressure drilling (MPD), and casing while drilling (CwD). However, selecting the suitable LCM and the optimized fluid formulation is vital to the lost circulation remedy's success.

The primary objective of this study is to evaluate the effectiveness of smart material in treating lost circulation in geothermal formations. The smart material is a shape memory polymer (SMP) that can be programmed to activate by formation temperature. Once activated, its particle size increases to plug large fractures and stop mud losses. SMP evaluation is conducted on a large-scale flow loop under high-temperature conditions (above 300°F). The experimental evaluation includes SMP activation with temperature, fluid rheology, wellbore hydraulics, fracture sealing, and SMP transportation in the annulus under a broad range of operating parameters, such as concentration, drill pipe rotational speed, inclination angle, and flow rate. Furthermore, a computational fluid dynamics (CFD) study was conducted to upscale the experimental results and predict the LCM transportation in the annular section of geothermal wells in the field dimensions.

The novelty of this study is the use of shape memory polymer that has the potential to plug large fractures in geothermal formations with minimal risk of plugging downhole drilling and logging tools. Moreover, this study introduces a novel experimental setup to test different lost circulation materials under high-temperature conditions. The introduced large-scale testing is unique and crucial in LCM evaluation to ensure better results in geothermal fields.

Chapter 1: Introduction

1.1 Overview of Lost Circulation Problem in Geothermal Formations

40 to 60% of the geothermal project's cost is spent on drilling operations, which significantly impacts the feasibility of geothermal exploration and developments (Bavadiya et al., 2019). The high drilling cost results from the prolonged drilling time caused by the high downhole temperature, depth, and complex nature of geothermal formations (Finger and Blankenship, 2010; Kruszewski and Wittig, 2018). High temperatures cause formidable challenges to the drilling operation, such as degradation of drilling mud and cement, damage to casing and cement sheath, and failure of downhole tools (Mohamed et al., 2021a). The hard and abrasive geothermal formation extends the drilling time, wears the drill bit, and damages the downhole equipment due to the increased vibrations (Baujard et al., 2017; Bavadiya et al., 2017; Miyazaki et al., 2019). Additionally, many issues are encountered in geothermal drilling operations, such as wellbore stability, lost circulation, and well control problems. These issues are mainly caused by the complex fracture networks and narrow mud windows observed in most geothermal reservoirs (Kiran and Salehi, 2020; Magzoub et al., 2021b; Mohamed et al., 2021a; Vollmar et al., 2013).

Lost circulation is a challenging event faced during drilling operations (Alkinani et al., 2019). More than 10% of the nonproductive time was spent curing lost circulation while drilling in the Gulf of Mexico between 1993 and 2003. In the United States, 10 to 20% of the geothermal well cost is spent on lost circulation treatments (Lavrov, 2016). Moreover, in severe cases, lost circulation causes well control problems, leading to a loss in lives and resources (Magzoub et al., 2021b). Lost circulation in geothermal wells is more challenging than oil and gas wells because of the high temperature, low fracture gradient, and large and complex fractures (Lavrov, 2016; Magzoub et al., 2020; Ravi et al., 2006; Tare et al., 2001). The low fracture gradient narrows the

mud window, which is the difference between fracture and pore pressure (Salehi and Nygaard, 2011). Controlling the wellbore pressure in narrow mud window drilling is challenging; consequently, lost circulation events are likely to occur, which increases the number of casing strings, drilling cost, and non-production time (NPT) (Magzoub et al., 2020).

Practically, loss prevention in the first place is more effective than lost circulation treatments (Alsaba, 2015; Magzoub et al., 2020). Loss prevention is achieved by adequately designing drilling muds, good hole cleaning, and optimized wellbore hydraulics. The prior knowledge of formation properties and advanced drilling technologies mitigate the consequences of lost circulation events (Magzoub et al., 2020). However, lost circulation events in weak and fractured formations are common because controlling wellbore pressure is challenging to attain. In such cases, drilling engineers should take prompt actions to cure the losses and regain well control. This technique is known as the corrective method, in which the mud circulation is restored after losses occur (Alsaba, 2015). The appropriate treatment method is selected and designed based on the loss severity: seepage, severe, or complete loss. The corrective methods are classified into three categories: using lost circulation materials (LCMs), LCM pills, and cement squeeze (Wagle et al., 2018).

Many lost circulation materials are used to treat fluid losses in geothermal, oil, and gas wells. LCMs are added to the drilling mud in various concentrations, depending on the loss severity and downhole conditions. Selecting and optimizing the LCM mud formulation is vital to ensure optimal treatment results. Mohamed et al. (2021) summarized the lost circulation materials commonly used in drilling operations. LCMs can be classified based on the particle shape into three main groups: granular, flakey, and fibrous materials. Several studies were carried out to study the sealing performance of common LCMs under different testing conditions (Akhtarmanesh et

al., 2016; Alsaba, 2015; Alsaba et al., 2014; Ezeakacha et al., 2017; Javeri et al., 2011; Lee and Taleghani, 2020; Loeppke et al., 1990; Magzoub et al., 2021a and 2021b; Mansure, 2002).

Despite the advancements in LCMs and drilling technologies, more research is still required to overcome the limitations of current lost circulation materials. Sealing complex fracture networks, plugging downhole tools, and formation damage induced by LCMs create severe problems for loss treatments (Magzoub et al., 2021b; Mansour et al., 2017). More advanced lost circulation materials were introduced to cure losses under critical downhole conditions, where most conventional LCMs fail. Blends of LCMs, encapsulated pills, nanoparticles (NPs), and shape memory polymers (SMPs) are good examples of these smart LCMs.

1.2 Problem Statement and Motivation

Despite the recent advancements and developments in lost circulation materials, the treatment success or failure depends on understanding the mechanisms of fracture sealing and downhole conditions. Selecting the suitable LCM type, concentration, and particle size still presents a significant challenge to the lost circulation treatment. Moreover, there are many limitations for the current LCMs that can be summarized as follows: i) The high-temperature conditions present in geothermal formations deteriorate the properties of fluid formulations and sealing efficiency of these LCMs, ii) The conventional lost circulation materials fail to efficiently seal large and complex fractures exist in the geothermal formations, iii) When LCMs with large particles are used in an attempt to bridge these large fractures, the risk of plugging downhole tools are very high, and iv) Conventional LCMs are considered a primary source of formation damage as they invade the drilled formations and significantly reduce the well productivity.

Additionally, a very limited number of studies on shape memory polymer applications in lost circulation were performed. These studies mainly focused on sealing efficiency experiments conducted in small-scale laboratory equipment. This type of experiment is not a good

representation of the lost circulation phenomenon, and different results may yield in field applications. Moreover, no experimental study was performed to investigate SMP activation, rheology, wellbore hydraulics, and solid particle transportation and dispersion of a mud containing shape memory polymer under large-scale high-temperature conditions. Previous studies did not investigate the impact of operational parameters, such as well inclination, annular velocity, and drill pipe rotational speed.

The motivation of this study is promoted by the promising results of shape memory polymer in previous lost circulation laboratory studies. The shape memory polymer showed great potential in sealing large fractures with minimal risk of plugging drilling and logging tools. Optimizing SMP-based drilling formulation can effectively seal large fractures encountered while drilling geothermal and high-temperature formations with a high success rate to solve the lost circulation problem, reduce the geothermal drilling cost, and increase the feasibility of geothermal projects.

1.3 Research Objectives

This study investigates the performance of a smart material at high temperatures as a lost circulation material for geothermal drilling applications, considering the LCM activation, rheology, wellbore hydraulics, and LCM transportation under various operating conditions. This evaluation is crucial for geothermal drilling applications to optimize the lost circulation treatment to efficiently seal large fractures in geothermal wells and avoid excessive Non-Productive Time (NPT). The smart LCM is a thermoset shape memory polymer (SMP) that can be activated with formation temperature. The main objective of this study is to introduce a novel, efficient, and economically feasible solution for the most encountered problem in geothermal drilling, lost circulation. Optimizing the SMP-based mud formulation and operating conditions would significantly improve the sealing efficiency and set the stage for broad applications of this smart

LCM globally, with minimal drilling time. The objectives of this study can be summarized in the following:

1. Study the effect of shape memory polymer on mud rheology and wellbore hydraulics under high-temperature conditions.
2. Study the activation process of the smart LCM at high temperatures.
3. Evaluate the smart LCM dispersion and transportation under various operating conditions to optimize the lost circulation treatment.
4. Investigate the SMP sealing efficiency on a large scale and under high-temperature dynamic conditions.
5. Compare the smart LCM performance with the conventional LCMs used for geothermal drilling applications regarding rheology, dispersion, and sealing efficiency.
6. Develop a numerical model to upscale and predict the smart LCM transportation at a broader range of operating conditions.

1.4 Research Hypotheses

The research hypotheses are based on the available studies in literature discussing the lost circulation issue in high-temperature conditions. The factors affecting SMP sealing efficiency were studied. The following hypotheses are considered in this research study:

- The thermoset shape memory polymer can be programmed during the manufacturing process and activated downhole with formation temperature and increase its particle size to seal large and complex fractures in geothermal formations.
- The SMP activation process may occur in the drill pipe and clog drilling tools if the activation temperature is not well optimized in the programming process.

- Shape memory polymer is compatible with water-based drilling mud. However, the SMP particles may accumulate in the wellbore in some conditions.
- The shape memory polymer causes minimal formation damage and can be removed afterward.

1.5 Research Scope and Methodology

This study consists of four main parts to cover the work scope and attain the main objectives of this study. These parts include a comprehensive literature review, material selection and characterization, experimental study, and computational fluid dynamics (CFD) simulation. The workflow of this study is shown in Figure 1.1, and the scope of each part is discussed in the following sections.

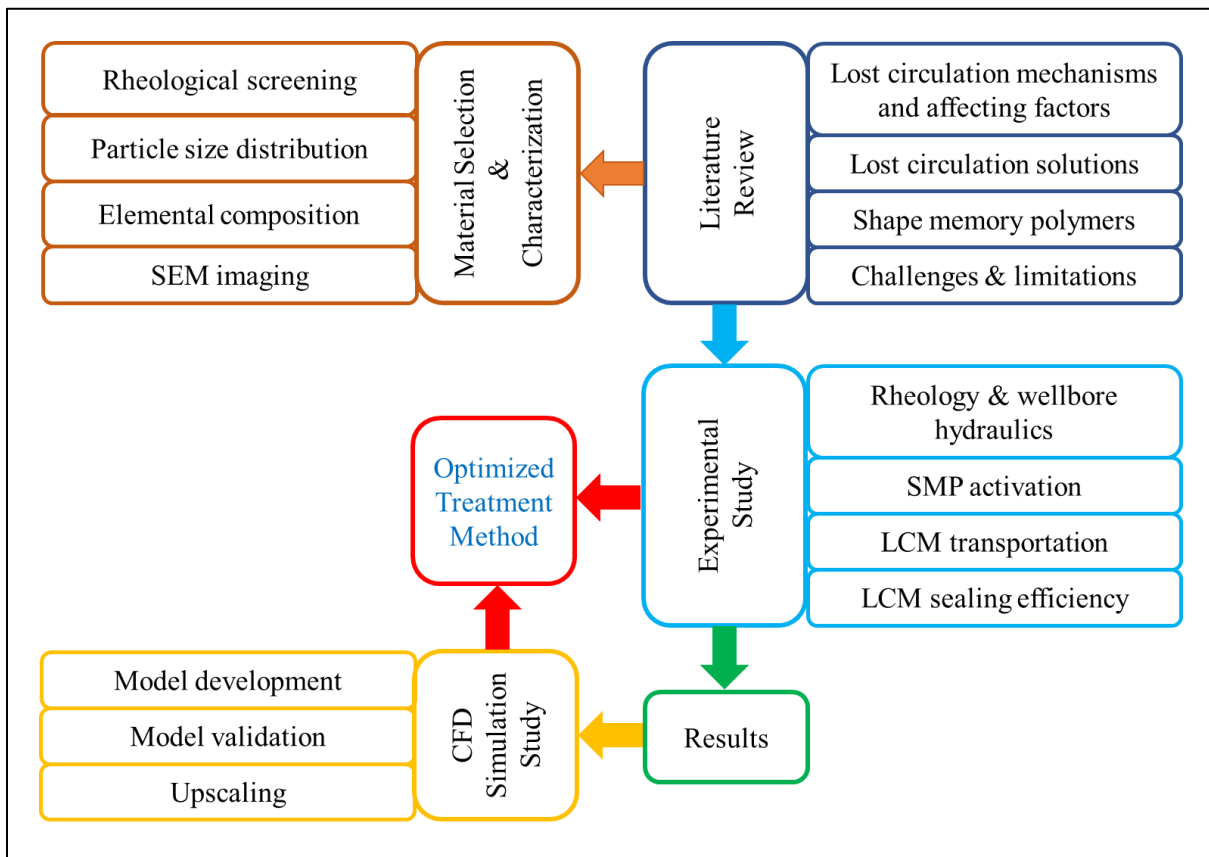


Figure 1.1: Workflow of the research methodology.

- i. **Literature Review:** The primary objective of this task is to provide a comprehensive review of the geothermal drilling challenges, lost circulation problem, mud loss mechanisms and affecting parameters, and the available field solutions to the lost circulation issue. The research gap in the literature was identified, then the lost circulation challenges and limitations were discussed. Understanding the lost circulation problem and associated issues helps design an efficient method to mitigate the lost circulation in geothermal formations. It also helps design the experimental work, considering the research gap in evaluation methods.
- ii. **Material Selection and Characterization:** This task includes a rheological screening for several drilling fluid additives to prepare a stable base mud that can withstand the high testing temperature and yield optimum results with the smart LCM. Several viscosifiers were tested using an HPHT rheometer to provide enough mud viscosity to keep the LCM suspended throughout the experiments. This task also involves a full characterization of the selected lost circulation materials by measuring the particle size distribution, elemental composition, and morphological properties. These properties are crucial in selecting and designing the lost circulation material to ensure a successful treatment method in field operations.
- iii. **Experimental Study:** In this task, four phases of experiments were conducted to fully evaluate the performance of shape memory polymer in treating lost circulation. In the first phase, the SMP activation process was studied using the visualization data of annular flow to prove the thermal activation of shape memory polymer. The second phase of experiments investigate the impact of SMP on drilling fluid rheology and wellbore hydraulics. In the third phase, the LCM dispersion in the drilling mud was studied under a broad range of experimental parameters to evaluate the SMP transportation and ensure the treatment method is effectively optimized. The final phase of experiments evaluates the sealing efficiency of SMP and other conventional

LCMs under high-temperature dynamic conditions using 3D printed discs with different fracture sizes and geometries. The details of all the experimental phases are well described in Section 4.3.

- iv. ***Computational Fluid Dynamics Study:*** The CFD simulation study was integrated with the experimental work to upscale the experimental results and extend the findings to a broader range of operating parameters. The simulation study is a multiphase flow fluid dynamic study that aims to simulate and investigate the LCM dispersion and transportation by the drilling mud in the annulus. First, the analysis was performed on an annular section that matches the experimental setup dimensions. The experimental results were used to evaluate the simulation model and validate the results. After the model was validated, the model was run using a larger scale and a broader range of parameters to provide a robust tool to predict the smart LCM performance under various operating conditions. The CFD study is discussed in more detail in Section 4.4.

Chapter 2: Literature Review

This chapter discusses the major challenges encountered while drilling in geothermal formations, and focuses in lost circulation problem. A comprehensive literature review was conducted on the main filtration mechanisms of water-based and oil-based drilling fluids in different formation types to better understand the lost circulation and affecting factors to help select and optimize treatment methods.

2.1 Overview of Geothermal Energy

The term “geothermal” is originally from the Greek words “gê and thérn,” meaning earth heat. Geothermal energy is considered one of the most significant renewable and clean energy sources due to the associated benefits. Geothermal energy provides sustainable and affordable energy sources, diverse energy portfolios, efficient heating and cooling, and minimized pollution (U.S. Department of Energy, 2019; Wight and Bennett, 2015). The concept of geothermal energy lies in using earth heat as an energy source for different applications (Finger and Blankenship, 2010). These applications include the direct use applications such as heating, bathing, cooking, other industrial applications, and electricity generation (U.S. Department of Energy, 2019). Geothermal energy is generated by circulating a working fluid downhole to transfer the earth’s heat to the surface. The source of working fluid is mostly the geothermal formation but, in some cases, where permeability is very low or in the absence of formation fluids, the geothermal applications rely on injecting cool water from the surface, circulating it through geothermal formations, then producing it at higher temperatures (Finger and Blankenship, 2010).

Generally, there are three classifications of geothermal formations based on downhole temperature; low-temperature formations (less than 300°F), medium-temperature formations (300°F-390°F), and high-temperature formations (above 390°F) (Kruszewski and Wittig, 2018).

The downhole temperature is considered one of the main constraints to geothermal applications. The type of geothermal application is defined based on the nature and downhole temperature of geothermal formations. For instance, geothermal heat pumps are commonly utilized in low-temperature formations, while electricity production is economic from medium and high-temperature geothermal resources (U.S. Department of Energy, 2019). Another form of geothermal application is enhanced geothermal systems (EGS), where fracturing operations are performed to increase the formation permeability and allow adequate fluid injection and production from such geothermal formations (Finger and Blankenship, 2010).

Recently, new geothermal systems have been introduced to overcome the issue of low permeability and fluid flow in geothermal formations. The new system is known as the closed-loop geothermal system (CLG). The main concept of CLG is to circulate a fluid through two deep sealed wells in different configurations to transfer the downhole temperature to the surface for electricity generation. However, available studies are not enough and are still ongoing to evaluate the drilling operations, well configurations, operational parameters, and working fluid to optimize the energy production from these systems (Van Horn et al., 2020). The common thing between existing applications of geothermal energy is that they all require drilling operations to access the geothermal reservoirs and unlock the geothermal energy potential. Figure 2.1 illustrates the typical applications of geothermal energy.

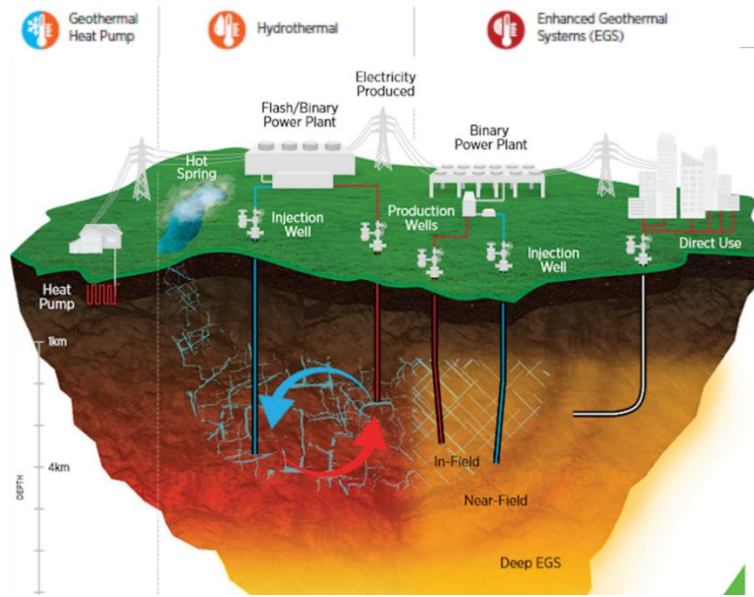


Figure 2.1: Common applications of geothermal energy (U.S. Department of Energy, 2019).

2.2 Geothermal Drilling and Associated Challenges

The increasing energy demand and growing environmental concerns about fossil fuels opened great opportunities for geothermal energy exploitation. Thus, a significant increase in the number of geothermal projects has been observed lately, including exploration, drilling, and production activities (De Angelis et al., 2011; Kiran and Salehi, 2020; Reinsch et al., 2015). There is a high similarity between oil&gas and geothermal sectors, especially in drilling operations. This similarity comes in the high temperatures encountered downhole and the extended depths required to reach the targeted formations (Bavadiya et al., 2019; Capuano, 2016; Teodoriu et al., 2019). Therefore, with the proper knowledge transfer, the technological advancements introduced for oil&gas development can significantly and efficiently serve geothermal projects worldwide (Teodoriu, 2015; Teodoriu et al., 2019). These advancements are in drilling bits, casing, cement, logging and testing tools, and other drilling techniques such as measure-while-drilling (MwD), logging-while-drilling (LwD), casing-while-drilling (CwD), and managed pressure drilling (MPD). However, the type of produced fluid and the nature of producing formations represent the

primary differences between high-pressure high-temperature (HPHT) oil&gas and geothermal wells (Capuano, 2016; Vollmar et al., 2013).

Due to the harsh conditions encountered in geothermal formations, geothermal drilling operations are very challenging in terms of well design, well control, wellbore integrity, material selection, and other drilling issues such as lost circulation (Chemwotei, 2011; Finger and Blankenship, 2010; Kiran and Salehi, 2020; Mohamed et al., 2021a; Shadravan and Amani, 2012; Vollmar et al., 2013). The hard and abrasive formations and high downhole temperature increase the technical limitations on selecting casing material, downhole tools, cement, and drilling mud additives. Consequently, the urge for more technological advancements is increasingly high to cope with the growing number of geothermal projects (Finger and Blankenship, 2010).

Special drilling fluid and cement formulations with high thermal resistance are required to drill and complete geothermal wells efficiently and without any issues that may result from fluid thermal degradation. Thermal stresses resulting from temperature variations are also believed to be one of the main reasons for casing damage. When they exceed the yield stress of casing material, these thermal stresses cause thermally induced fatigue (Shadravan and Amani, 2012; Teodoriu, 2015; Wu et al., 2020). Most of the produced fluid contains dissolved amounts of carbon dioxide and hydrogen sulfide gasses, which causes corrosion to the casing and limits the material selection for downhole drilling tools. Moreover, there are other causes for casing failure in geothermal wells, such as wear and overloading while casing and drilling operations (Kruszewski and Wittig, 2018; Teodoriu, 2015; Teodoriu et al., 2019).

The geothermal formations are commonly volcanic rocks such as granodiorite, granite, and quartzite that are hard and abrasive (Vollmar et al., 2013). Their hardness increases the wear on drill bits that shortens the drill bit life (Baujard et al., 2017) and increases the vibration on the drill

string, causing failure to the downhole equipment (Bavadiya et al., 2017). Moreover, the geothermal formations are naturally weak and contain complex fracture networks. These fractures induce challenging issues to the drilling operations, such as wellbore integrity issues, and are responsible for the high number of lost circulation events encountered in geothermal drilling operations (Mohamed et al., 2021a). All the abovementioned issues will interfere with drilling, casing, completion, testing, and production activities, leading in some severe cases to a total loss of geothermal wells (Kruszewski and Wittig, 2018).

The high cost of drilling operations in geothermal reservoirs is considered a significant challenge that highly impacts geothermal developments (Bavadiya et al., 2019; Randeberg et al., 2012; Vollmar et al., 2013). According to Bavadiya et al., 2019, the exploration and development drilling operations constitute 40-60% of the total cost of geothermal projects, as shown in Figure 2.2. This high cost significantly affects the geothermal project's feasibility, and the proper means to reduce the geothermal drilling cost are still needed. Randeberg et al. (2012) suggested several means to minimize the geothermal drilling cost, starting by understanding the complexity of geothermal reservoirs and identifying the major expenses in drilling operations. They also concluded that the knowledge transfer from the oil&gas industry to the geothermal sector and automated operations would significantly improve the drilling performance and increase the geothermal project's feasibility (Falcone and Teodoriu, 2008; Petty et al., 2009). Moreover, the geothermal industry should encourage investment in developing advanced technologies to drill geothermal formations to ensure efficient and fast drilling operations (Randeberg et al., 2012).

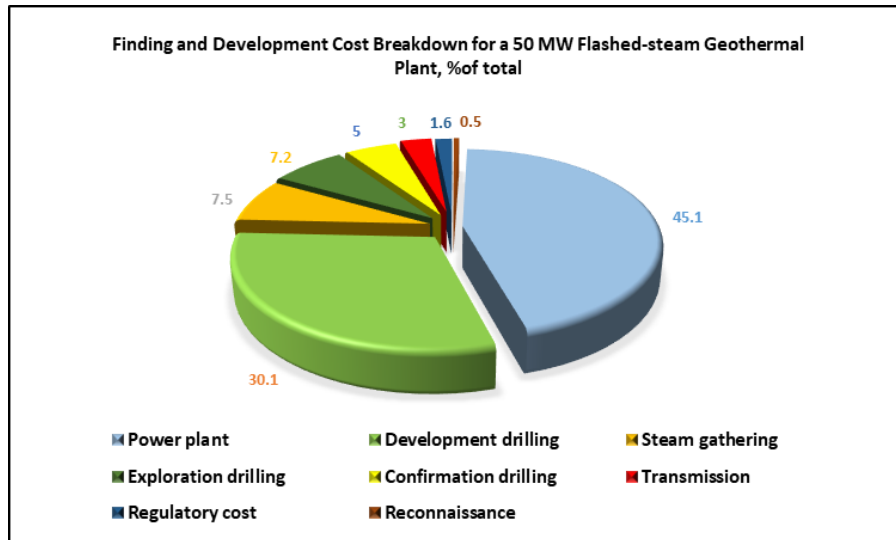


Figure 2.2: Cost allocation for a 50 MW geothermal plant (Mohamed et al., 2021a).

Another challenge to geothermal drilling is the lack of drilling and operational data because a small number of geothermal wells are being drilled annually compared to oil and gas wells (Kruszewski and Wittig, 2018). Taking the United States as an excellent example for the countries leading in geothermal energy, less than 100 geothermal wells were drilled in 2008, while more than 50,000 oil and gas wells were drilled in the same year (Finger and Blankenship, 2010). The high uncertainty that may result from the lack of drilling data necessitates the technology transfer from the oil industry to improve the performance of geothermal drilling operations. Mohamed et al. (2021) summarized the main challenges encountered in geothermal wells drilling, as shown in Figure 2.3.

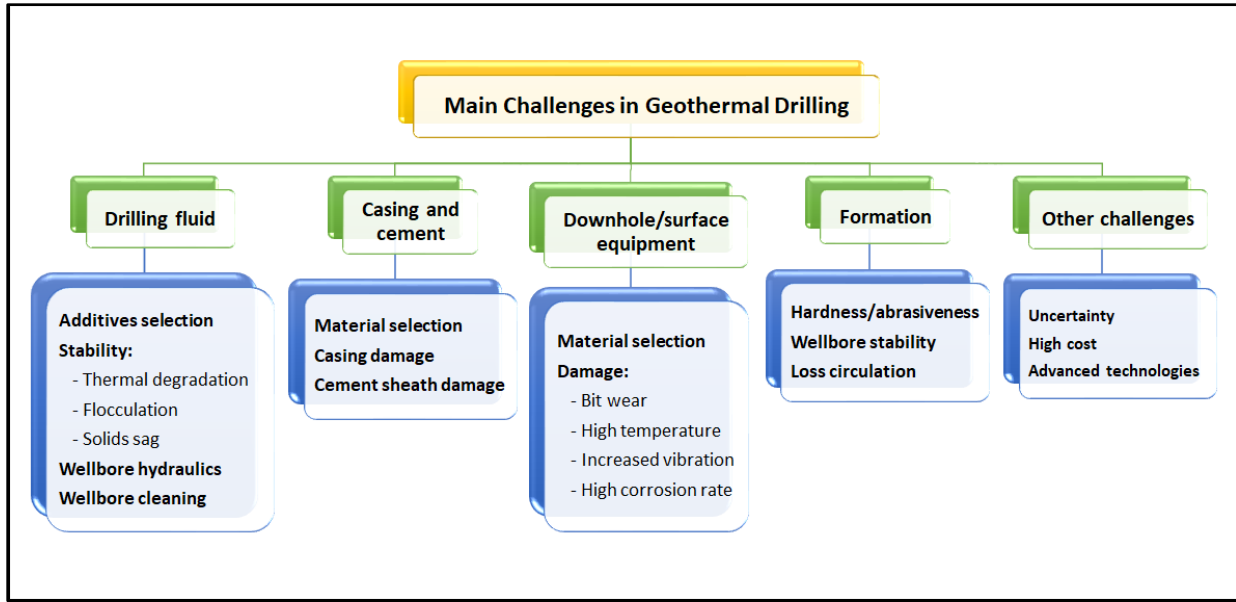


Figure 2.3: Main challenges in geothermal drilling operations (Mohamed et al., 2021a).

2.3 Lost Circulation Problem

Drilling fluids are introduced to the drilled formation to attain many functions, mainly to suspend and transfer the drilled cuttings to the surface, control the formation pressure, maintain the wellbore stability, and lubricate the drill bit. Overbalanced drilling is the most common drilling technique, where well control is achieved by applying enough hydrostatic mud pressure. Consequently, the drilling mud tends to invade the formation and forms mud cake on the wall of the well. There is an acceptable rate for mud invasion according to the drilling practices. The high invasion rates would cause formation damage and reduce the well productivity (Caenn et al., 2017; M. E. Hossain and Al-Majed, 2015).

Lost circulation is the partial or total loss of drilling fluid into the drilled formation through natural rock permeability, natural fractures, or induced fractures. It is considered one of the challenging events faced during drilling operations (Alkinani et al., 2019). Lost circulation events introduce many issues to the drilling operations and increase the drilling time and cost. For instance, in the Gulf of Mexico, treating mud loss events was responsible for more than 10% of

the non-productive time (NPT) between 1993 and 2003. Around 10-20% of the geothermal well cost in the United States is spent on lost circulation treatment (Lavrov, 2016). In severe cases, mud losses may jeopardize the well control, causing a loss in lives and revenue (Magzoub et al., 2021a).

The increased downhole temperature, large and complex fracture networks, and low fracture pressures make the lost circulation in geothermal formation more challenging than in oil and gas wells (Lavrov, 2016; Magzoub et al., 2020; Ravi et al., 2006; Tare et al., 2001). The geothermal formations are naturally weak and have a low fracture gradient, restricting the operational mud window and making the pressure control more difficult (Salehi and Nygaard, 2011). Therefore, the possibility of mud loss events and the drilling cost increase due to the increase in NPT resulting from running more casings in the well (Magzoub et al., 2020). Moreover, the increased temperature encountered in geothermal reservoirs complicates the drilling operations because the fracture gradient is affected by the formation and mud temperature (Zhang, 2019).

2.4 Mechanisms of Mud Filtration and Relevant Factors

As defined earlier, mud loss or lost circulation is the partial or complete loss of drilling mud into the drilled formation through natural rock permeability, natural fractures, or induced fractures. The two main parameters in the mud losses are the driving mechanism and the loss mechanism. Mud losses are generally driven by the wellbore pressure exerted mainly by the hydrostatic mud pressure and annular frictional pressure losses. When this pressure is higher than the pore pressure, the mud tends to invade the formation through different means such as formation permeability and natural caverns and fractures. Moreover, some induced fractures will result when the wellbore pressure exceeds the fracture gradient, causing additional mud losses. These induced fractures usually occur in narrow mud windows, such as depleted reservoirs, deepwater wells, and inclined wells. The induced in such formations are attributed to different reasons. For Instance, the induced fractures in depleted reservoirs are caused by the drop in fracture gradient due to the extended

production period. While in deepwater wells, the density of seawater is less than formation density which reduces the overburden pressure thus, reducing the breakdown pressure.

Generally, mud losses in water-based muds are classified based on the amount of loss, which indicates the loss severity. Seepage loss, partial loss, and total loss are the three types of losses. The loss is considered a seepage loss when the loss rate is less than 25 bbl/hr, a partial loss when the loss rate ranges between 25 and 100 bbl/hr, while higher loss rates are considered total losses. Conversely, the classification is different in oil-based mud, where loss rates higher than 30 bbl/hr are classified as severe losses. This classification has been used in the industry for many years to determine the loss severity and select the best treatment method. However, this classification only considers the amount of loss regardless of the formation type, downhole conditions, and the loss mechanism. All these factors should be considered when selecting and optimizing the treatment method. More descriptive classification is discussed in the next section.

2.4.1 Filtration Mechanisms in Fractured and Non-Fractured Formations

A more descriptive classification is adopted, considering the formation type. In this classification, the losses are divided into three categories based on the escape mean: losses through pore throat or formation permeability, losses through fractures, and losses through vugs and caverns. Seepage losses are associated with high-permeability formations with large pore throats, and partial losses occur commonly in unconsolidated sand, gravel, and microfractures. Conversely, total or severe losses are encountered in formations containing large fractures, vugs, or caverns (Ghalambor et al., 2014).

In non-fractured formations, mud losses occur merely through the formation permeability. Thus, the mud filtration process in such formations depends on the permeability and filtration time. The first stage of filtration is the invasion of spurt loss that occurs in the early time of filtration,

then more solid particles from the drilling fluid invade the formation due to the differential pressure. These solid particles start to deposit inside the drilled formation forming an internal mud cake. The internal filter cake prevents solid particles from penetrating deeper into the formation; therefore, solid particles tend to deposit on the wellbore forming an external mud cake, as shown in Figure 2.4.

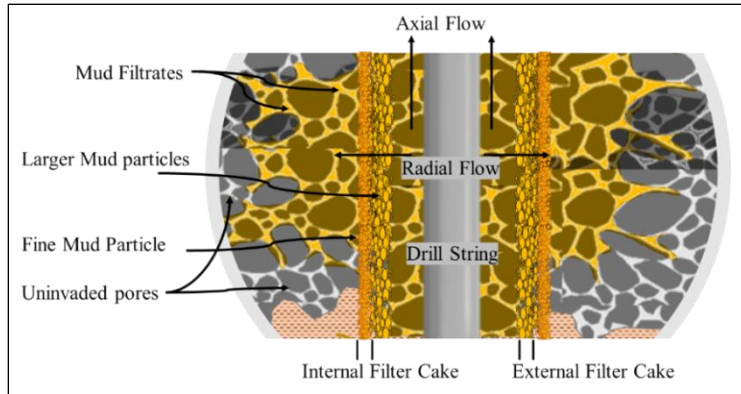


Figure 2.4: Schematic of the wellbore in mud filtration process (Magzoub et al., 2021).

Filter cake formation is crucial during drilling operation as it minimizes mud losses and improves the wellbore stability. The filter cake evolution occurs over time depending on the drilling fluid formulation, formation permeability, and operational parameters. A thin impermeable filter cake is ideal for drilling operations because it stops mud losses, does not interfere with cementing and casing operation, minimizes the possibility of differential sticking, and is easier to remove before production.

On the other hand, fractured formations are responsible for 90% of mud losses. Mud losses in fractured formations occur through induced or natural fractures. Induced fractures are encountered in low fracture gradient formations such as weak formations, depleted reservoirs, and inclined wells. The loss mechanism in fractured formations is impacted by wellbore pressure, mud properties, and fracture conductivity. Connected fracture networks cause severe mud losses because of their high permeability. Many studies were performed to study the loss mechanism in

fractured formations. It was reported that the fracture size, orientation, and LCM concentration are the main factors affecting the sealing performance.

Regardless of the formation type, the factors affecting loss mechanism and severity are divided into controlled and uncontrolled factors. The uncontrolled factors are the preexisting downhole conditions such as fracture gradient, temperature, rock type, porosity, permeability, and existing fracture size. In contrast, the controlled factors can be optimized during the lost circulation treatment. They include mud type, mud properties, LCM type and concentration, tripping and rotational speed, and circulation rate. These factors are discussed in detail in section 2.5.

Moreover, determining the loss mechanism is vital in selecting and optimizing the lost circulation treatment method. The mud pit level and loss rate are good indicators of the loss mechanism. Figure 2.5 compares the mud loss profile in fractured and non-fractured formations. In non-fractured formation where losses occur due to formation permeability, mud losses increase gradually with time, then drop slowly after passing the loss interval, while the pit level drops gradually and stops after passing the loss interval. Conversely, a sharp increase in the loss rate and a sharp drop in the pit level are observed in fractured formations; then, both profiles drop gradually with time. On the other hand, the loss rate increases sharply in formations containing caverns or vugs to reach the highest rate then maintain that rate. Simultaneously, the opposite trend is observed with mud level in the pit, indicating a complete lost circulation.

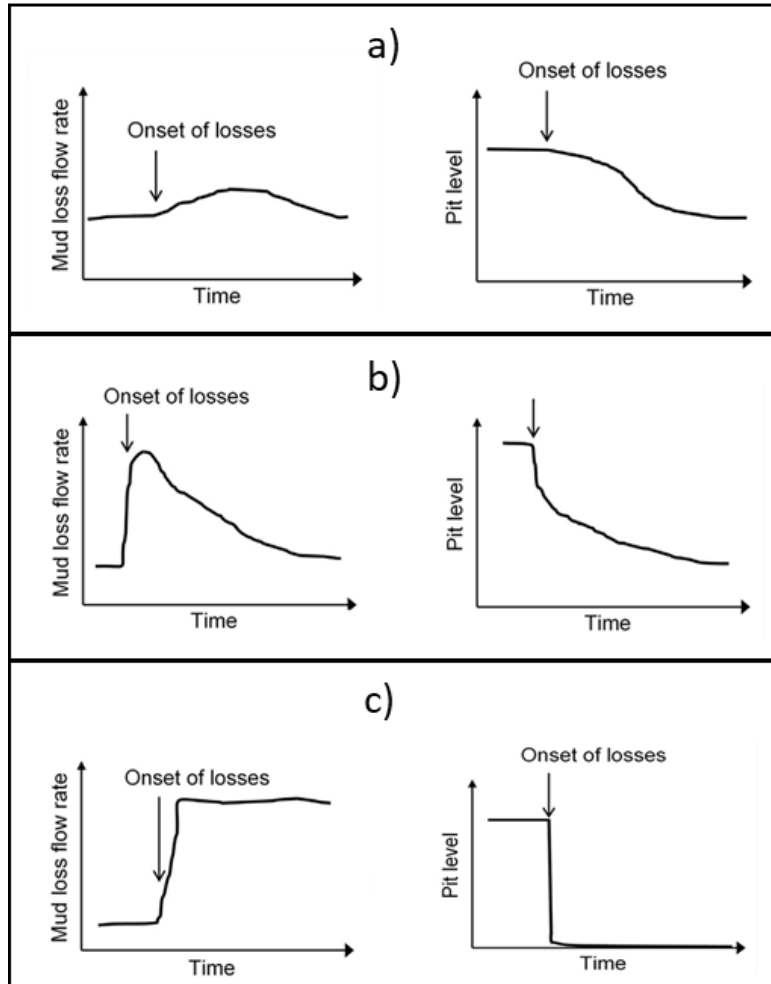


Figure 2.5: Mud loss profile in a) permeable formation, b) fractured formation, and b) caverns and vugs (Chilingarian and Vorabutr, 1983).

2.4.2 Filtration Mechanisms in Aqueous and Non-aqueous Drilling Fluids Systems

Depending on the base fluid used to prepare the mud, drilling mud systems are classified into water-based, oil-based, and gas-based muds. Water-based muds include freshwater muds and saltwater muds. In oil-based muds, the base fluid can be diesel, oil, mineral oil, or synthetic oil. The mud system significantly impacts the lost circulation operation technically and economically because Oil-based and water-based muds perform differently at the same conditions, and their cost varies greatly. The significant differences between aqueous and non-aqueous fluids are the temperature tolerance and filtration properties.

Generally, the main mechanisms of mud filtration discussed in section 2.4.1 apply to both aqueous and non-aqueous drilling fluids. However, the filter cake properties and filtration rate highly depend on the mud system. The non-aqueous muds form a much thinner and less permeable filter cake, with much less filtrate volume than aqueous muds. Despite the better filter cake characteristic in non-aqueous drilling fluids, filter cake removal is more challenging than aqueous muds (Mohamed et al., 2019; 2020). Moreover, mud losses can result from the mud interaction with the drilled formations. For instance, big caves can occur when drilling salt formation with water-based mud, causing severe or total mud losses.

Many studies were performed to investigate the filtration performance and filter cake characteristics in both aqueous and non-aqueous muds. Most studies reported that oil-based muds outperform water-based muds in terms of filtration rate and filter cake properties. The less permeable filter cake observed with oil-based muds is attributed to the emulsification of the brine phase in the oil phase. It was also reported that changing the filter cake wettability from water-wet to oil-wet reduces the brine invasion into drilled formations, improving the filtration performance (Brege et al., 2010). One great example of the difference in filtration performance between WBM and OBM is the study conducted by Allan et al. (2019). They evaluated the filtration performance of two different formulations of drilling fluids (OBM and WBM) with a density of 9 ppg under elevated temperatures. They reported a more than 80% reduction in filtrate volume when using the oil-based mud.

2.5 Factors Affecting Mud Losses

The lost circulation problem is affected by many factors categorized into chemical, geochemical, geomechanical, and operational factors. In this section, all the factors affecting the mud losses are discussed in detail.

2.5.1 Chemical and Geochemical Factors

Chemical factors are the factors associated with the chemical nature and composition of drilling fluids. These factors are mud type, mud additives, and lost circulation materials. Drilling muds are mainly divided into water-based mud (WBM), oil-based mud (OBM), and aerated mud. The mud composition highly affects the filtration rate and filter cake properties. OBM is well known to have a better filtration performance than WBM. OBM forms a much thinner and less permeable filter cake, with much less filtrate volume than WBM. This good filtration performance is attributed to high thermal stability and emulsification of the brine phase in the oil phase. OBM contains asphalt, gilsonite, and clays as filtration control additives.

In contrast, WBM is prepared by adding mud additives to the water as a base fluid. WBM also consists of polymeric additives to control fluid loss and clay swelling. The filtration performance of WBM depends on the mud rheology and conventional lost circulation materials. Mud additives are added to drilling fluids to optimize the mud properties, control fluid losses, and mitigate the effect of mud filtrate on drilled formations such as clay swelling and formation damage. For instance, mud pH is a vital parameter that controls colloidal suspension, such as bentonite. Thinners or dispersants are also mixed with WBM to improve the rheological and filtration performance of the mud and enhance the filter cake characteristics. Mud composition represented by the concentrations of such additives significantly impacts the amount of losses and filter cake properties.

Several studies were conducted in laboratories to synthesize and evaluate mud additives to optimize the mud system and improve its performance. Evaluating these additives and studying their impact on the mud formulation is crucial before field implementation. These additives may change the chemistry of other additives and negatively affect the drilling operation. Moreover,

these additives may interact with the drilled formations, causing additional mud losses or other complications such as formation damage.

On the other hand, the geochemical factors are defined as the factors associated with the drilled formations impacting the fluid losses. These factors are essential to consider in drilling operations and lost circulation treatments. They include the formation lithology and mineral composition that cannot be changed or controlled during drilling operations. Due to their importance, researchers modify the standard filtration setups to accommodate actual core samples rather than filter papers or ceramic discs to study the filtration performance in more representative filtration mediums. Furthermore, the lost circulation treatment is affected by the grain size, orientation, and cementing materials. These factors greatly influence the porosity and permeability that are considered vital formation properties in filtration mechanisms. Rock cementation determines the formation strength that is also considered a significant factor in mud losses, mainly through induced fractures.

Moreover, the drilled cuttings generated from the drilling operation mix with the drilling fluid and alter its properties, especially the fine particles that are difficult to separate using solid control equipment on the surface. Depending on the rock composition, the generated cuttings change the rheological properties and filtration performance differently. To address the lithology effect on mud filtration, several studies were performed to evaluate the filtration performance of drilling fluids in various formation types, such as sandstone, carbonate, and shale formations.

Bageri et al. (2019) studied the effect of drilled cuttings on the drilling fluid properties and filter cake properties using different sandstone formations such as arenite, calcareous, argillaceous, and ferruginous. They mixed fine particles with drilling fluid in various concentrations and measured drilling mud's rheological and filtration properties. The authors tested the same WBM formulation

using a ceramic filter disc as a filtration medium; however, the formation type was the main difference. They found that the formation type significantly impacts the filtration performance and filter cake properties. Ferruginous cuttings enhanced the filter cake sealing properties and reduced its thickness, while the argillaceous cuttings degraded the filter cake porosity and permeability, allowing the fine particles to penetrate deeply in the filtration medium. The effect of mineral composition on filter cake properties is summarized in Figure 2.6.

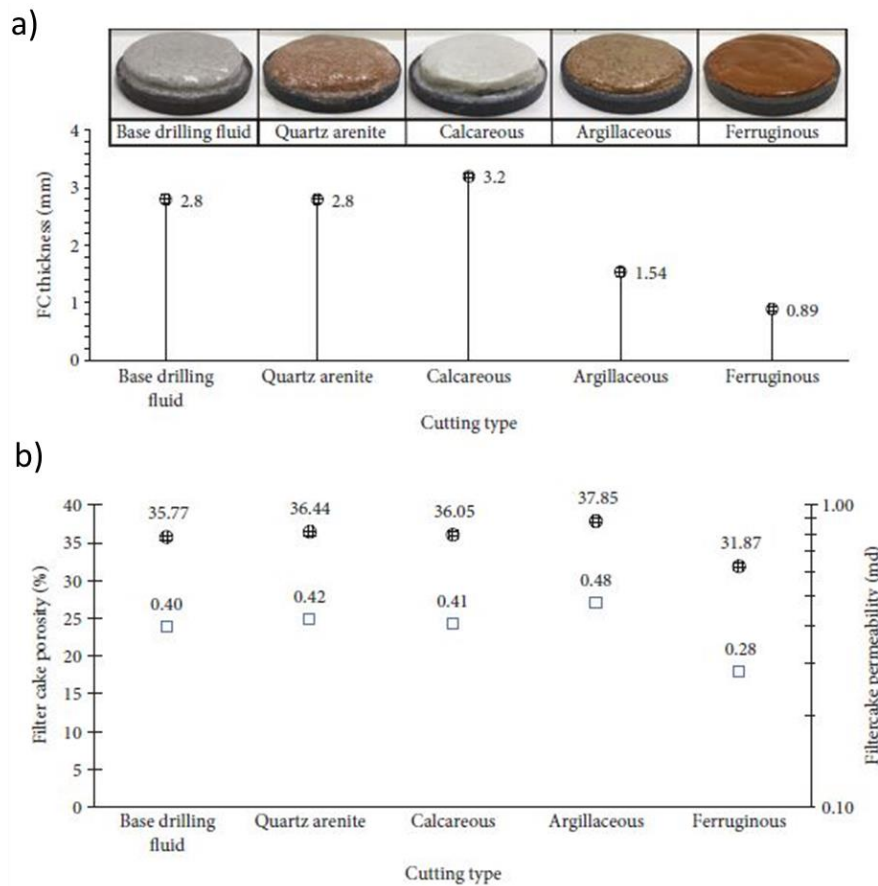


Figure 2.6: Effect of drilled cuttings on a) filter cake thickness and b) filter cake porosity and permeability (Bageri et al., 2019).

2.5.2 Geomechanical Factors, In-Situ Stresses, and Thermal Stresses

As discussed earlier, lost circulation occurs through formation permeability, fractures, caverns, and vugs. Losses through fractures are challenging and responsible for 90% of mud losses.

Geomechanical factors are related to the formation stresses that impact the fracture initiation and propagation into the formation. Drilling operations disrupt the stresses distribution around the wellbore due to the absence of formation rocks. In addition to other functions, drilling fluids are introduced into the wellbore to improve the well integrity and stabilize the wellbore. However, the improper design of drilling muds or parameters deteriorates the wellbore integrity and causes complications. For instance, the ECD uncontrollably increases beyond the fracture gradient in some cases and induces some fractures or makes the microfracture propagate, causing mud losses. It is vital to distinguish these induced fractures from natural fractures.

In addition to mud pressure, the in-situ formation stresses influence fractures propagation and well stability. The stresses are mainly divided into vertical and horizontal stresses. The well inclination highly impacts the stresses around the wellbore. For example, drilling a horizontal well in the direction of maximum horizontal stress yields less well stability than in the direction of minimum horizontal stress. Also, vertical wells are usually more stable than inclined and horizontal wells. Moreover, other factors such as rock elasticity, formation temperature, and mud temperature affect the well stability and fracture pressure. Vertical stresses in elastic rocks generate horizontal stress components, which impact the formation breakdown pressure.

Mud temperature is another crucial factor that affects the stresses around the wellbore. Mud temperature reduces the wellbore temperature and changes the fracture gradient. The effect of mud temperature is more pronounced in high-temperature formations, such as geothermal formations. The sudden cooling and heating generate tensile stresses and cause the near-wellbore fracture gradient to be exceeded, inducing fractures that form an escape pathway to the mud losses. The reduction in fracture gradient in several deep-water wells is clear evidence of the cooling effect that led to many lost circulation events. Another field test conducted in shallow sand and shale

formations in Texas (3081 ft) confirmed the temperature effect on fracture gradients. It was found that increasing the mud temperature to around 60°F increased the fracture gradient by 1.5 ppg (Zhang, 2019). Zhang (2019) conducted a modeling study on the effect of mud temperature on the stresses around the wellbore and breakdown pressure. He concluded that cooling the mud reduces both tangential stresses and breakdown pressure (Figure 2.7). Cooling the mud to 50°F decreased the tangential stresses in the maximum horizontal stress by 9.26%, as shown in Figure 2.7a.

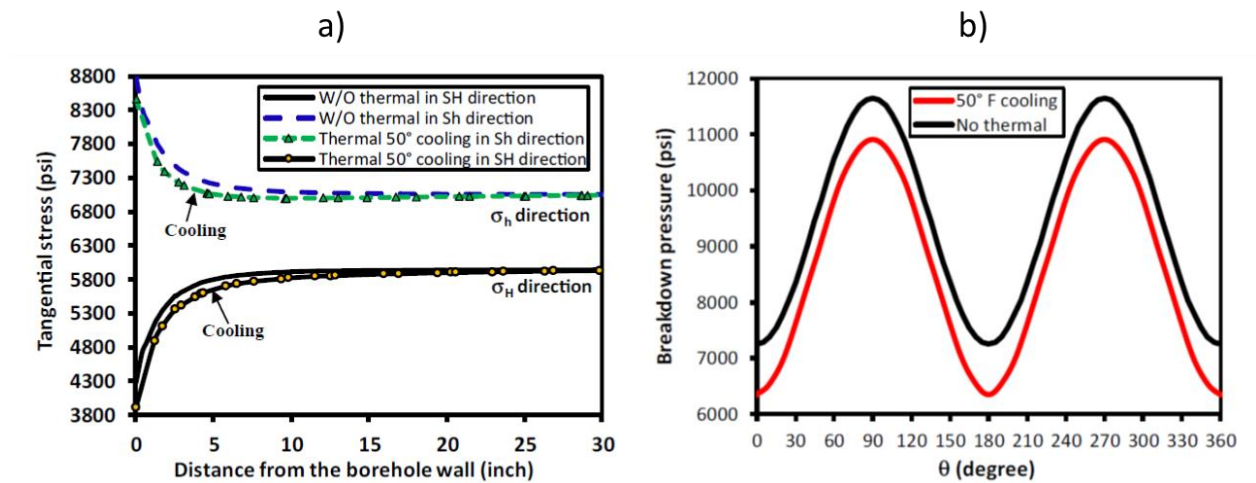


Figure 2.7: Cooling effect on a) tangential stresses and b) breakdown pressure (Zhang, 2019).

Moreover, in-situ stresses are significant factors in the preventive methods of lost circulation, particularly wellbore strengthening techniques. In these methods, the hoop stresses around the wellbore are improved by adding LCM pills to increase the rock resistance to fracture propagation. Several models are introduced to model the wellbore strengthening, such as the stress cage model, fracture propagation resistance model, and fracture closure stress model. The concept and assumptions of these models vary. For instance, the compressive forces transferred to the bridging particles at the fracture mouth are assumed to increase the hoop stresses in the fracture closure stress model. Thus, the fracture is initiated first before the bridging particles are forced into the fracture. These bridging particles isolate the fracture tip from wellbore pressure. In contrast,

bridging occurs close to the wellbore in the stress cage models, and fluid filtrates invade the fracture walls into the formation. Several numerical models were developed to represent the wellbore strengthening and simulate mud losses through fracture propagation. Linear rock elasticity is assumed in most of these models, neglecting the effect of formation porosity, fluid flow, and pore pressure.

2.5.3 Impact of Fracture Size on Mud Losses

Fracture size is essential in lost circulation in natural or induced fractures. The fracture conductivity highly depends on the fracture width and length. As the fracture size increases, the fracture conductivity increases, increasing the loss and loss rate. Several laboratory studies were performed to study the effect of fracture size on mud losses. one example of these studies is the experimental evaluation of fracture size impact on mud losses conducted by Ezeakacha et al. (2017). Using a dynamic filtration drilling simulator, they tested the mud losses on three fractured cylindrical discs with different sizes and orientations, 500 microns and 1000 microns. They concluded that the fracture size and orientation greatly affected the fluid losses. A significant increase in filtrate volume was observed when drilling mud was tested in large fracture sizes.

2.5.4 Impact of Rheology on Mud Losses

Rheological properties play a significant role in the drilling operation and impact several drilling issues such as filtration and suspension properties, hole cleaning, fluid stability, and wellbore hydraulics. Mud losses are affected by rheological properties in different ways. In non-fractured formations where the formation permeability is the only pathway for mud invasion, mud losses are managed by optimizing mud properties and rheology. Previous studies confirmed that the rheological properties of drilling mud highly impact filtration performance and lost circulation (Kulkarni et al., 2013). The primary factors that dominate mud loss through natural fractures are

drilling fluid rheology, wellbore pressure, and hydraulic aperture of the fracture. Sun and Huang (2015) investigated the impact of mud rheology on lost circulation in natural fractures. Their main conclusion was that the high shear rate rheology is essential in controlling the mud losses as it affects the losses during the early filtration time.

Equivalent circulation density (ECD) is a vital hydraulic parameter that affects mud losses. ECD is defined as the effective mud density exerted on the formation accounting for the pressure losses in the annulus. In general, the higher the ECD, the higher mud losses invade the formation. However, the increase in ECD beyond fracture gradient induces fractures in the drilled formation, causing partial or total mud losses, especially in weak and depleted formations (Murray et al., 2013). Therefore, ECD should continuously be optimized to avoid such induced losses. Moreover, controlling the ECD and mud rheology is a well-known method to mitigate mud losses.

The Pierce field in the UK is an excellent example of this technique, where severe mud losses were encountered, and no progress in drilling operation could be made. Two options were considered: reducing the ECD to its minimum by decreasing the pump flow rate or by optimizing and reducing the rheological properties. The first option was unsuccessful because lowering the mud flow rate deteriorates the hole cleaning, increases the ECD, and ultimately causes additional losses. On the other hand, the organophilic clay content and the oil-water ratio were optimized to reduce the rheological properties, especially the low-end rheology. Consequently, subsequent wells were drilled successfully without mud losses (Murray et al., 2013; Wilson, 2014).

Additionally, mud rheological properties contribute significantly to the hole cleaning efficiency and suspension capability of drilling fluids. The yield point of drilling mud represents the fluid's capability to suspend solid particles and drilled cuttings. Based on a simulation study, Busahmin et al. (2017) stated that plastic viscosity, yield point, and gel strength are controlling

factors on the cuttings transport efficiency. Poor hole cleaning or fluid stability present formidable challenges to the drilling operation and loss circulation treatment. The accumulated cuttings or weighting materials increase the frictional pressure losses by reducing the annular space, thus increasing the ECD. As discussed earlier, the uncontrolled increase in ECD may induce fracture into the formation and increase the losses, as shown in Figure 2.8. Furthermore, poor rheological suspension capability means that the mud cannot carry lost circulation materials efficiently; consequently, less sealing efficiency will result because less LCM concentration than the optimum concentration will get to the loss zone.

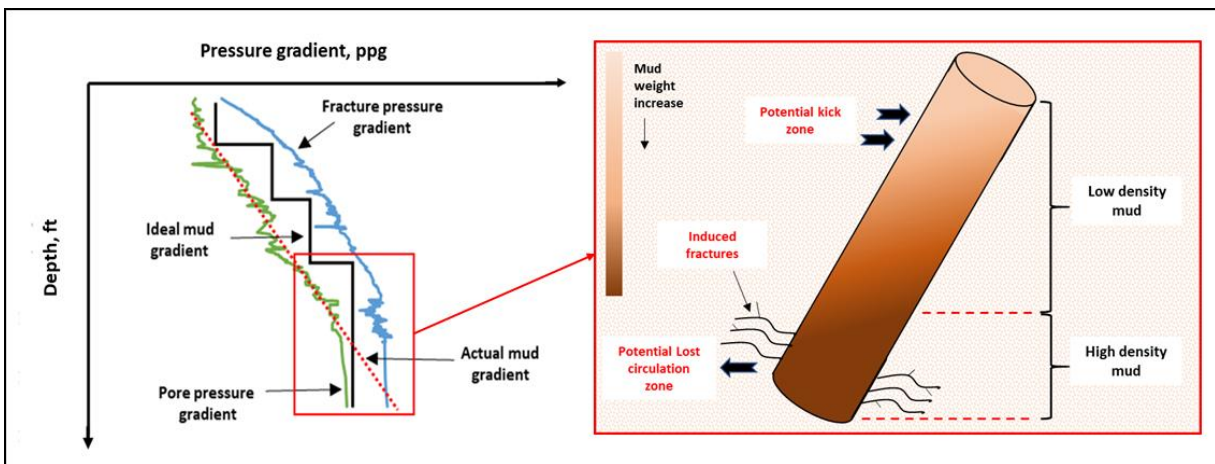


Figure 2.8: Complications of accumulated cuttings or solids sag phenomenon (Mohamed et al., 2021a).

2.5.5 Impact of Temperature on Mud Losses

Downhole temperature is considered one of the preexisting conditions that cannot be controlled during lost circulation events. Temperature affects the mud losses and lost circulation treatment in many ways, mainly by altering mud and formation properties. The change in mud rheology caused by the high temperature encountered downhole was observed in the lab and fields. A substantial increase in yield stress of bentonite mud at elevated temperatures has been reported in previous studies. This increase is attributed to clay swelling and flocculation at high temperatures. Also, the high temperature degrades the polymeric additives and LCMs, which causes a deterioration of

rheological properties and sealing efficiency (Mohamed et al., 2021a). This effect will be discussed in more detail in section 3.4. Additionally, the change in rheological properties impacts the wellbore hydraulics, suspension capability, and other drilling parameters related to lost circulation. The effect of mud rheology on mud losses was well discussed in section 2.5.4.

Moreover, the temperature is one of the controlling parameters in many LCMs methods. For instance, polymeric gel formulations are designed to work at a specific temperature because the temperature significantly influences polymers crosslinking. Temperature also controls the activation of smart LCMs such as shape memory polymers. This material is designed to work in a specific temperature range between the activation and melting temperatures. The activation cannot be attained below this range, and exceeding the melting temperature will degrade the LCM, causing the lost circulation treatment failure. Therefore, the downhole temperature is a crucial factor in selecting and optimizing the lost circulation treatment.

On the other hand, high temperature exposes the drilled formations to thermal stresses that impact the rock strength and fracture gradient. Temperature variations resulting from the sudden cooling and heating generate tensile stresses and reduce the near-wellbore stresses. This decrease in wellbore stresses lowers the fracture gradient, resulting in induced fractures that form an escape pathway to the mud losses. The effect of thermal stresses was discussed in detail in section 2.5.2.

2.5.6 Impact of Pressure on Mud Losses

When mentioning the pressure in lost circulation problems, we mean the wellbore pressure, pore pressure, and fracture pressure, representing the mud window. Usually, the formation pressure is an uncontrollable parameter in drilling operations. Therefore, the mud should be carefully designed to function without causing any problems. First, the mud density is optimized to avoid the excessive hydrostatic pressure exerted by the mud column. At the same time, the rheological

properties are designed to yield optimum ECD and wellbore hydraulics to prevent any induced fractures. The differential pressure is the primary driving mechanism of mud invasion; the higher the wellbore pressure, the more mud losses into the formation.

During overbalanced drilling, the wellbore pressure should always be higher than the pore pressure and lower than the fracture gradient. However, in many cases, controlling the wellbore pressure is challenging, especially in weak and depleted formations. Exceeding the fracture gradient causes induced fracture, resulting in a significant increase in mud losses. Therefore, many drilling techniques control the mud pressure to prevent losses, such as managed pressure drilling (MPD) and underbalanced drilling (UBD). Moreover, other operational parameters are optimized to avoid increased wellbore pressure, such as swap and surge pressure. For instance, increasing the surge pressure from 450 to 650 psi at a depth in the range of 7,500-10,000 ft is equal to a 1.2 ppg increase in the mud density. Thus, controlling the wellbore pressure properly can prevent and mitigate the lost circulation problem.

2.5.7 Effect of Rotational Speed, Mud Rate, and Wellbore Geometry on Mud Losses

Rotational speed and circulation rate are operational factors that can be controlled during the drilling operation and lost circulation treatment to achieve optimal results in the field. In addition to the area, circulation rate determines the flow regime and impacts the frictional pressure losses used in wellbore hydraulics calculations. Usually, the higher the flow rate, the more frictional pressure losses and the higher ECD. This increase in ECD when it exceeds the fracture gradient causes induced fractures and additional mud losses. Conversely, low circulation negatively impacts the hole cleaning. The poor hole cleaning leads to the formation of a cutting bed that reduces the annular space and increases the frictional pressure losses, leading to mud losses.

Therefore, the mud circulation rate should be optimized and continuously monitored to avoid any complications in the drilling operation.

Another essential property in lost circulation treatment is the suspension capability of the drilling mud. The excellent suspension capability improves LCM transportation and ensures no complications from accumulated LCM particles. In addition to mud properties, circulation rate and drill pipe rotation effectively enhance the solid particles' transportation and dispersion in drilling mud. The pipe rotation agitates and erodes the cutting bed and improves the LCM dispersion, especially at low flow rates. The rotational speed also affects the rate of penetration (ROP) and the amount of generated cuttings, impacting the hole cleaning.

On the other hand, in most cases, wellbore geometry is an uncontrollable parameter that impacts the lost circulation and mud losses. Wellbore geometry directly affects the flow regime, wellbore stability, and frictional pressure losses. As the well diameter decreases, the annular space between the drill pipe and the well decreases. This decrease will significantly increase the mud velocity and frictional pressure losses. The higher the frictional pressure losses, the higher the ECD and the more mud losses. The optimum flow rate for proper hole cleaning is also affected by the wellbore size. Moreover, wellbore geometry alters the stress distribution in and around the wellbore; consequently, changing the fracture gradient may lead to induced fractures and additional mud losses into the formation.

2.6 Statistical Assessment of Mud Losses in Different Formations

Partial or complete mud losses introduce many issues to drilling operations. Mud losses are common in drilling operations; lost circulation is encountered in 20 to 25% of the drilled wells worldwide. They are one of the major causes of prolonged drilling time and the high cost of drilling operations. The increase in drilling cost is due to the cost of drilling fluid lost into the formation and the downtime spent on curing the losses. For instance, in the Gulf of Mexico, treating mud

loss events was responsible for more than 10% of the non-productive time (NPT) between 1993 and 2003 (Magzoub et al., 2021).

One contributor to the drilling cost increase is the high cost of drilling muds. The drilling fluid cost varies significantly with the mud type; WBM, OBM, or SBM. However, 25 to 40% of the total drilling cost is the cost estimate of drilling muds. Therefore, losing this percentage would significantly impact the feasibility of drilling operations. Moreover, the consequences of mud losses may add additional costs to the drilling operations. According to Al Maskary et al. (2014), about one billion dollars is spent annually on lost circulation events worldwide, including the materials cost and rig time.

Another contributor to the increased drilling cost is the time spent on curing mud losses and regaining the well control. Around \$800 million is the estimated annual cost of NPT due to lost circulation events. According to the analysis conducted by Rohani (2012) on NPT during drilling offshore gas wells, 12.8% of the NPT was attributed to the lost circulation events lost circulation in deep wells (more than 15,000 ft), while shallow wells (less than 15,000 ft) were responsible for 12.7% of the down time, as shown in Figure 2.9. This analysis was performed on offshore gas wells drilled between 1993 and 2002. He also reported that mud losses add around 27 \$/ft to the drilling cost. This additional cost affects the economics of drilling operations, impacting the feasibility of oil&gas and geothermal formations.

Mud losses occur while drilling in geothermal formations frequently. Geothermal formations are naturally weak and contain large and complex fracture networks. The high temperature encountered in geothermal wells degrades the drilling mud and lowers the fracture gradient. Additionally, geothermal wells are prone to lost circulation induced by the cool mud that reduces the hoop stress around the wellbore. All these reasons make the lost circulation more

challenging in geothermal wells than in oil&gas wells. Lost circulation and other related issues significantly increase the geothermal drilling cost to constitute around 40-50% of the total cost of geothermal projects (Mohamed et al., 2021a). Approximately 10-20% of the exploration geothermal well cost in the United States is spent on lost circulation treatment. In the Hengill geothermal area in Iceland, lost circulation and wellbore instability are the leading causes of drilling issues in 18 out of 24 drilled wells (Lavrov, 2016).

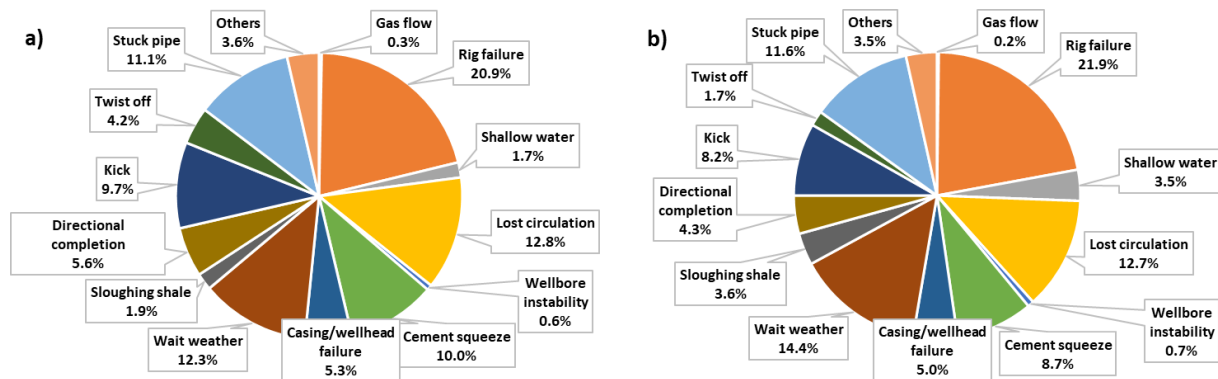


Figure 2.9: NPT percentages for offshore gas wells: a) deep wells and b) shallow wells (Modified after Rohani, 2012).

Cole et al. (2017) analyzed the leading causes of non-productive time during geothermal drilling. Their study is based on daily drilling data obtained from 38 geothermal wells drilled in the United States since 2009. They found that lost-circulation formations are responsible for most of the NPT (7%) with an average of 100 hrs of NPT per well (Figure 2.10), adding around \$185,000 to the rig cost for each well. They reported that the cost added by lost circulation varies in the range of \$2M to \$28M for a 50-MW geothermal field with 10-20 geothermal wells.

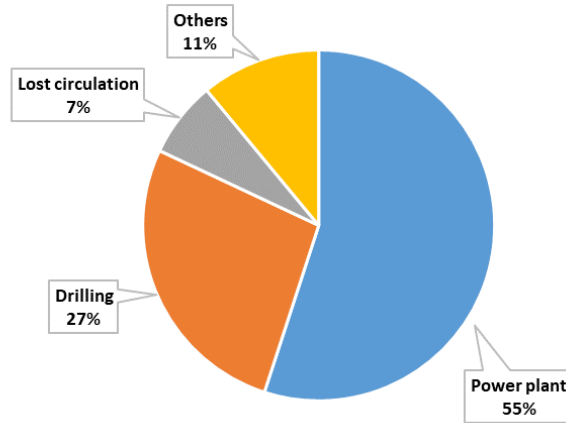


Figure 2.10: Cost allocation for a 50-MW geothermal power plant (Modified from Cole et al., 2017).

The severity of lost circulation events is impacted by formation type and formation properties, such as permeability, porosity, and fracture dimensions. Therefore, total and severe mud losses are more common in fractured carbonate formations. For instance, in Iran, it is reported that 35% of drilling wells encountered lost circulation events in carbonate formations. While in Saudi Arabia, ballooning and mud losses were experienced in 42% of the wells drilled in the Khuff carbonate formation. Severe mud losses are highly expected in caved formations such as salt formations. It is reported that drilling 1,500 ft above the salt formations costs several million dollars.

Moreover, 29% of mud losses are encountered in limestone, shale, loose sand, and depleted sand formations. Rosenberg and Gala (2012) evaluated the lost circulation in different depths and lithologies in the Gulf of Mexico. 48% and 32% of mud losses occurred at 100-1000 ft and 1000-5000 ft, respectively. At the same time, most mud losses (29%) occurred while drilling in shale and loose/depleted sand formations. Figure 2.11 shows the statistics of lost circulation events with depth and formation type.

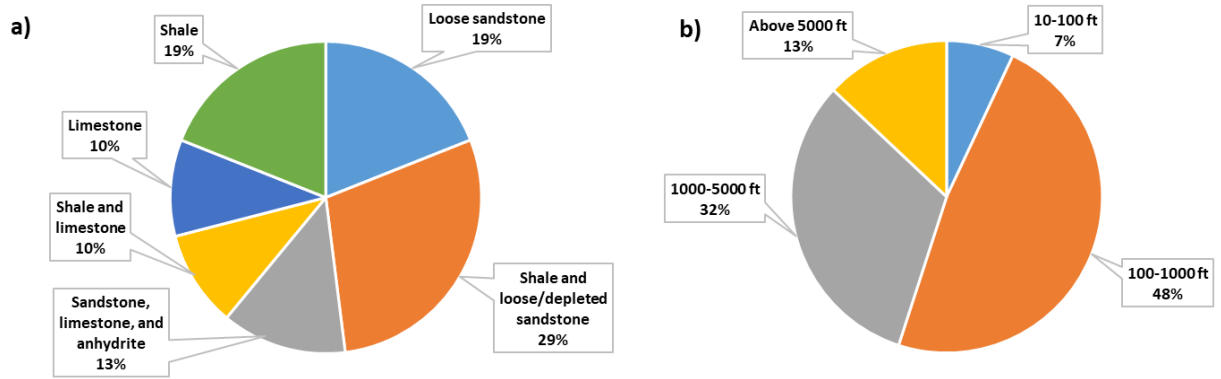


Figure 2.11: Statistics of mud losses with a) formation type and b) depth (Modified from Rosenberg and Gala, 2012).

Chapter 3: Lost Circulation Treatment Methods and Applied Solutions

3.1 Overview of Field Practices

As discussed earlier, the lost circulation problem is challenging and costs the industry huge effort, time, and resources. Therefore, lost circulation prevention, early detection, and prompt remedial actions are the main factors to mitigate the consequences of mud losses, such as hole instability, pipe sticking, and well control issues. Generally, there are two main methods to avoid the effects of mud losses. These methods are the preventive method and the corrective method. Preventive methods can be defined as the actions taken before the loss occurs, while the techniques used after the loss occurs are the corrective methods.

Preventing mud losses in the first place is the priority and more effective than curing the losses (Alsaba, 2015; Magzoub et al., 2020). Avoiding mud losses would reduce the NPT spent on curing losses and save the industry time, effort, and resources. Moreover, the failure of lost circulation treatments is quite often, which will require more trials and NPT to regain the well. Preventive methods mainly rely on good field practices and wellbore strengthening methods.

Field practices include optimizing drilling mud formulations, optimizing drilling fluid properties and wellbore hydraulics, ensuring good hole cleaning, and controlling the drilling parameters such as mud pump pressure. Therefore, sufficient and accurate knowledge of downhole conditions and drilled formation using advanced drilling technologies and previous drilling data would help design the drilling operation to mitigate the lost circulation consequences (Magzoub et al., 2020). Another efficient practice used in drilling rigs is to control the operational parameter during drilling and circulation operations. For instance, during tripping operations, running the drill pipe slowly in the well will reduce the surge pressure that may cause lost circulation sometimes. Additionally, wellbore strengthening techniques are efficient practices to prevent

losses. Wellbore strengthening is achieved by adding appropriate LCMs to the drilling mud formulation or replacing the mud with LCM pills before reaching the expected loss formation. Consequently, the formation fracture gradient increases, and the loss tendency is minimized.

Although the preventive methods are efficient and easy, the nature of drilled formations and downhole conditions in some cases are very challenging. For example, mud losses are very common in narrow mud-window drilling, where drilled formations have low fracture gradients, and controlling downhole mud pressure is difficult. In such cases, lost circulation events are inevitable, and drilling engineers should be prepared to take prompt actions to avoid further complications. This procedure is called the corrective method, in which the mud circulation is regained after losses take place (Alsaba, 2015). Several remedy actions are taken to cure mud losses depending on the loss amount and severity: seepage, severe, or total loss. These methods are classified into three main groups: using lost circulation materials (LCMs), LCM pills, and cement squeeze (Wagle et al., 2018).

Several case studies about the success and failure of lost circulation treatments were reported in the literature, describing the causes, applied solutions, and the learned lessons. For instance, drilling a 12” hole in the Azar oilfield in Iran is a clear example of loss circulation case studies, where different preventive methods were tried. While drilling in one of the troublesome formations, a complete loss occurred. 110 bbl of mica pill was introduced into the wellbore to stop the losses. The treatment was successful, and loss was reduced gradually to reach only 35 bph. Again, mud loss increased suddenly to 150 bbl, while lowering the mud weight and adding another LCM pill failed to stop the losses. Consequently, 100 bbl of cement slurry was pumped to serve as a cement plug to stop the losses (Rahmanifard et al., 2014).

3.2 Conventional LCMs

Lost circulation materials are additives mixed with the drilling fluid formulation to seal fractures and stop mud losses in oil, gas, water, and geothermal wells. LCMs are added to the mud formulation in different concentrations, depending on the loss severity and downhole conditions. Selecting the appropriate LCM type and optimizing the mud formulation are significant factors in ensuring successful treatments in the field. LCM selection depends on many factors such as downhole conditions, sealing efficiency, availability, cost, and environmental impact of LCM. Generally, there are different classifications for lost circulation material based on the shape and purpose. Depending on the treatment type, preventive or corrective method, LCMs are classified into two main groups: bridging or plugging materials. On the other hand, based on the shape, LCMs are divided into three main categories: granular, flakey, and fibrous material.

Granular materials are the common additives used to stop lost circulation because they are relatively inexpensive and have many good properties such as large surface area, hardness, and wide particle size range. This type of LCMs includes calcium carbonate, walnut, graphite, gilsonite, perlite, coal, marble, and expanded aggregate. Flakey and fibrous LCMs are also used for bridging and sealing fractures in the loss zones. The large particles form a bridge on the fracture opening, while small particles seal the voids. Flakey and fibrous LCMs are used in both wellbore strengthening and lost circulation treatment. However, they have low mechanical strength. The common LCMs used in drilling operations are summarized in Table 3.1.

Many laboratory studies were performed to evaluate the sealing efficiency of common LCMs at various testing conditions (Akhtarmanesh et al., 2016; Alkinani et al., 2019; Alsaba, 2015; Alsaba et al., 2014; Ezeakacha et al., 2017; Javeri et al., 2011; Loeppke et al., 1990; Luzardo et al., 2015). In addition to these LCMs, several studies were also conducted to evaluate some

LCMs produced from natural resources and such as plants, date seeds, and banana peels (AlAwad et al., 2018; Amanullah and Arfaj, 2018; Nasiri et al., 2018; Sauki et al., 2017).

Despite the advancements in lost circulation materials, more research is still needed to overcome the limitations of conventional lost circulation materials. Conventional LCMs fail to seal large and complex fracture networks due to particle size limitations. When large particles are used, plugging downhole equipment (such as LWD and MWD) is likely. LCM particles also cause formation damage when they invade the producing formation. Moreover, some health and environmental impacts are associated with some of these materials (Magzoub et al., 2021b; Mansour et al., 2017). These impacts are discussed in detail in Chapter 6. To overcome such challenges, advanced LCMs were introduced to stop mud losses under critical downhole conditions, where most conventional LCMs fail. Encapsulated pills, acid/water-soluble LCMs, LCMs Blends, nanoparticles (NPs), polymeric gels, and shape memory polymers (SMPs) are good examples of such advanced LCMs.

Table 3.1: Common LCMs used in drilling operations (Mohamed et al., 2021a)

LCM	Type	Specific gravity	Temperature		Remarks
			Maximum tested	Successful up to	
Calcium Carbonate	Granular	2.71	149 °C (300 °F)	126 °C (260 °F) alone /149 °C (300 °F) in blends	High Solubility to acid and low pH muds
Cellophane Flakes	Flake	1.42	149 °C (300 °F)	149 °C (300 °F)	Typically used in blends/ Highly damaging to productive formations/ High resistance to shear when wet.
Graphite	Granular	1.9-2.3	149 °C (300 °F)	149 °C (300 °F)	Can reduce seal efficiency at HT due to lubricity effect/ It should not be used in blend at HT conditions/ It is not affected by temperature when used alone
Black Walnut Shells	Granular	1.1	260 °C (500 °F)	260 °C (500 °F)	They have fiber-like structures on the surface that could prove helpful in sealing fractures
Mica	Flake	2.4-3	260 °C (500 °F)	260 °C (500 °F)	Typically used in combinations with other LCM's/ Standard concentration: 28.53 kg/m ³ (10 lb/bbl)/ Should be used with care due to high SG

Perlite	Granular	1.1	204 °C (400 °F)	204 °C (400 °F)	Used with cement only in Shallow Depths/ It does not resist pressures higher than 13.8 MPa (2000 psi).
Mixed Nut Shells	Granular	1.2	149 °C (300 °F)	149 °C (300 °F)	More Effective at higher temperatures (swelling)/ More effective on their own than in blends/ Good from a solid degradation point of view
Thermoset Rubber	Granular	1.48	149 °C (300 °F)	149 °C (300 °F)	LCM capabilities rapidly degrade with temperature/ Higher concentrations than 71.33 kg/m ³ (25 lb/bbl) can be detrimental
Cellulosic fibers	Fiber	1.2-1.5	100 °C (212 °F)	100 °C (212 °F)	-
Cotton Seed Hulls	Mixed/Mostly flakes	0.32	121 °C (250 °F)	93 °C (200 °F)	-
Plastic Foil	Flake	1.4	260 °C (500 °F)	-	Although the normal degradation temperature of PVC is low, plastic foil is still listed as a geothermal LCM, which implies that other materials might be used in the plastic foil composition
Alder Wood	Granular	0.37	204 °C (400 °F)	Completely degraded at 204 °C (400 °F)	Not Suitable for geothermal applications due to low thermal resistance
Coal	Granular	2.3	204 °C (400 °F)	156.6 °C (330 °F)	%30 loss of seal strength up to 156.6 °C (330 °F)/ Poor Mechanical Properties
Foam Wedge	Flake/Fiber	Variable	82 °C (180 °F)	82 °C (180 °F)	Requires time to strengthen the seal
Expanded Aggregate	Granular	2.6	204 °C (400 °F)	204 °C (400 °F)	Poor Mechanical Properties/ High Density/ Very abrasive/ Seals created were very unreliable
Gilsonite	Granular	1.06	121 °C (250 °F)	More than 110 °C (230 °F)	Typically Used in cement Slurries/ Low S/E ratio suggest poor to medium plugging capabilities/ Poor Mechanical Properties
Marble	Granular	2.7	187 °C (370 °F)	187 °C (370 °F)	-
Tires	Granular	~1.15	90 °C (194 °F)	90 °C (194 °F)	Very low price and high availability

3.3 Unconventional LCMs

3.3.1 Nanoparticles (NPs)

The applications of nanomaterials have been recently extended in the oil&gas sector for different purposes, including enhanced oil recovery, well stimulation, and drilling. Nanomaterials are synthesized materials with a particle size in the range of 1–100 nm. They have distinctive properties under various operating conditions, such as high surface area and high thermal conductivity. The main advantages of using NPs in drilling fluids are controlling fluid loss, improving rheological and filter cake properties, reducing formation damage, lubrication, and

overall drilling cost. NPs are used with drilling fluids to attain certain functions such as fluid loss control, improved rheological performance, hole cleaning, and shale inhibition. Cheraghian (2021) presented an excellent review of the applications of NPs in drilling fluids, including materials, sizes, recommended concentrations, and drilling fluid types.

Several studies were performed to evaluate the use of NPs in reducing mud losses. For instance, Mahmoud et al. (2018) conducted an experimental study to investigate the effect of ferric oxide nanoparticles on the properties of calcium bentonite-based drilling mud. They found out that Fe_2O_3 NPs significantly improved the filtration performance of drilling mud by reducing the filtrate volume and filter cake thickness, as shown in Figure 3.1.

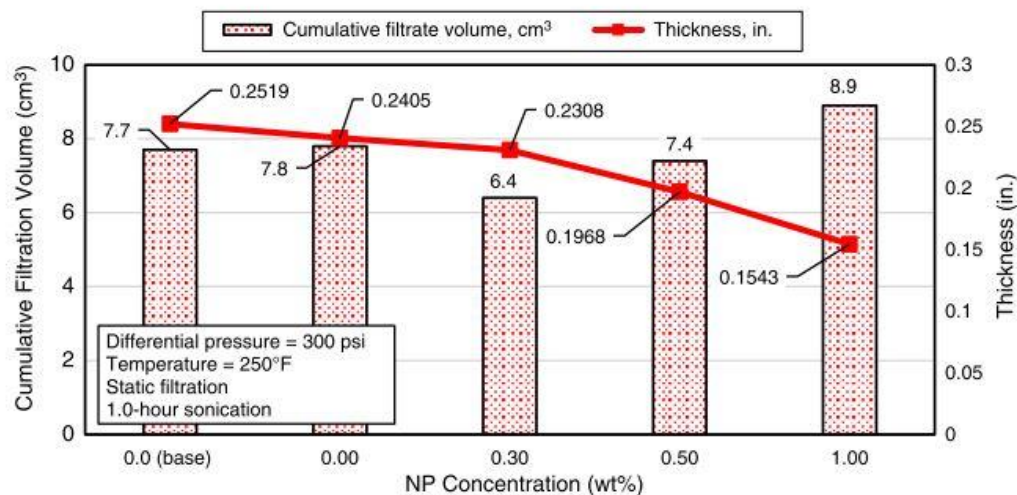


Figure 3.1: Effect of ferric oxide NPs on the filtration performance of drilling mud (Mahmoud et al., 2018).

3.3.2 Polymeric Gel

Polymers are used widely in the oil&gas and geothermal industries because they have many good characteristics. Polymers are relatively inexpensive than other chemicals, pumpable, and suitable for operational purposes. They are classified based on their structure, polymerization mode, origin, and molecular forces. Generally, polymers are classified into biopolymers and synthetic polymers. Polymeric gels contain a polymer base and a crosslinker. Different organic and inorganic

crosslinkers are used to prepare polymeric gels. Crosslinkers are selected based on the application, downhole conditions, cost, and environmental impacts.

Polymeric gels have been introduced for various applications such as sand control, water shut-off, cementing and well stimulation, and lost circulation treatments. Crosslinking temperature, gelling mechanism, gel strength, thermal and chemical stability, and gelling time are the significant factors to be considered in all applications to ensure optimal results. Moreover, the breaking mechanism of polymeric gels is vital for cleaning purposes (Hamza et al., 2019).

Polyacrylamide (PAM) is a commonly used polymer in the oil and gas industry crosslinked with polyethyleneimine (PEI). PAM is a water-soluble polymer prepared by polymerization of acrylamide monomer with a bifunctional crosslinking agent, while PEI is an organic crosslinker. The PAM/PEI solution is broadly used in water flooding and water shutoff applications. It has unique rheological characteristics, a broad range of molecular weight, and low cost. Several studies were performed in laboratories to evaluate the stability, optimum concentration, rheological properties, reaction kinetics of PAM/PEI solutions (Magzoub et al., 2021).

The fundamental concept of using polymeric gels for lost circulation and wellbore strengthening is to mix the gel with drilling formulation or pump it downhole as a separate pill. The gel is injected inside the formation as liquid and set for some time to form a gel. The mature gel will form a hard seal inside the fractures and stop the mud losses. Many studies were performed to evaluate the effectiveness and performance of polymeric gels in lost circulation treatments. Hamza et al. (2019) reviewed the polymeric gel formulations used in loss circulation and wellbore strengthening applications considering the mechanical strength, compatibility with drilling mud additives, rheological properties, thermal stability, and environmental concerns. The special additives used with gel formulations such as nanomaterials have also been discussed.

For instance, Magzoub et al. (2021) proposed a screening method to optimize the formulation and mixing procedure of PAM/PEI using the rheological behavior. Their approach achieved promising findings, where gel formulations were optimized to yield optimal rheological performance and sealing efficiency. 80% reduction in the fluid loss was observed when PAM/PEI gel was compared with conventional lost circulation material, as shown in Figure 3.2. Other gel formulations used in lost circulation applications are summarized in Table 3.2.

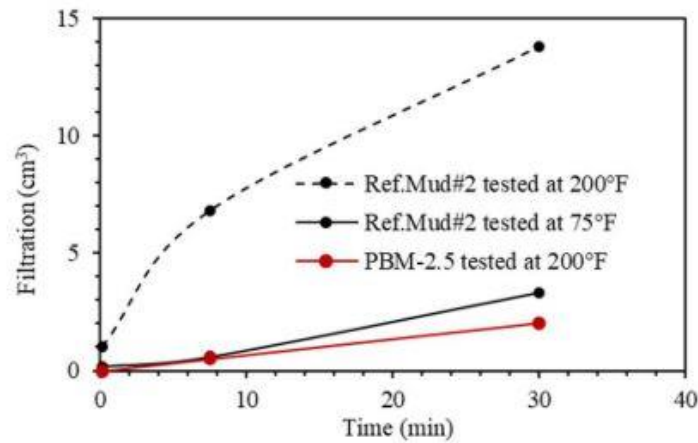


Figure 3.2: Filtration performance of PAM/PEI gel (PBM-2.5) and reference mud (Magzoub et al., 2021).

Table 3.2: Summary of polymeric gel systems used in lost circulation application (Hamza et al., 2019)

Polymer/Crosslinker	Temperature, °C	Gel strength/Gelation time
3 wt.% HPAM/1.2 wt.% PEI.	120	9.8 times the base solution/200 min
2 wt.% HPAM-derivative/1.2 wt.% PEI	100	3 times the base solution/204 min
0.5 wt.% PAM/0.4 gm phenol and 0.37 gm formaldehyde	Room temperature	Class C
Multifunctional gel solution	up to 100	-
HPAM/chromic III carboxylate. Synthetic water hydrated polymer	-	400 times the original size
CACP mixed with retarder, fibrous cellulose polymer, and polymer with calcium carbonate	90	3–7.5 MPa
Modified polymer	-	-
Urethane 902, Butyl Sealant, polysulfide polymer, and Hotpour 164	-	Gelation time about 5–30 min
7 wt.% copolymer of acrylamide and PATBA, 2 wt.% KCl, and 8 wt.% carbonate retarder	Up to 176.7	40 min without retarder and 600 min with 8 wt.% carbonate retarder at 176.7 °C

Smart anionic shape memory polymer activated by heat	70	34.5 MPa
The oil-absorbent polymer formed by 6 gm of MMA, 18 gm of HMA, 16 gm of BA, and 5 gm of EAC	300	Increased from 3 to 9 Pa after using 3 wt./vol.% of the oil absorbent polymer
0.7 wt.% lignosulfonate/acrylamide graft copolymers 5.72 kg/m ³ (HPS) (not recommended for drilling), 2.85 kg/m ³ CMC and XG	30 and 55	-
acrylamide-based solution mixed with hydroxyl and carboxyl-based ingredients (commercially named as XNGJ-3)	Became a gel at 80	bear up to 21 MPa

3.3.3 *Shape Memory Polymer (SMP)*

Shape memory polymer is one of the recent technological advancements in the lost circulation material. SMP is a smart polymer programmed to have a temporary shape/size under specific conditions and regains its original shape once triggered with an external stimulus (Huang et al., 2005; Meng and Li, 2013). Light, pH, electricity, heat, moisture, enzymes, and magnetic field are the common mechanisms used to trigger shape memory polymers (Fan and Li, 2018; Liu et al., 2009; Mather et al., 2009). SMPs are used widely in many applications such as sealants, actuators, self-healing, smart textile, and medical applications (Fan and Li, 2018).

Thermoset polymers are the most common SMPs programmed and activated using thermal energy (Lakhera et al., 2012). SMP is heated to a specific temperature (programming temperature) during the programming cycle and deformed by applying an external load. Then, SMP is cooled below its glass transition temperature while the load is still exerted. Once the load is removed, the deformed shape will be maintained, as shown in Figure 3.3a. When SMP is heated to a temperature higher than the programming temperature, the stored energy will be released as mechanical stresses and the original shape will be restored (Figure 3.3b). Since activation can be optimized, SMPs have a great potential to overcome the conventional LCMs limitations, where large particles may plug downhole drilling tools such as MWD and logging tools. Moreover, shape memory polymers are easy to process, cheap, highly elastic, and versatile (Liu et al., 2009).

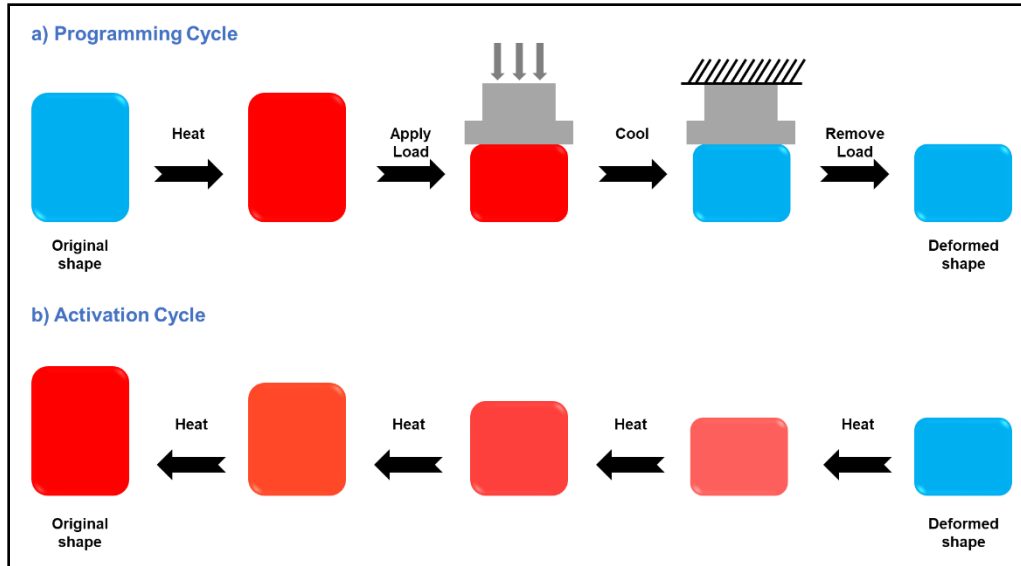


Figure 3.3: Programming and activation cycle of shape memory polymers (Mohamed et al., 2021c).

Shape memory polymers were recently introduced for lost circulation material, and many laboratory studies were performed to evaluate their sealing efficiency. However, there is no field application reported in the literature. Mansour et al. (2017) proposed a novel expandable lost circulation material based on a shape memory polymer to treat mud losses. Their LCM material is designed for low-temperature applications (70°C). Their new material yielded promising results, where a high sealing pressure and low mud loss were achieved. They also concluded that the expandable LCM could release 13 MPa stress, increasing the hoop stresses around the wellbore.

However, the experiments were performed using permeability plugging apparatus (PPA) at static conditions, which do not represent the actual filtration process. Afterward, they conducted another study to investigate the SMP performance under dynamic conditions. It was found that the SMP worked much better when mixed with fiber (Mansour et al., 2018). Moreover, the ultimate temperature was limited to 120°C as SMP melts beyond this temperature. This temperature is not suitable for geothermal applications where high temperatures are encountered downhole.

Another study was conducted by Magzoub et al. (2021a, 2021b) to evaluate the sealing efficiency of SMP at high temperatures (149°C) for fracture sealing in geothermal formations. In addition to the conventional PPA, they built a new flow loop setup to simulate the sealing process under dynamic conditions. 14-inch fabricated aluminum discs and cylindrical granite core samples were used as a filtration medium. Filtration mediums contain a fracture of two different sizes: 2000 and 3000 microns. SMP was found to be an excellent candidate to cure mud losses in geothermal formations with additional wellbore strengthening features. They also confirmed the findings of Mansour et al. that SMP and fiber blend provides better sealing efficiency (Figure 3.4).

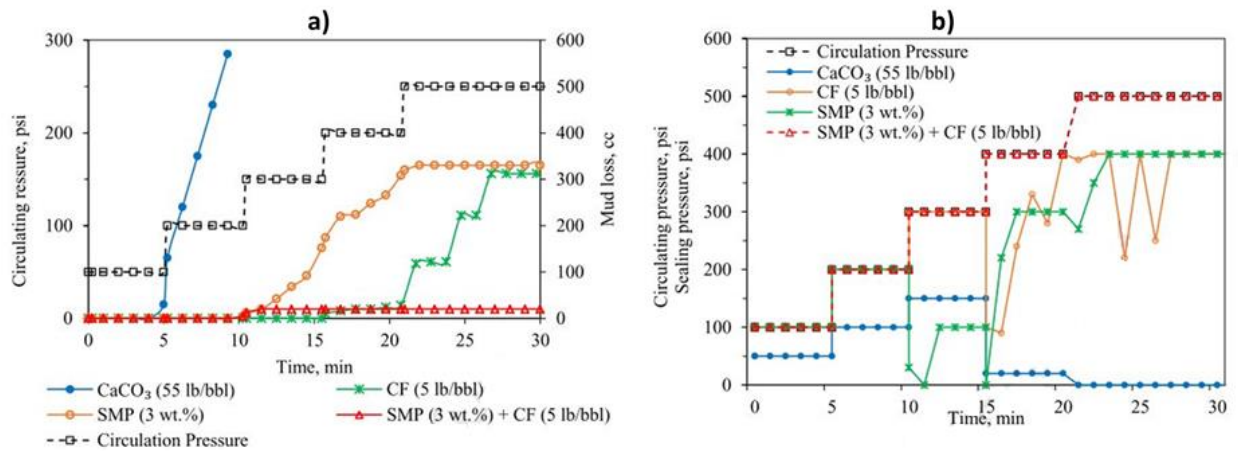


Figure 3.4: Sealing performance of SMP and other LCMs in 1000-micron fracture: a) mud loss and b) sealing pressure (Magzoub et al., 2021a).

For a successful application, formation type, lithology, mud properties, and LCM type and concentration should be considered before treating the lost circulation. Rheological properties play a vital role in loss prevention and treatment. They significantly affect wellbore hydraulics and LCM transportation. For instance, the uncontrolled increase in ECD may induce some fractures in the drilled formation, consequently increasing fluid losses and complicating the drilling operation (Wastu et al., 2019). Moreover, previous studies focused on evaluating the sealing efficiency of

SMP on a small laboratory scale without considering SMP transportation and its impact on fluid rheology and hydraulics.

Therefore, this work aims to study SMP activation, transportation, sealing efficiency, and its impact on mud rheology and wellbore hydraulics at high temperatures using a large-scale flow loop. A broad range of parameters is considered in this work, such as SMP concentration, annular velocity, inclination angle, and pipe rotational speed. Also, the SMP performance is compared with other conventional LCMs such as walnut, calcium carbonate, and cedar fiber. A detailed description of the material and methods used to conduct this work are presented in chapter 4.

Formation damage is one of the main disadvantages of lost circulation material. Formation damage is caused by the mud filtrate invasion and the filter cake formed on the well and inside the formation. Fine particles and mud filtrates invade the drilled formation and interact with formation rocks and fluids. These interactions alter the formation properties such as wettability, porosity, and permeability, reduce productivity, and cause other complications such as clay swelling. Filter cake formation is vital in drilling operations to minimize the mud invasion into the drilled formations. However, the formed filter is considered a barrier when starting the production, and it may also impact casing and cementing operations; therefore, the formed filter cake should be removed.

Several methods were developed to remove the formed filter cake depending on the filter cake composition and downhole conditions. The removal methods are either by mechanical means or chemical dissolution, while the latest is more common. Lost circulation material is added to the drilling mud to seal fractures and reduce the mud invasion. The LCM particles deposit on the fracture mouth and form a bridge to prevent mud losses. In this case, LCMs constitute the majority of filter cake compositions. Therefore, removal efficiency mainly depends on LCM solubility in the removal fluid.

The application of shape memory polymer in drilling operations is recent and has not been tried in the field. Developing an efficient removal method to dissolve this type of LCM is essential to ensure optimal cleaning. Conventionally, thermoset polymers are difficult to dissolve except when using powerful chemicals at HPHT conditions. Novel polymers with dynamic exchange reactions have been recently developed, enabling dissolution under mild conditions. The epoxy resin, which is the main component of SMP, can be dissolved by various organic solvents such as acetone and toluene. However, SMP is a cured resin that is hard and more challenging to dissolve than liquid resins. Kuang et al. (2018) proposed a solvent-assisted dynamic transesterification method to dissolve an anhydride-epoxy thermoset. The TBD-alcohol solution effectively broke the ester bond in the cured epoxy, leading to epoxy dissolution below 180 °C, as shown in Figure 3.5. Therefore, as a part of this work, we will conduct series of experiments to evaluate the SMP solubility in various solvents to optimize fluid formulations for cleaning SMP.

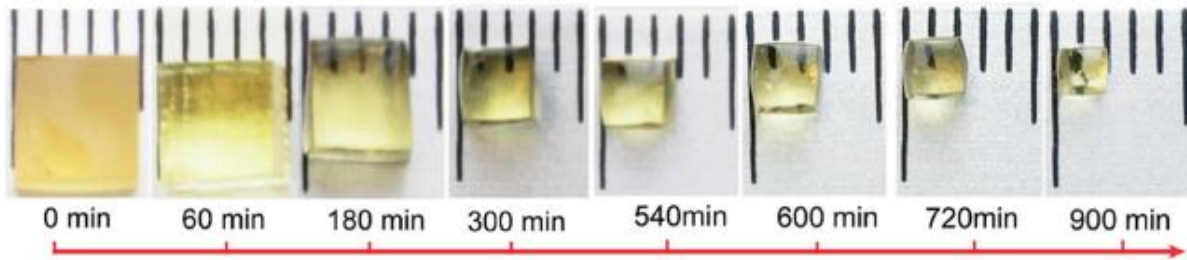


Figure 3.5: The change in cubic epoxy size soaked in 0.35 M TBD-EG at different times at 170°C (Kuang et al., 2018).

3.4 Temperature Constraints

High temperatures present formidable challenges to the drilling operations and complicate the lost circulation problem. Lost circulation materials are limited by their thermal resistance. When the temperature exceeds the thermal resistance, LCMs thermally degrade, which causes a failure in the lost circulation treatment. High temperature promotes the thermal degradation of polymeric additives and impacts the rheological properties of drilling fluids (Amani and Al-Jubouri, 2012a,

2012b; Avci and Mert, 2019). For instance, bentonite mud flocculation due to high temperature is often observed at temperatures above 250°F (Zilch et al., 1991).

The deterioration in rheological properties significantly impacts wellbore hydraulics and the suspension capability of drilling fluids. Consequently, the mud fails to suspend the drilled cuttings and LCM particles sufficiently. The accumulated solids increase the ECD, which may induce some fractures, increasing the mud losses. Moreover, the poor suspension affects the LCM sealing efficiency because the LCM particles are not homogeneously distributed, and less concentration will get to the fracture.

Moreover, the temperature limits the application of unconventional lost circulation methods. For instance, the crosslinking mechanism of polymeric gels is significantly impacted by the downhole temperature. Shape memory polymers do not activate below a specific temperature, and they melt when the downhole temperature exceeds their melting point. From the abovementioned, formation temperature is one of the essential parameters to consider when selecting and optimizing the LCM pill.

3.5 Recommended Particle Size Distribution

Particle size distribution is one of the essential properties that must be considered when optimizing the lost circulation material. The particle size significantly impacts the LCM sealing efficiency because small particles invade the formation and fail to seal the fracture. In contrast, large particles cannot get into the fracture to form the seal. Therefore, a combination of large and small particles is required for better sealing efficiency. Large particles form a bridge on the mouth of the fracture, and small particles fill the voids.

Different theories have been introduced to determine the proper size distribution of LCMs. The first theory of selecting the appropriate particle size is the ideal packing theory (IPT) presented

by Andreasen and Anderson (1930). The IPT relates the cumulative filtrate volume to the particle diameter by Equation 3.1.

$$\text{Cum Vol \%} \propto d^x \dots\dots\dots (3.1)$$

$x=1$ when particles are evenly distributed, $x < 1$ when particle distribution is shifted towards the smaller size, and $x > 1$ when the larger size dominates.

Another rule was proposed by Abrams, which suggests that the mean particle size of the LCM should be equal to or slightly greater than one-third of the average pore size of the filtration medium. Abrahams also suggested that the bridging solids should be at least 5 vol.% of the LCM pill. Abrahams' theory is widely used to select the optimum particle size; however, it only considers the mean particle size and does not look at the whole particle size distribution. Later, many theories were introduced, considering the full range of particle size. For example, Vickers et al. (2006) considered the whole particle size range to select the proper size of bridging materials (D_{10} , D_{25} , D_{50} , D_{75} , and D_{90}). They suggested that the optimal sealing occurs when:

- D_{10} is larger than the smallest pore throat
- D_{25} is equal to $1/7$ of the mean pore throat
- D_{50} is larger or equal to the $1/3$ of the mean pore throat
- D_{75} is less than $2/3$ of the largest pore throat
- D_{90} is equal to the maximum pore throat.

Moreover, several studies were performed to investigate the effect of LCM particle size on sealing efficiency. All these studies stressed on the importance of particle size distribution on mud losses and concluded that the wide range of LCM particle size yields better sealing performance. However, in some cases, the particles size is insignificant, especially in viscous pills where the sealing mechanism is entirely different.

3.6 Advanced Field Technologies

In addition to using LCMs, other drilling technologies can be used to avoid and mitigate lost circulation problems, such as underbalanced drilling (UBD), managed pressure drilling (MPD), and casing while drilling (CwD). Underbalanced drilling (UBD) is an old drilling method used drilling mud invasion into the drilled formation to preserve the permeability of producing formations and avoid any damage. The fundamental concept of UBD is to keep the hydrostatic mud pressure below the formation pressure by using lightweight muds such as air-based muds. Consequently, no mud cake will form, which minimizes the possibility of differential sticking and formation damage. Therefore, the formation fluids tend to flow into the wellbore then to the surface. This influx will be controlled and handled at the surface using surface equipment. Excellent examples of such equipment are drilling choke manifold (DCM), rotating control device (RDC), and multiphase separators.

UBD has been widely used to mitigate lost circulation problems in the past years. Several field case studies were reported in the literature addressing the success of using UBD in lost circulation prevention. For instance, in South Texas, lost circulation rates were up to 100 gpm, and using this technique helped significantly mitigate the problem and save a considerable cost and time. However, the high cost and technical limitations of this technique put more burden on the drilling operations. UBD costs 30% more than conventional drilling operations. Additional surface and downhole tools are required, and wellbore instability issues are also likely, especially in weak, high permeable, and fractured formations. Moreover, some safety concerns exist due to the difficulty of controlling the well, where the risk of kicks is higher than overbalanced drilling.

Managed pressure drilling (MPD) is a flexible and adaptive drilling process used to precisely control the mud pressure in the wellbore and annulus. Unlike conventional drilling, MPD does not require changing the mud system to meet any changes to the formation pressure. Instead,

the mud pressure is controlled by adjusting the backpressure applied from the surface. MPD is a quick and efficient technique used to prevent mud losses and reduce the NPT, especially in narrow mud-window drilling. MPD technique allows prompt intervention to any pressure variation observed during drilling operations. Therefore, MPD requires proper training to the rig crew and appropriate selection of the MPD method, depending on the encountered problem. Several case studies of using MPD were reported in the literature. For example, in the Gulf of Mexico, previous studies showed that the MPD technique could achieve a 25-33% reduction in the NPT. However, extra surface and subsurface tools are required for the MPD method, which is sometimes costly or unavailable on the site. Figure 3.6 illustrates the mud pressure profile in the case of underbalanced, conventional, and managed pressure drilling.

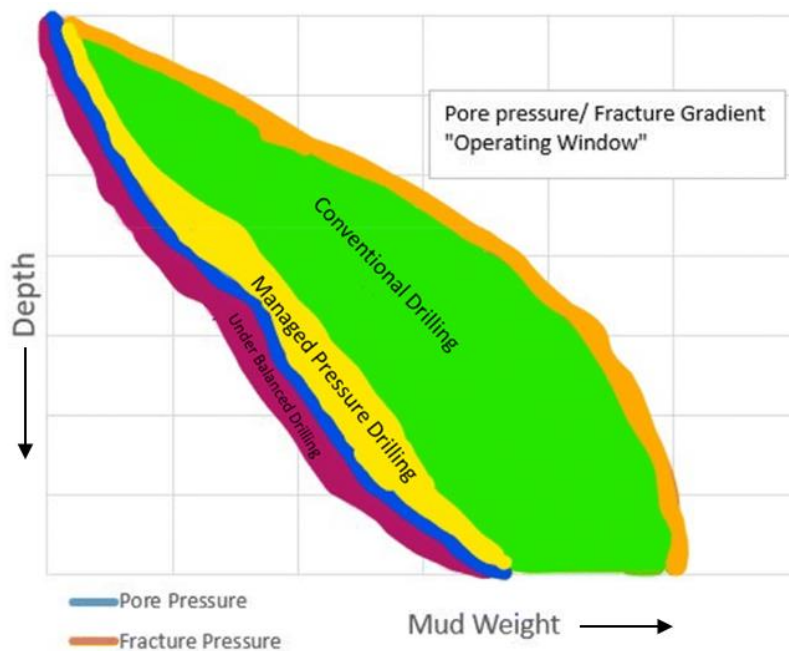


Figure 3.6: Illustration of the mud window in underbalanced, conventional, and managed pressure drilling (Huque et al., 2020).

Casing while drilling (CwD) is a revolutionary technology used in drilling operations to mitigate some of the drilling problems. These problems are mainly associated with the long exposure of drilled formation to the drilling fluids, such as lost circulation and formation damage.

CwD reduces the drilling time spent on pulling the drill pipe and running the casing. It also uses smaller rigs and less fuel thus, reducing the environmental footprint (Patel et al., 2019). Moreover, it helps form a filter cake with good characteristics due to the plastering effect resulting from the smaller annular space than in conventional drilling. To achieve such filter cake, the ratio between casing size and wellbore should range between 0.75 to 0.9 (Karimi et al., 2011).

The concept of CwD lays on using a standard casing string as drill pipe to transmit rotation to the drill bit and circulate drilling mud. The used casing can be utilized as a liner or a full-length casing string up to the surface. CwD is classified into four types: CwD with a retrievable system, CwD with a non-retrievable system, liner drilling with a retrievable system, and liner drilling with a non-retrievable system (Figure 3.7).

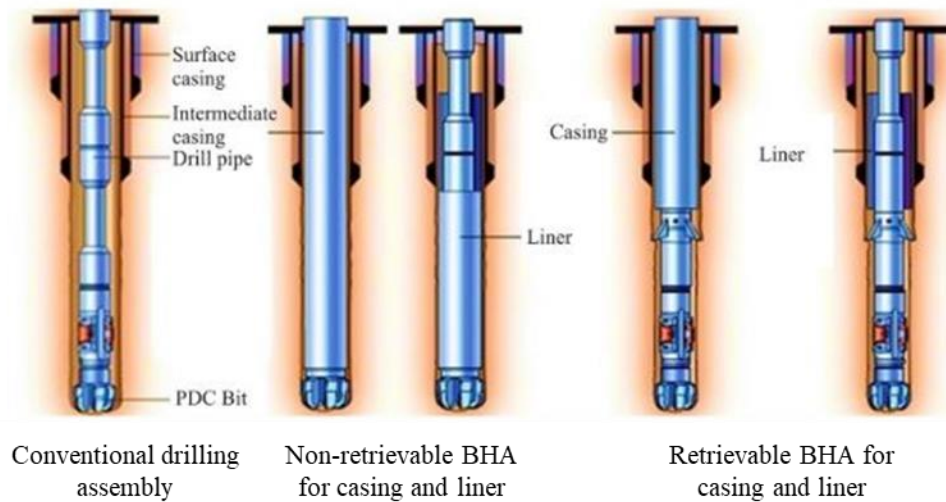


Figure 3.7: Types of CwD systems (Patel et al., 2019).

Although CwD offers many benefits to the drilling operation and improves the filter cake properties, as reported in many cases, many challenges are faced when using CwD technology. The large casing size requires higher torque to rotate the casing string than drill pipe, and the smaller annular space makes it challenging to manage wellbore hydraulics, especially in deep wells. If the drill bit is not correctly selected to complete drilling up to the casing depth, the whole

casing string must be retrieved to change the bit, which significantly increases the NPT. Additionally, fatigue failure is a common problem with the casing connections, particularly in high deviated wells. Therefore, some analyses must be done before drilling operation to determine the safe rotational speed. Moreover, the high cost of manufacturing drilling rig components significantly impacts the feasibility of CwD technology.

3.7 Current Research Gap

Despite the advancements in lost circulation materials, more research is still needed to overcome the limitations of conventional lost circulation materials. Due to particle size limitations, conventional LCMs fail to seal large and complex fracture networks. When large particles are used, difficulty in mud pumping, increased ECD, and plugging downhole equipment (such as LWD and MWD) are likely. The large LCM particles also put some limitations on bit nozzles selection. LCM particles also cause formation damage when they invade the producing formation. Moreover, some health and environmental impacts are associated with lost circulation materials.

Alternatively, researchers proposed other advanced materials for lost circulation treatment, such as LCM blends, nanoparticles, polymeric gels, and encapsulated pills. However, the optimization of this material is challenging, and the high manufacturing cost and associated environmental concerns significantly limit their use. On the other hand, advanced drilling technologies (UBD, CwD, MPD) also have limitations. For instance, these technologies are not recommended in drilling exploration wells, where information about drilled formations and downhole conditions is inadequate. Also, fatigue problems in casing connections are common in the casing while drilling operations.

The shape memory polymer is one of the recent advancements in lost circulation treatment, and few studies have been conducted to evaluate such material in treating lost circulation. All the conducted studies focused on testing SMP sealing efficiency using small-scale laboratory

equipment without considering SMP transportation and its impact on fluid rheology and hydraulics. The findings of previous studies were promising; however, the small-scale laboratory equipment: i) does not simulate the actual field conditions and dimensions, ii) is limited with particle size, and iii) may yield inaccurate results when large particles are tested because large particles may block the tubes and valve openings. Therefore, further research studies are required to evaluate SMP sealing efficiency on a larger scale to optimize the drilling fluid formulations for field deployment.

Moreover, for a successful application, formation type, lithology, mud properties, and LCM type and concentration should be considered before treating the lost circulation. Rheological properties play a vital role in loss prevention and treatment. They significantly affect wellbore hydraulics and LCM transportation. For instance, the uncontrolled increase in ECD may induce some fractures in the drilled formation, consequently increasing fluid losses and complicating the drilling operation (Wastu et al., 2019). Inefficient LCM transportation impact LCM placement and sealing efficiency because less LCM concentration would get to the fracture, and accumulated LCM particles alter wellbore hydraulics. They also cause other complications, such as increased ECD and pipe sticking. Furthermore, SMP activation when mixed with drilling mud was not thoroughly studied and visually confirmed in previous studies.

Thus, the evaluation of shape memory polymer as lost circulation material is still in the early stages. More research is required to study SMP activation, transportation, sealing efficiency, and its impact on mud rheology and wellbore hydraulics at high temperatures using large-scale experimental setups. A more comprehensive evaluation of such advanced materials would help optimize the LCM mud formulation to yield more successful results in field operations.

Chapter 4: Laboratory Experimental Methods

This chapter describes the experiments performed to evaluate the shape memory polymer for treating lost circulation events in geothermal formations. The experimental setup, experimental parameters, design of experiments, experimental methods, and laboratory procedures are discussed. This chapter also contains the methodology followed to develop the computational fluid dynamics (CFD) model used to upscale the experimental results and predict the SMP transportation in the annulus at different conditions and field dimensions.

4.1 Design of Experiments (DoE)

The smart lost circulation material used in this study is a thermoset shape memory polymer (SMP) that activates at temperatures above 149°C (300°F). This work is a comprehensive experimental evaluation of the smart LCM by studying rheology, wellbore hydraulics, activation process, sealing efficiency, and LCM dispersion and transportation. The smart LCM was added to a base drilling mud designed in the lab using rheological screening for several drilling additives. The smart LCM was added to the base fluid in different concentrations to study the effect of concentration and other parameters on the LCM performance. SMP performance was also compared with three other conventional lost circulation materials commonly used in field operations. These LCMs are calcium carbonate, cedar fiber, and walnut. The experimental evaluation was mainly conducted in the built high-temperature flow loop discussed in Section 4.2, and some laboratory methods were used to characterize the different LCMs. The experimental study was conducted mainly in six phases. Table 4.1 lists all experimental stages and their objectives. These phases and experimental methods are discussed in detail in the subsequent sections.

Table 4.1: Experimental phases and methodology

Phase	Objective	Methodology
Phase -1	Material selection and base drilling mud preparation	Literature review, rheological screening
Phase -2	Lost circulation material characterization	Elemental compositional analysis (EDS), morphology (SEM), particle size distribution
Phase -3	Study the smart LCM activation process	Flow loop experiments, visualization data analysis, image and video processing, particle size distribution
Phase -4	Study the pipe and annular flow of LCM muds	Rheology, wellbore hydraulics, flow loop experiments, data analysis
Phase -5	Fracture sealing experiments	Fractured-discs preparation, dynamic filtration using the flow loop setup
Phase -6	Post experiment analyses	Computational fluid dynamics simulation study

The primary data acquired in the flow loop experiments were differential pressure, pressure, temperature, flow rate, pipe rotational speed, and visualization data obtained using high-speed cameras. The acquired data were processed and analyzed to obtain the rheological behavior, wellbore hydraulics, activation process, LCM transportation, and sealing efficiency. The flow loop experiments considered a broad range of experimental parameters. These parameters are LCM type, LCM concentration, inclination angle, flow rate, pipe rotational speed, fracture size, and fracture complexity. For fracture sealing experiments, the main parameters used to evaluate the LCM sealing efficiency are flow rate and differential pressure built across the fractured discs. Figure 4.1 shows the detailed plan of this study.

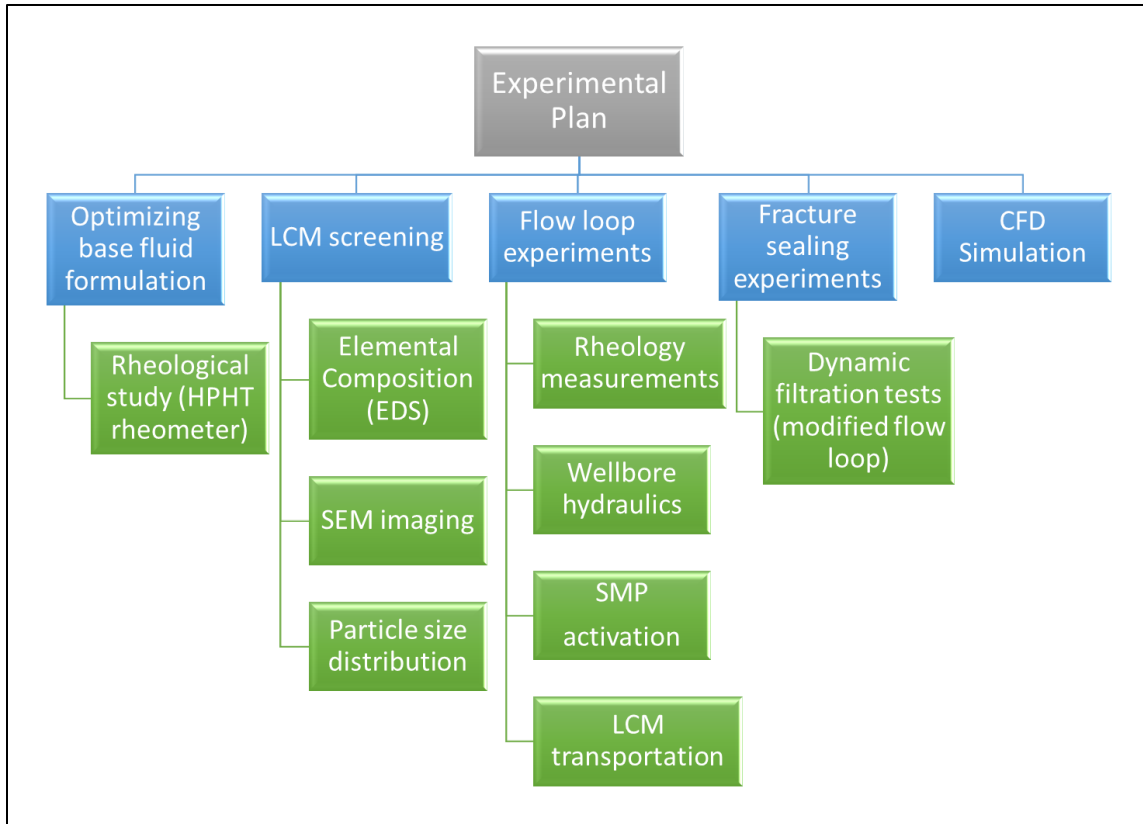


Figure 4.1: The detailed plan of this study.

4.2 Experimental Setup Description

Testing LCM materials is usually conducted using small laboratory equipment in static or dynamic conditions, such as static and dynamic filtration setups, plugging permeability apparatus, and dynamic filtration drilling simulator. However, this laboratory equipment does not fully represent the actual field conditions, and it also fails when large particles are used. Solid particles may clog the tubes and valve openings, leading to inaccurate results and failure in field operations. In this study, a novel experimental setup was built to evaluate lost circulation material in large-scale and high-temperature dynamic conditions to avoid the limitations of existing laboratory techniques. The experimental setup is a large-scale flow loop consisting of five systems: mud mixing and circulation system, heating system, rheology measurement system, main test section, and data acquisition system. The flow loop components are pressure and temperature rated up to 150 psi

and 350°F. Figure 4.2 illustrates the setup schematic design and main parts, and each system is described in detail in the subsequent sections.

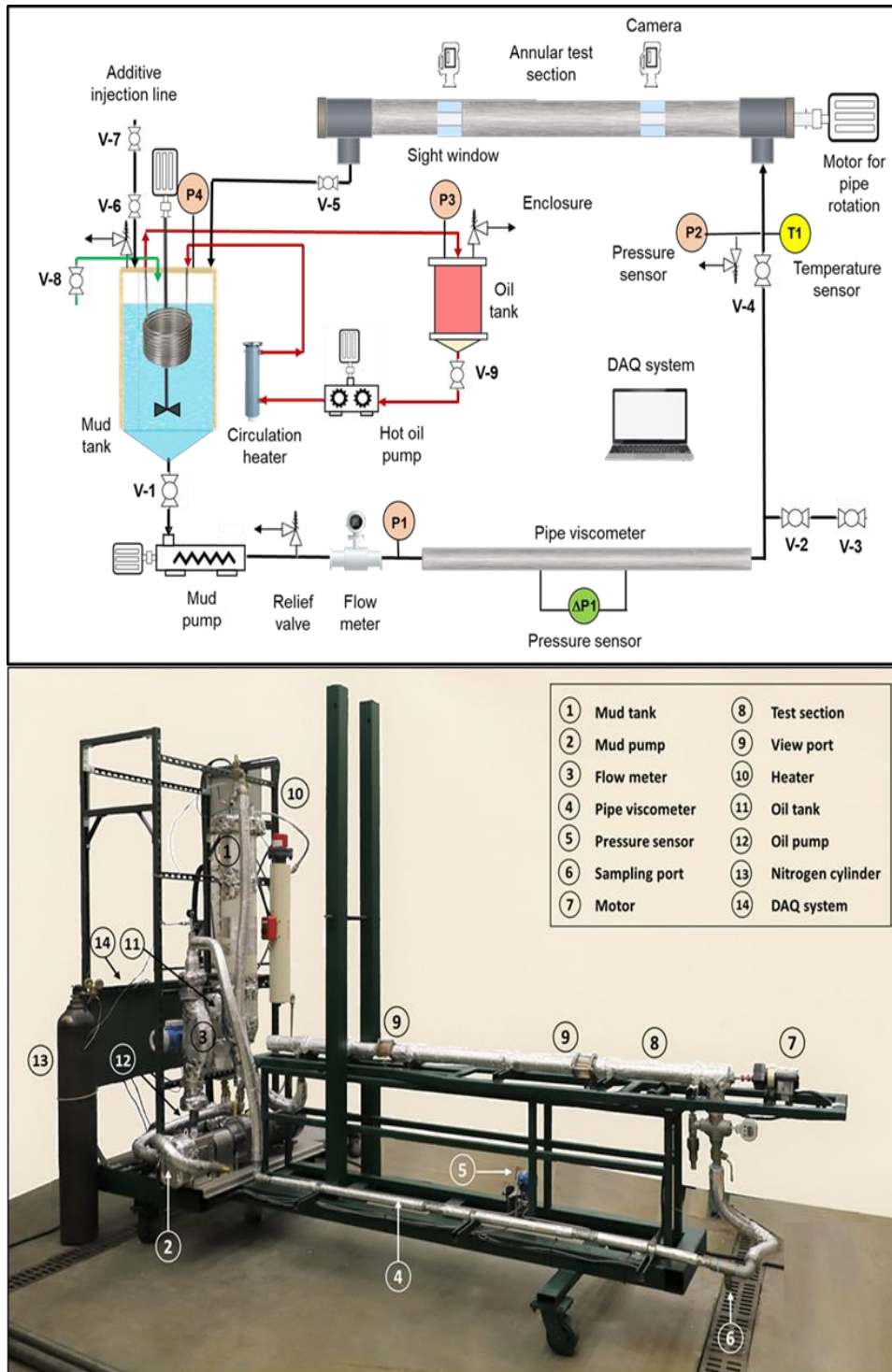


Figure 4.2: Schematic design and components of the high-temperature flow loop.

4.2.1 Mud Preparation and Circulation System

The function of the mud preparation and circulation system is to mix the mud sample and circulate it through the flow loop setup. This system consists of a stainless-steel mud tank with a capacity of 10.5-gal. A variable-speed agitator was installed on the top to mix the mud and keep the fluid homogeneous throughout the experiment. The tank also has an additive injection line installed at the top to add drilling fluid additives and lost circulation materials. The circulations system also consists of a lobe mud pump to circulate the fluid sample at various flow rates, ranging from 0 to 40 gpm, with a maximum differential pressure of 150 psi. The mud pump can withstand solids of up to 18 mm with a maximum concentration of 40 wt.%. The pump was customized with this unique design to test solid-loaded drilling mud with minimal issues. 2-inch stainless-steel flexible pipes were added to connect the flow loop components and allow mud circulation. Additionally, several control valves were installed to control the flow direction and help operate and clean the system, while relief valves were added to the system for safety measures to safely operate the experimental setup and protect its main components.

4.2.2 Heating System

The heating system was designed to heat the drilling mud and maintain the desired testing temperature throughout the experiment. The main components of this system are:

- A stainless-steel oil tank with a capacity of 7 gallons was added to contain the heating oil with a temperature and pressure of 650°F and 200 psi, respectively.
- A relief valve was installed on the top of the oil tank to avoid overpressure while heating.
- A control valve was added to the oil tank to control the oil flow.

- A pump to circulate the heating oil at various flow rates (maximum of 85 gpm) and temperature of 650°F. The oil circulation rate can be controlled to optimize the heating rate and final mud temperature.
- A circulation heater with a power of 6000 W and a maximum temperature of 550°F was added to heat the oil.
- The hot oil is circulated inside the mud tank through a stainless-steel coil, where the heat is transferred from the hot oil to the mud.
- Pressure and temperature sensors were added to the flow loop to monitor the fluid pressure and temperature.

The heating system is a closed system, where the oil is circulated through the oil tank, heater, and stainless-steel coil. The heat is transferred from the hot oil to the mud, and then the oil returns to the oil tank at a lower temperature, where it is circulated to the heater again. The heating rate is optimized by controlling the heater temperature and circulation rate. All the flow loop systems were thermally insulated to minimize the heat losses across the experimental setup and maintain the testing temperature.

4.2.3 Rheology Measurement System

The primary function of this system is to measure the flow characteristics of drilling mud and investigate the lost circulation material effect on mud rheological properties under different conditions. The measured rheological properties are also used to analyze the wellbore hydraulic parameters. Wellbore hydraulic parameters are essential in designing drilling operations, and they impact LCM transportation in the wellbore. The rheology measurement system consists of a stainless-steel pipe viscometer with a diameter of 1 inch and a length of 9 ft. The pipe viscometer helps avoid the limitations of rotary viscometers commonly used to test the rheological properties

of drilling fluids containing large solid particles. A differential pressure transmitter (DP cell) was connected to the pipe viscometer through two capillary lines. The DP cell measures the differential pressure across the pipe viscometer, which can be used to determine the mud rheological behavior. To eliminate the end effects, the capillary lines are 3 ft apart with a 3 to 4 ft distance from the viscometer's inlet and outlet. The capillary tubes were installed precisely at the same level and distance from the DP cell to ensure accurate differential pressure readings. The DP cell has a measurement range of -5 to 5 kPa with an accuracy of $\pm 0.05\%$. This system also consists of a flow meter to measure the mud circulation rate. The differential pressure value corresponding to each flow rate was recorded and used to obtain the flow characteristics and rheological properties of LCM mud samples. The detailed procedure of the analysis is discussed in more detail in Section 4.4.4.

4.2.4 Main Test Section

The main test section is two concentric stainless-steel pipes with a diameter of 1" and 2" to simulate the drilling mud circulation in the annulus. The inner pipe was attached to a motor to simulate the drill pipe rotation in the range of 0 to 150 RPM, while the outer pipe represents the drilled hole. The outer pipe was designed to have two viewports to visualize the annular flow with the aid of two high-speed cameras. The sight glass on the view ports can withstand a maximum pressure of 150 psi at 450°F. The total length of the main test section is around 10 ft, and it is mounted on the moving part of the experimental setup frame. The moving part allows changing the inclination from 45° up to 90° (from vertical) to simulate the fluid flow in inclined and horizontal wells. The inclination angle can be adjusted by lifting the downstream side of the moving part using an overhead crane. At the same time, safety pins were added to the setup to secure the test section at

the desired inclination angle. The recorded videos and images were analyzed to study the SMP activation, LCM transportation, and mud flocculation.

In the second phase of experiments, the flow loop design was modified to conduct the fracture sealing experiments and evaluate the sealing efficiency of different LCMs. The modifications were mainly done on the main test section by removing the inner pipe from the system and installing the fractured disc. The fractured disc was installed inside the viewport to enable real-time visualization of the plugging process. Several fractured discs were designed using the Tinker Cad software. The fracture disc was designed as a hollow cylinder containing a fractured disc in the middle perpendicular to the flow direction. The fractured disc has an outer diameter of 6.63 cm to fit inside the viewport. The disc design has lips at both ends to secure the disc inside the viewport. It also has openings on the sides to detect the plugging process. Different disc designs were created by changing the fracture width and complexity to evaluate the sealing efficiency at different fracture sizes. These sizes are 2000 and 3000 microns, and the third disc was designed to contain a complex fracture network with 2000 microns in width. The fractured discs were prepared by a 3D printer using carbon fiber material. The printing material can withstand a maximum testing temperature of 350°F.

Moreover, a differential pressure transmitter was added to the main test section to determine the sealing efficiency by monitoring the frictional pressure change across the fracture throughout the experiments. The differential pressure transmitter has a high-pressure range that can measure maximum differential pressure of 30 psi. The capillary lines of the DP cell were installed on both ends of the main test section. Figure 4.3 illustrates the schematic design of the fractured disc and the modified test section.

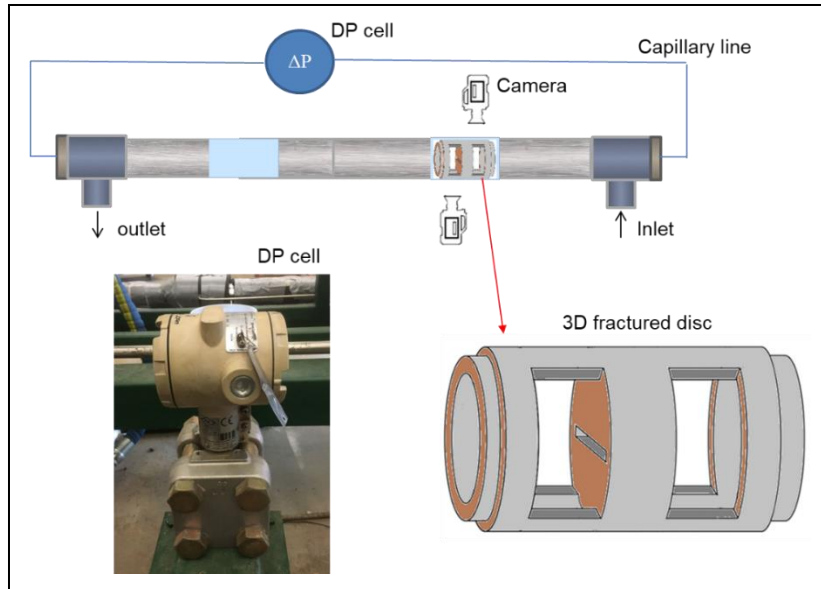


Figure 4.3: Schematic design of the modified main test section for fracture sealing experiments.

4.2.5 Data Acquisition and Control System

This system is mainly used to start and stop the experiments, control the experimental parameters, and monitor and record the obtained data throughout the flow loop experiments. The obtained data are pressure, temperature, flow rate, differential pressure, density, photos, and videos. The data acquisition computer was equipped with a multi-channel data acquisition card (DAQ). All measurement devices were connected to the DAQ card. The measured data was converted into digital numeric values and then sent to, processed, and displayed on the PC monitor. Visual basic-based software was developed to process and record the measured data. The software was also designed to send specific voltage to the variable frequency drives (VFDs) through the DAQ card to start/stop the experiment and control the mud and oil circulation rate. The developed software can also ramp up/down the mud circulation rate in a previously set sequence to conduct the rheology measurements. Some other safety features were added to the software to stop the oil pump and heater when the temperature exceeds the testing temperature by a particular margin. Table 4.2 lists the limitations of the developed flow loop setup.

Table 4.2: Range of experimental parameters of the flow loop setup

Parameter	Range
Temperature	21-160°C (70-175°F)
Pressure	1,035 KPa (150 psi)
Inclination angle (from vertical)	45°-90°
Flow rate	0-2.52 x10 ⁻³ m ³ /s (0-40 gpm)
Pipe rotational speed	0-150 RPM

4.3 Testing and Calibrating the Flow Loop Setup

4.3.1 Heating and Pressure Testing

Pressure testing was performed to ensure that the experimental setup worked efficiently without any leakage. The pressure test was conducted in two stages; 1) Test the heating system lines and tank using nitrogen and heating oil, and 2) Test the mud tank, test section, pipe viscometer, and flowlines using water and nitrogen. The test was performed in two stages because the setup is divided into two separate systems. First, the heating system was tested with nitrogen starting with the oil tank. The tank was isolated from the other system components by closing the valves. The tank was tested until 100 psi, and the pressure was monitored for more than 10 hrs using the data acquisition system and pressure gauges. Then the test was conducted on the whole heating system by following the same procedure. After the heating system passed the pressure test with nitrogen, the tank was filled and pressure tested with heating oil. Oil was circulated throughout the heating system at different flow rates using the oil pump, and no leakage was observed in the heating system. Afterward, the pressure test was performed on the mud tank and test section using nitrogen gas, following the same procedure. The pressure test was repeated with water by running the mud pump at various flow rates. The flow loop system passed the pressure testing successfully, and no leakage was observed.

The heating system was then tested by running different experiments with water to check the heating efficiency and optimize the insulation. The heating test was performed in three stages: without insulation, one insulation layer, and two insulation layers. Without insulation, the system showed a low heating rate of 39.5°F/hr, and due to the high temperature losses and safety concerns, the heating was stopped after the fluid temperature reached around 200°F. Adding one layer of insulation improved the heating rate by 26.8%, with a rate of 50.1°F/hr. The mud temperature reached 287°F in 4 hrs, and the heating was stopped for safety because the surface temperature of the system was higher than 150°F. Then, another insulation layer was added to the whole system, and the test was repeated. After adding the second layer of insulation, the heating rate was further increased by 26.1% to reach 63.2 °F/hr heating rate. In around 3 hrs, the fluid temperature reached 300°F, and the test was stopped after reaching 320°F. The surface temperature of the insulation was below 100°F, which makes the system efficient and safe to operate.

After the flow loop was modified for fracture sealing experiments, the setup was heated using a water-based fluid to test the thermal stability of the 3D printed discs. The base fluid was heated to the maximum testing temperature (350°F). The infill printing density was varied to attain a stable fractured disc design. The infill printing density represents how much material the disc contains, and the remaining percent is pore space. With an infill printing density of 50%, the fractured disc successfully maintained its stability up to 350°F, and the disc was used for several experiments without any deformation.

4.3.2 Setup Calibration

First, all flow loop instruments were tested by checking the input and output signals to ensure all devices were functional and appropriately connected to the DAQ card. These instruments are temperature sensors, pressure sensors, flow meters, and differential pressure

transmitters. The output signals were calibrated to ensure accurate results. Afterward, the pipe viscometer's accuracy was validated by conducting rheology experiments using water-based polyanionic cellulose (PAC-R) solutions at two various concentrations, 0.8 and 1.5 wt.% PAC-R. The rheology measurements were performed at 120 °F and atmospheric pressure. The flow rate was varied from 2 to 36 gpm using the mud pump, and the differential pressure readings were recorded with the flow rate. These measurements were converted into shear stress and shear rate, and the flow curve was constructed for each testing fluid. The results were compared with a rotational viscometer (Fann-35A) for validation. By excluding the turbulence data, the pipe viscometer data showed a good agreement with the rotational viscometer, indicating that the pipe viscometer would yield accurate rheology measurements (Figure 4.4).

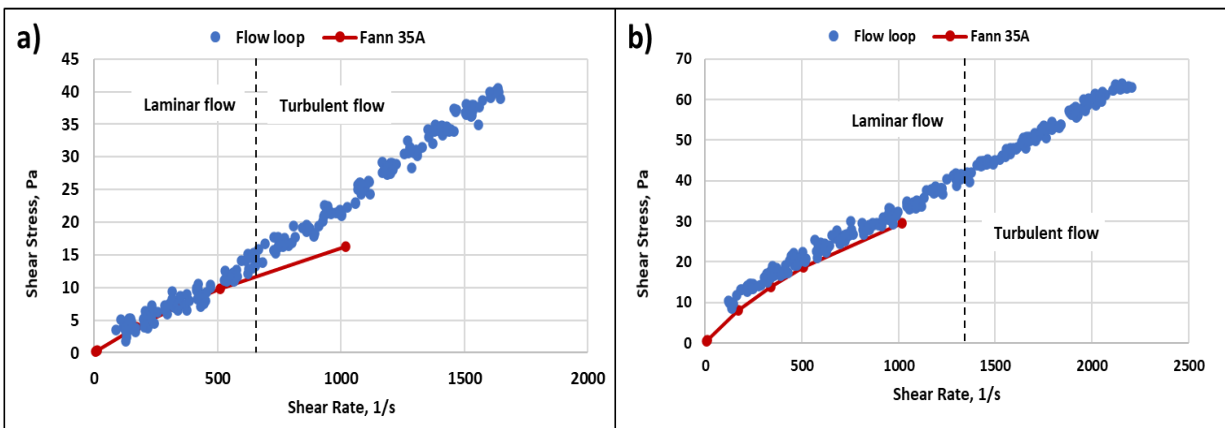


Figure 4.4: Calibration data for PAC-R solution at 120 °F: a) 0.8 wt.% and b) 1.5 wt.%.

4.4 Experimental Methods and Procedures


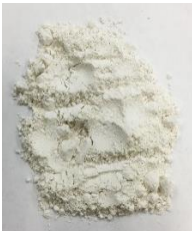


4.4.1 Material Selection, Preparation, and Characterization

This study evaluates a smart polymer as a lost circulation material by studying its activation process, transportation, sealing efficiency, and its effect on mud rheology and wellbore hydraulics. The smart LCM is a thermoset shape memory polymer (SMP) programmed to activate by formation temperature (at 300°F) and regain its original shape and size. Once SMP is thermally

activated, the particle size increases, which helps seal the large fractures and stop mud losses with minimal risk of plugging the downhole tools. The shape memory polymer was prepared using 93 wt.% tris[2-(acryloyloxy) ethyl] isocyanurate monomer and 7 wt.% photo-initiator diphenyl (2,4,6-trimethyl benzoyl) phosphine oxide. After mixing, the resin was cured using ultraviolet (UV) light and post thermal curing to ensure a high conversion rate from monomers to a fully cured polymer structure. The cured polymer was characterized by measuring the heat flow, absorption, heat flow, conversion rate, stress recovery, compressive strength, and viscoelastic properties to optimize the preparation process. After the optimum polymer structure was achieved, the resin was poured into cylindrical molds and left to harden. Afterward, the hardened polymer was programmed by applying heat and load, as described in Figure 3.3 in Section 3.3.3. then the deformed shape was ground to produce the lost circulation material with the required particle size distribution (840-2,360 μm).

In this experimental study, the SMP performance was also compared with other conventional lost circulation materials. These commercial LCMs are calcium carbonate, walnut, and cedar fiber. These additives were obtained from a service company. SMP and other LCMs were characterized in the laboratory by measuring the particle size distribution, elemental composition, and morphological properties. The particle size distribution was measured by a particle size analyzer using the laser diffraction technique. The surface characteristics and elemental composition were determined using scanning electron microscopy (SEM) and energy-dispersive X-ray spectroscopy (EDS) techniques. Table 4.3 summarizes the main properties of the LCMs used in this study, while, Figure 4.5 shows their particle size distribution.

Table 4.3: Properties of used lost circulation materials

Material	Appearance	Density, kg/m ³	Particle size
Shape memory polymer (SMP)	 Granular	950	840-2,360 μm (Average of ~1,400 μm)
Calcium carbonate	 Granular	2,710	Average of 88.2 μm
Walnut	 Granular	1,300	840-2,360 μm (Average of ~1,400 μm)
Cedar fiber	 Fibrous	1,700	53-2,360 μm (Average of 550 μm)

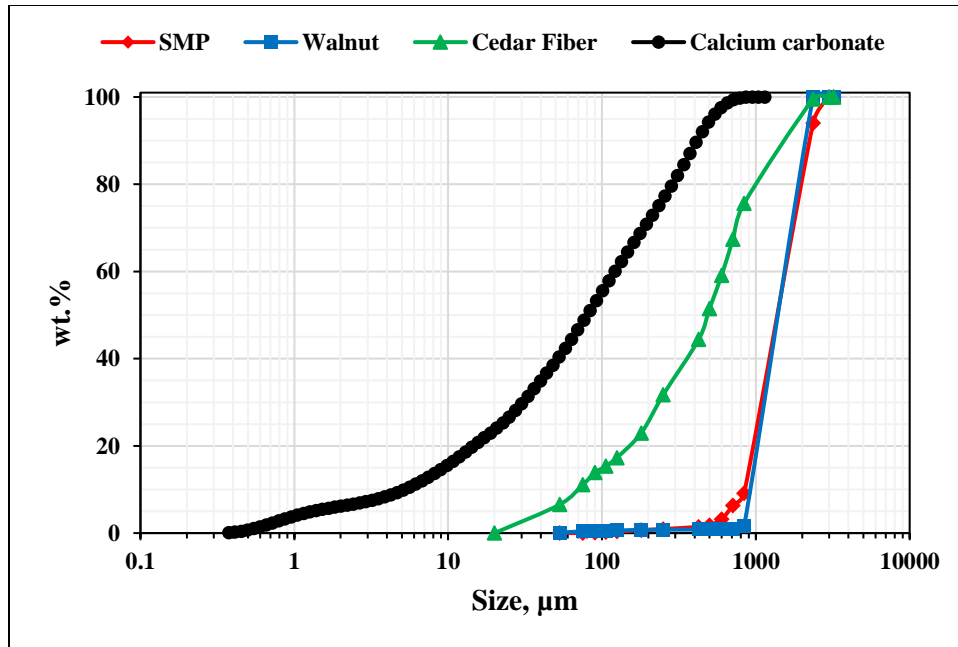


Figure 4.5: Particle size distribution of used LCMs.

4.4.2 Rheological Screening of the Base Fluid

This screening aims to evaluate different drilling fluid additives to be used as viscosifier for the base fluid. Viscosifiers are used to maintain the rheological properties of the drilling fluid system to efficiently suspend the drilled cuttings and solid particles within the fluid system. Before performing flow loop experiments, a set of rheology experiments was conducted to optimize the base drilling fluid formula on a small scale. Several additives were evaluated by measuring the rheological properties at high-temperature conditions using an HPHT rheometer. These additives are low viscosity polyanionic cellulose (PAC-L), regular viscosity polyanionic cellulose (PAC-R), xanthan gum polymer (XC), hydroxyethyl cellulose (HEC), and other synthetic polymers such as THERMA-CHEK, POLYAC PLUS, and THERMA-VIS. The additives were obtained from a service company. The screening criteria are i) high thermal stability (above 150°C) to efficiently suspend the LCM particles, and ii) clear appearance to allow flow visualization. The tested

additives are commonly used in the industry as primary viscosifiers, secondary viscosifiers, and/or fluid loss control additives. The properties of these additives are shown in Table 4.4.

Table 4.4: Properties of the tested additives

Additive	Appearance	Specific gravity	Thermal stability, °F	Main uses	Recommended concentration, lb/bbl
Xanthan gum	Dispersible beige powder	1.5	250	Viscosifier	1.0-2.0
HEC	White to light tan powder	1.38-1.4	205-210	Viscosifier and filtration control	2-7
THERMA-VIS	White powder	1.0	700	Viscosifier	1.0-4.0
PAC-R	White or tan powder	0.8	300	Filtration control and secondary Viscosifier	0.5-2.0
PAC-L	White or tan powder	0.8	300	Filtration control	0.5-3.0
POLYAC PLUS	White granular powder	0.8	400	Filtration control	0.25-1.0 (fresh water) 1.0-3.0 (salt water)
THERMA-CHEK	White or cream powder	1.32	400	Filtration control and secondary viscosifier	1.0-3.0 (fresh water) 4.0-8.0 (salt water)

Various fluid samples were mixed by adding the additives individually to tap water in different concentrations (1 to 5 lb/bbl). The samples were prepared at room temperature using a variable-speed mixer and left for 20-24 hrs to hydrate to ensure consistent results. Then, a 50-mL sample was taken from each fluid formulation and poured into the sample cup to measure the rheological properties. The experiments were conducted at 400 psi to prevent evaporation. The

first rheology experiments were performed at a constant shear rate of 170 1/s, while the temperature was increased gradually from room temperature (21°C) to 190 °C (375°F) to evaluate the thermal stability of the fluid samples. In the second phase, the thermal stability of the stable additives was evaluated with time by running the experiment at 175 °C for 3-4 hrs to ensure that the drilling mud was stable throughout the flow loop experiments. The experimental conditions are summarized in Table 4.5.

Table 4.5: The experimental parameters of the rheology screening

Parameter	Range
Base fluid	Tap water
Temperature	21-190°C (70-375 °F)
Pressure	400 psi
Shear rate	170 1/s
Concentration	1-5 lb/bbl

4.4.3 LCM Mud Preparation

To conduct the flow loop experiments, several drilling mud samples were prepared by mixing the base fluid with SMP and other conventional lost circulation materials. A total fluid volume of 10.5 gallons was mixed in the mud tank for every experiment. During mud preparation, the mud tank was isolated from the setup by closing the control valve at the bottom of the tank. The mud components were added separately to the tank, starting with the water and mud additives. Each additive was added slowly and mixed for a specific time, depending on the fluid formulation. The mud agitator was run throughout the mixing process and experiments to maintain the fluid homogeneity. After preparation, the mud was left in the tank for 20-24 hrs to hydrate and ensure consistent results. The lost circulation material was added to the tank during the experiments at the

desired testing temperature through the additive injection line. The additive injection line remained closed throughout the experiment to prevent mud evaporation.

4.4.4 Rheology Experiments and Wellbore Hydraulics Analyses

The primary objective of these experiments was to evaluate the effect of SMP and other LCMs on the rheological properties and wellbore hydraulic parameters. Rheology experiments were conducted at different temperatures (21-160°C) using the pipe viscometer in the flow loop. The mud circulation rate gradually increased from 0 to 40 gpm, and the corresponding differential pressure across the pipe viscometer was recorded. Each flow rate was kept for a few minutes to ensure stable and accurate readings. The measured flow rate and differential pressure were used to determine the rheology model that best described the drilling mud and obtain the flow characteristics of each mud sample using the following procedure:

- i. The flow rate (Q) and differential pressure (ΔP) data, obtained from the flow meter and pipe viscometer, were converted from gallon per minute (gpm) and inch water (in H₂O) to cubic meter per second (m³/s) and pascal (Pa). The differential pressure measurements were taken after 1.2 m from the inlet and before 0.9 m from the outlet of the pipe viscometer. Therefore, the analysis did not consider the correction for the end effect.
- ii. The wall shear stress (τ_w) and nominal Newtonian wall shear rate ($\dot{\gamma}_{nom}$) were obtained using the viscometer diameter (D= 0.02286 m) and length (L= 0.9144 m) by applying Equations 4.1 & 4.2.

$$\tau_w = \frac{D \Delta P}{4 L} \dots \dots \dots (4.1)$$

$$\dot{\gamma}_{nom} = \frac{8V}{D} \dots \dots \dots (4.2)$$

- iii. τ_w and $\dot{\gamma}_{nom}$ data was plotted on a logarithmic scale and fitted with a straight line to check for the Power-law model's applicability. The consistency (K) and flow index (n) Were obtained from the curve fitting. Consistency corresponds to the intercept with the y-axis, while the flow index is the slope.
- iv. Fluid properties and n data were used to plot the laminar flow limit line and check the laminar flow for all the data points. The points falling on or to the right of the laminar flow limit line correspond to the turbulent flow. The turbulent flow data were excluded from the analysis. Equation 4.3 was used to plot the laminar flow limit line for power-law fluids (Alderman and Pugh, 2004).

$$\tau_c = \frac{\rho D^2}{8} \left[\frac{n}{404} \frac{\left(\frac{1+3n}{4n}\right)}{(n+2)^{\frac{(n+2)}{(n+1)}}} \right] \left[\frac{8V}{D} \right]^2 \dots \dots (4.3)$$

- v. Another method was also used to check for laminar flow to validate the results. Fanning friction factor (f) and the generalized Reynolds number (Re) were calculated for the laminar and turbulent flow data using Equations 4.4-4.6 and plotted on a log-log scale. The transition from laminar to turbulent was detected when the points deviated from the straight line. The deviated points correspond to the turbulent flow.

$$f = \frac{\tau_w}{\frac{1}{2} \rho v^2} \dots \dots \dots (4.4)$$

$$Re = \frac{8\rho\bar{v}^2}{K\dot{\gamma}_w^n} \dots \dots \dots (4.5)$$

where,

$$\dot{\gamma}_w = \frac{3n+1}{4n} \dot{\gamma}_{nom} \dots \dots \dots (4.6)$$

vi. After excluding the turbulent data, the wall shear stress (τ_w) was plotted against the nominal Newtonian wall shear rate ($\dot{\gamma}_{nom}$) on a logarithmic scale. The data was fitted, and the correct K and n were determined from the curve fitting, as discussed in step (iii). K and n were then used to calculate the shear stress (τ) at different shear rates ($\dot{\gamma}$) using the Power-law model (Equation 4.7). The calculated shear stress was plotted against the shear rate to construct the flow curve for each mud sample. The flow curve was established for shear rates ranging from 0.1 to 1000 1/s.

$$\tau = K\dot{\gamma}^n \dots \dots \dots (4.7)$$

vii. K and n were used to calculate the apparent viscosity at different shear rates to compare the performance of SMP with other LCMs. The apparent viscosity (μ_a) was determined using Equation 4.8.

$$\mu_a = K\dot{\gamma}^{n-1} \dots \dots \dots (4.8)$$

4.4.5 SMP Activation and LCM Transportation

4.4.5.1 SMP Activation

The shape memory polymer used in this study is a smart lost circulation material programmed to activate by formation temperature above 149°C. Once SMP is activated, it restores its original shape, and its particle size increases to seal large and complex fractures in geothermal formations effectively. In this part of the experiments, the activation process was studied by visualizing the annular flow. The viewport and high-speed camera were utilized to monitor the SMP particles. Two different experiments were conducted at 21°C and 160°C to detect the change in SMP particles with temperature. SMP was added to the mud at these two temperatures with a concentration of 1.0 wt.%. The experiments were run at a horizontal inclination and low circulation

rate to detect the particle size change easily. The captured videos were processed and analyzed using frame-by-frame video processing techniques. The particle size was then determined at both temperatures to confirm and evaluate the SMP activation process.

4.4.5.2 LCM Transportation

In this section, a series of experiments were performed to study the parameters affecting the LCM transportation in the annulus. These experiments were performed at a temperature of 160°C (320°F) and a broad range of experimental parameters. The experimental parameters considered in this section were LCM type and concentration, pipe rotational speed, flow rate, and inclination angle. The range of these parameters is listed in Table 4.6. The range of experimental parameters in this study was obtained from the field practice. However, because the experiments are time consuming and require large amounts of material, the experiments were conducted at selected values that can cover all the parameters' range. Thus, there is some gap in the acquired experimental data. For instance, the pipe rotational speed was changed from 0 to 75 to 150 RPM to cover the whole range of 0 to 150 RPM. This gap can be filled with the numerical study, described in more detail in chapter 6, to optimize the treatment in actual field operations. The annular flow was visualized, and videos were recorded throughout the experiment using the high-speed camera. Afterward, the visualization data was processed and analyzed to detect the LCM settlement. Frame-by-frame video processing techniques were utilized to determine the bed height of the accumulated LCMs. These experiments help identify the optimum operational parameters for better LCM dispersion to ensure efficient circulation treatments.

Table 4.6: The experimental parameters of LCM transportation experiments

Parameter	Range
LCM concentration	1.0 and 3.0 wt. %
Pressure	100 psi

Temperature	160°C (320°F)
Inclination angle from vertical	45, 67.5, and 90°
Mud circulation rate	1-20 gpm
Pipe rotational speed	0-150 RPM

4.4.6 Fracture Sealing Experiments

The fracture sealing experiments were conducted to evaluate the LCM sealing efficiency at high temperatures (160°C). The experiments were conducted at a horizontal inclination. Three fractured discs were designed with different fracture sizes and complexity. These fractured discs were created by a 3D printer using a carbon fiber mater that can withstand the testing temperature. The used fractured discs were 2000 microns, 3000 microns, and a complex fracture, as shown in Figure 4.6. The fracture sealing experiments were conducted using the following steps:

- i. The base fluid was prepared in the mixing tank by adding the synthetic hectorite clay as a viscosifier to the water and mixing it for around one hour to ensure complete dispersion.
- ii. The base fluid was left for 20-24 hrs to hydrate and yield consistent rheological performance.
- iii. The fluid was heated and circulated in the flow loop to ensure homogenous fluid temperature. When the testing temperature was reached, the circulation was stopped, and LCM was added to the mixing tank with a concentration of 1.0 wt.% and mixed for 30 min. The agitator in the tank was kept rotating to ensure better LCM dispersion throughout the experiment.
- iv. The experiment was started by circulating the LCM mud at a flow rate of about 10 gpm. The differential pressure across the fracture, flow rate, and videos were recorded during the experiment to capture the plugging process.

- v. The plugging can be confirmed by the increase in differential pressure, decrease in flow rate, and the captured videos.
- vi. The sealing experiments were conducted using the different fracture sizes and complexities to evaluate and compare the sealing performance of the different LCMs. The experimental parameters of fracture sealing experiments are summarized in Table 4.7.



Figure 4.6: 3D fractured discs used in this study: a) complex fracture, b) 3000 microns, and c) 2000 microns.

Table 4.7: The experimental parameters of fracture sealing experiments

Parameter	Description
LCM concentration	1.0 wt.%
Temperature	320°F
Pressure	40 psi
Flow rate	6 gpm
Inclination angle	Horizontal (0°)

Chapter 5: Experimental Results and Discussions

This chapter discusses the findings of the experimental studies conducted to evaluate the performance of shape memory polymer (SMP) and other lost circulation materials (LCMs). The rheological screening for selecting the base fluid formulation is discussed. The optimized base fluid formulation used to suspend the different LCMs is described. The LCM effect on rheological properties and wellbore hydraulic parameters is presented. The findings of the SMP activation process and LCM transportation in the annulus under the various testing conditions are also discussed. This chapter also presents the results of fracture sealing experiments of SMP and other conventional LCMs at different fracture sizes and complexity.

5.1 Base Fluid Selection and Rheological Screening

Drilling fluids play a significant role in the success and total cost of geothermal drilling operations (Chemwotei, 2011; Vivas et al., 2020). They are mainly used to control the well, transport drilled cuttings to the surface, lubricate and cool the drill bit, and maintain the wellbore stability (Bourgoyne et al., 1984; Caenn et al., 2011; E. Hossain and Al-Majed, 2015; Mohamed et al., 2020a). To ensure successful and efficient drilling operations, great attention should be put into selecting appropriate additives to optimize drilling fluid properties (Ahmed et al., 2020b; Mohamed et al., 2017; 2020b). Thermal stability and rheological properties are essential in selecting drilling fluid additives, especially under high-temperature conditions. Rheological properties affect drilling parameters such as fluid stability, rate of penetration, hole cleaning, wellbore hydraulics, filter cake formation, and mud losses (Basfar et al., 2020; Da Silva and Naccache, 2016; Gamwo and Kabir, 2015; Kulkarni et al., 2013; Pakdaman et al., 2019; Pandya et al., 2019a, 2019b; Zamora and Roy, 2000).

Thermal stability is a vital property for mud additives in geothermal drilling applications. The high temperature of geothermal formations promotes the thermal degradation of polymeric additives used with drilling mud. Thermal degradation can deteriorate the performance of drilling mud, which, in turn, decreases the drilling efficiency and increases the drilling cost and time (Amani and Al-Jubouri, 2012; Avci and Mert, 2019). Bentonite-based muds are commonly used to drill geothermal wells. However, bentonite clay flocculation at high temperatures causes an undesirable change in mud viscosity (Zilch et al., 1991). Thus, more stable viscosifying additives should be used to drill geothermal wells and prevent complications efficiently.

This rheological screening evaluated the thermal stability and rheological behavior of different polymeric and clay additives used with drilling fluid for geothermal drilling applications. The primary objective of this study was to optimize the base fluid formulation to perform the flow loop experiments and suspend the lost circulation materials. The selected additives were primary viscosifiers and filtration control additives that work as secondary viscosifiers. These additives were selected based on the thermal resistance (above 300 °F) and clear appearance. The screening was performed under different conditions by changing the testing temperature and additive concentrations. Further analysis was performed using the best additive by varying the shear rate and aging time to ensure a stable fluid formula.

5.1.1 Effect of Temperature

The temperature effect on the performance of drilling fluid additives was studied by measuring the apparent viscosity at a constant shear rate (170 1/s) and different temperatures using an HPHT rheometer. The experiments were started at room temperature; then, the temperature was gradually ramped up to 190°C (375°F). Figure 5.1 compares the performance of different viscosifiers with temperature. The used viscosifiers were bentonite, xanthan gum (XC), hydroxyethyl cellulose (HEC), and synthetic hectorite clay (THERMA-VIS). For comparison, the additives were added

with the same concentration of 3 lb/bbl, which is within the recommended use in field applications. Bentonite mud was prepared with a 30 lb/bbl concentration, an average of the recommended concentration per field practice. Deflocculant and dispersant were added to bentonite fluid to prevent clay flocculation and improve the rheological performance (Caenn et al., 2011; Hossain and Al-Majed, 2015).

As shown in Figure 5.1, temperature significantly impacted the apparent viscosity of all fluid samples. HEC yielded the highest viscosity of 400 mPa.s (cP) at room temperature; then, viscosity dropped sharply with temperature to reach around 1.5 mPa.s at 177°C (350°F), indicating poor thermal stability because of thermal thinning and/or degradation. XC polymer showed more stable performance with temperature than HEC. XC maintained a viscosity of around 100 mPa.s at 120°C (250°F). Above 120°C (250°F), the viscosity decreased dramatically to reach 3.0 mPa.s at 180°C (360°F). XC polymer was degraded at high temperatures through hydrolysis and oxidization mechanisms (Flynn, 2002), making this additive unsuitable for geothermal drilling applications. Bentonite mud showed a better performance with an apparent viscosity of 70 mPa.s until 93°C (200°F). Then, the apparent viscosity dropped gradually to around 40 mPa.s at 148°C (300°F) and maintained that viscosity until 190°C (375°F). However, bentonite mud can not be used in this experimental study because it produces unclear fluid, causing difficulty in visualizing the LCM particle flow.

In contrast, the synthetic hectorite clay (THERMA-VIS) showed a different viscosity profile. Its viscosity started at a low value (17 mPa.s), then increased gradually, reaching a viscosity of around 60 mPa.s at 148°C (300°F). The increase in viscosity was caused by the thermally induced activation of THERMA-VIS. This additive was initially designed to activate at

high temperatures to maintain the rheological properties required for geothermal drilling operations.

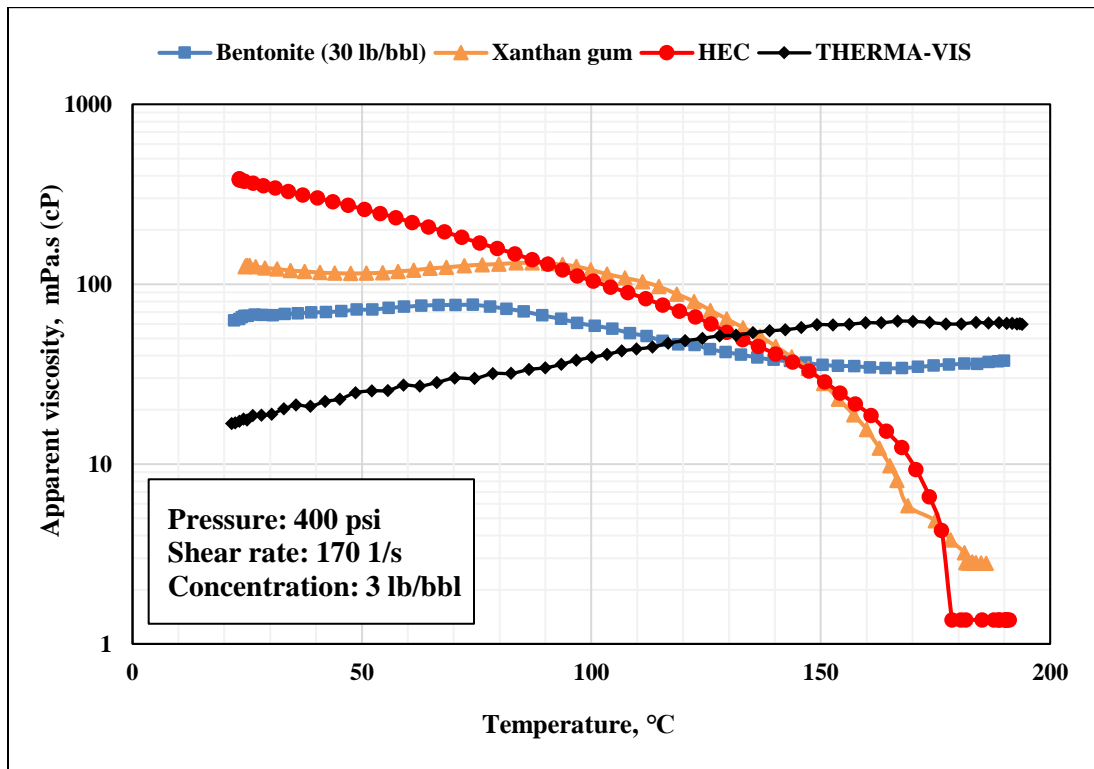


Figure 5.1: Effect of temperature on the apparent viscosity of different viscosifiers.

Figure 5.2 shows the effect of temperature on the apparent viscosity of fluids containing different fluid control additives. Regular polyanionic cellulose (PAC-R) showed the highest apparent viscosity at room temperature (30 mPa.s); then, the viscosity dropped dramatically to reach 1.0 mPa.s at 110°C (230°F). Similarly, Low-viscosity polyanionic cellulose (PAC-L) showed a viscosity of 18 mPa.s at room temperature, then decreased to 3.0 mPa.s at 120°C (250°F) and maintained that viscosity until 190°C (375°F). The sharp decrease in PAC-based fluid viscosity (PAC-L and PAC-R) at high temperatures (above 120°C/250°F) was due to hydrolysis and oxidization reactions that break the polymer chains (Flynn, 2002). Conversely, synthetic polymers (THERMA-CHEK and POLYAC PLUS) showed a slight reduction in the apparent

viscosity with temperature, indicating better thermal stability than PAC-based fluids. POLYAC PLUS showed a 3.0 mPa.s higher viscosity than THERMA-CHEK throughout the experiments.

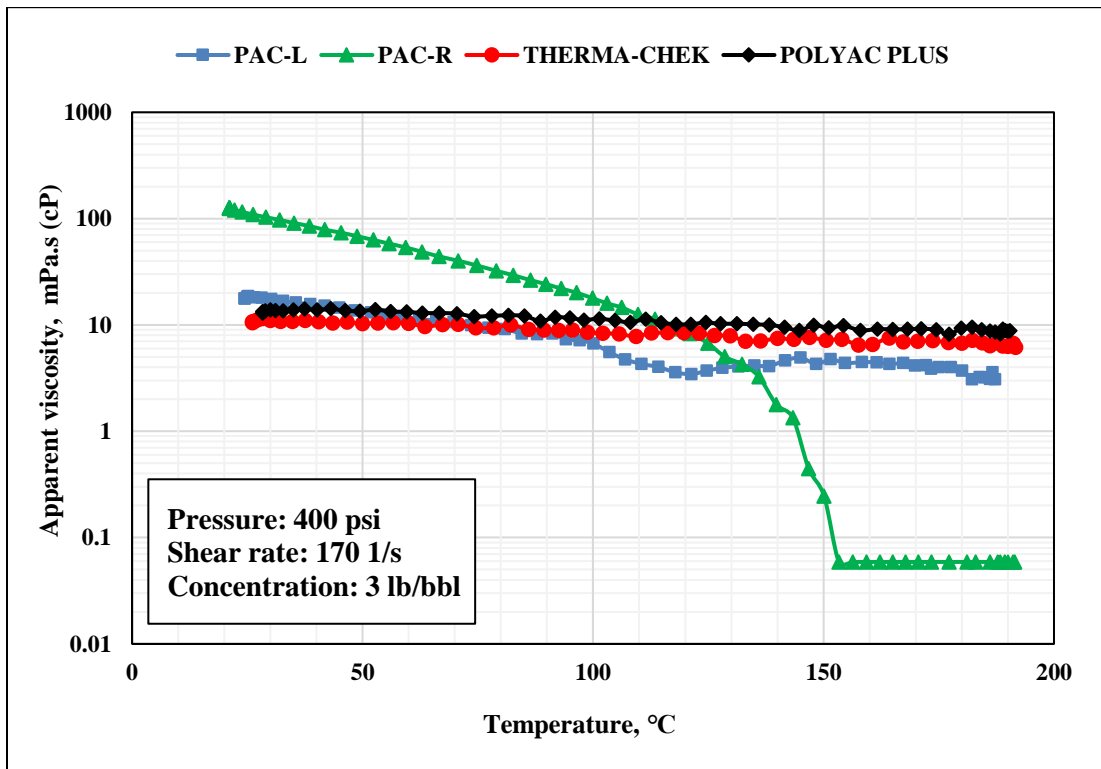


Figure 5.2: Effect of temperature on the apparent viscosity of different fluid loss control additives.

After the experiments, all fluid samples were recovered to check the temperature effect on the fluid appearance. All fluid samples were clear before they were exposed to high temperatures. After the exposure, as shown in Figure 5.3, the PAC-L-based fluid color completely changed to dark brown, confirming the complete thermal degradation at elevated temperatures. In comparison, fluids containing other additives showed a slight change in color with temperature. THERMA-VIS solutions exhibited the least change in color among other additives, demonstrating their superior thermal resistance and stability (up to 370°C/700°F).

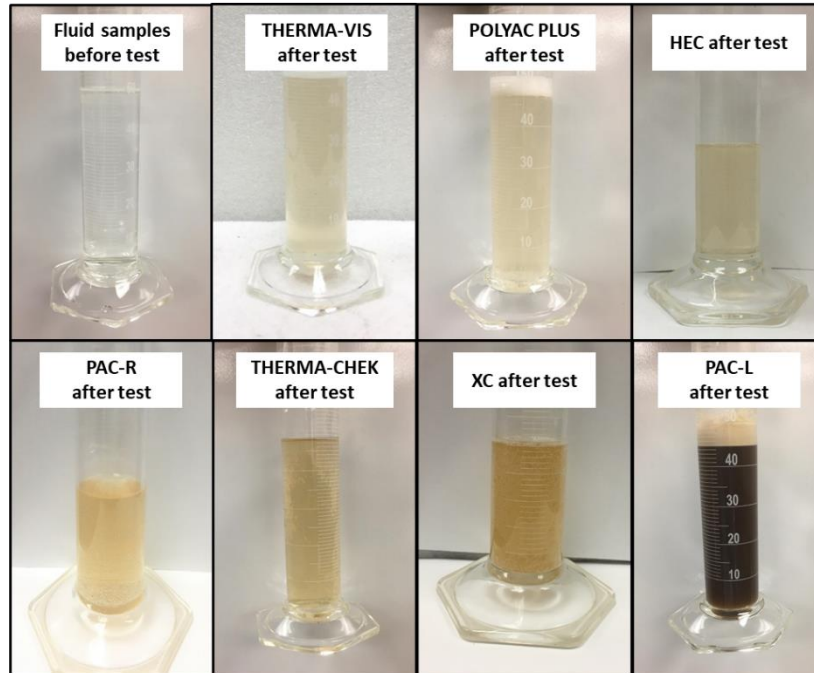


Figure 5.3: Fluid samples before and after rheology experiments (3.0 lb/bbl).

5.1.2 Effect of Additives Concentration

Several fluid samples were prepared in the laboratory by varying each additive's concentration from 1.0 to 5.0 lb/bbl to study the concentration effect on fluid rheology. On the other hand, bentonite clay was mixed with 10 to 30 lb/bbl as clay requires a higher concentration than polymers to build sufficient viscosity to fulfill drilling fluid functions. Figure 5.4 compares the concentration effect on fluid viscosity with temperature for bentonite, XC, HEC, and THERMA-VIS-based fluids. Concentration did not change the general trend of apparent viscosity with temperature for all these additives. As the concentration was increased, higher viscosity values were observed. XC-based and HEC-based fluids resulted in the highest viscosity of around 1,000 mPa.s at room temperature. For HEC-based and XC-based fluids, the viscosity difference due to concentration was not significant at high temperatures (150°C/350°F and above). The final viscosity was almost the same for all concentrations. Therefore, when using a viscosifier with low thermal resistance, increasing the concentration would not help maintain the required rheological behavior at high

temperatures. Conversely, bentonite samples maintained the same viscosity trend with temperature. The higher the concentration, the higher the viscosity.

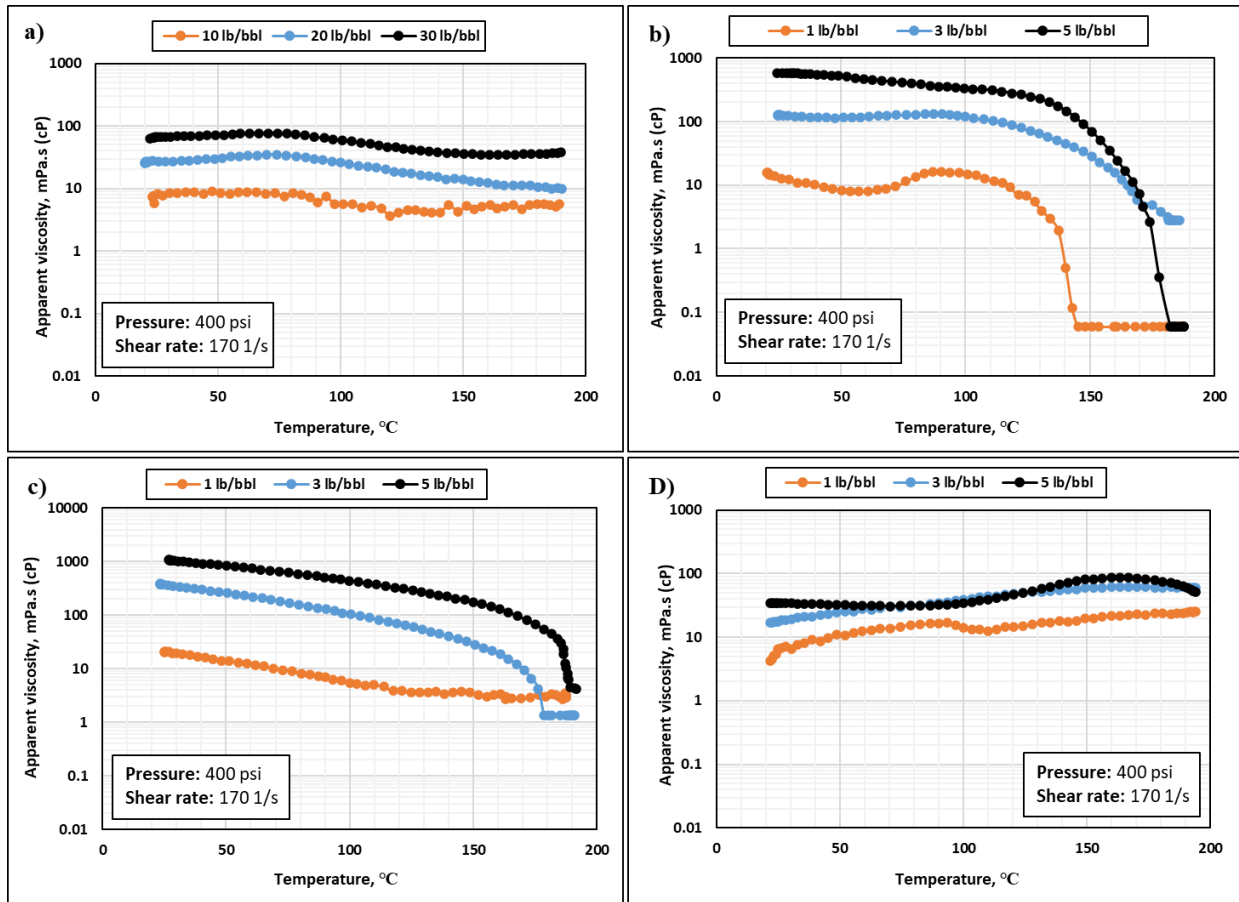


Figure 5.4: Effect of viscosifier concentration on fluid viscosity with temperature: a) bentonite, b) Xanthan, c) HEC, and d) THERMA-VIS.

In contrast, increasing THERMA-VIS concentration from 1.0 to 3.0 lb/bbl resulted in a 200% increase in the apparent viscosity throughout the experiment. However, increasing THERMA-VIS concentration to 5.0 lb/bbl negatively impacted the viscosity profile. 5.0 lb/bbl of THERMA-VIS showed a higher viscosity until 177°C/350°F (85 mPa.s); however, the viscosity dropped gradually and reached 50 mPa.s at 193°C (380°F). Figure 4.5 shows the fluid sample with 5.0 lb/bbl of THERMA-VIS after the experiments. It can be seen that the fluid formed a gel at a high temperature; therefore, the drop in viscosity was due to the slippery effect induced by

gelation, and it was not an actual viscosity reduction. The gel formation would significantly increase the frictional pressure losses and require very high pressure to circulate the mud, exceeding the equivalent circulating density (ECD) limit. The increased ECD causes complications in the drilling operation and may induce fractures into the formation when it exceeds the fracture gradient, leading to additional mud losses. Therefore, the optimum concentration for THERMA-VIS is a round 3.0 lb/bbl, and exceeding this concentration is not recommended.



Figure 5.5: Gelled THERMA-VIS on the rheometer's bob (5.0 lb/bbl).

Figures 5.6 shows the effect of PAC-L, PAC-R, THERMA-CHEK, and POLYAC PLUS concentrations on the apparent viscosity at different temperatures. The primary objective of these polymeric additives is to control fluid loss into the drilled formations. PAC-L, THERMA-CHEK, and POLYAC PLUS additives had minimal effect on fluid viscosity. PAC-L exhibited poor thermal resistance, and the viscosity dropped dramatically with temperature. Increasing the concentration did not have a significant impact on the thermal stability. THERMA-CHEK-based and POLYAC PLUS-based fluids with 1.0 lb/bbl additives exhibited low viscosity and a considerable drop in the apparent viscosity with temperature. When the concentration was increased to 3.0 lb/bbl, both additives showed a stable fluid formulation with a slight decrease in

the apparent viscosity with temperature. Fluid with POLYAC PLUS had a higher viscosity than THERMA-CHECK, with a difference of around 3.0 mPa.s throughout the experiments. Increasing the concentration of both additives to 5.0 lb/bbl showed an increase of 5.0 mPa.s in the viscosity at low temperatures; however, increasing the concentration had a detrimental effect on the thermal stability of the fluids. A dramatic decrease in the viscosity with temperature was observed. The apparent viscosity dropped to 1.0 mPa.s at elevated temperature, and the rheological performance was poor compared to the 3.0 lb/bbl fluid samples. The sharp reduction in the apparent viscosity was due to overtreatment. Therefore, the optimum concentration of these additives was approximately 3.0 lb/bbl, and exceeding this concentration could negatively affect the drilling fluid performance at high temperatures.

Fluid with PAC-R exhibited a high increase in viscosity. Fluid with 1.0 lb/bbl PAC-R showed an apparent viscosity of 30 mPa.s at room temperature. Increasing the polymer concentrations to 3.0 and 5.0 lb/bbl increased the apparent viscosity to 130 and 330 mPa.s, respectively. However, this additive was unsuitable for geothermal drilling due to its low thermal resistance, which was indicated by the sharp reduction in viscosity with temperature. Moreover, excessive mud viscosity is not favorable as it limits the performance of the fluid by increasing the frictional pressure loss in the annulus, drill pipe, and drill bit. Thus, such additives should be used at low concentrations.

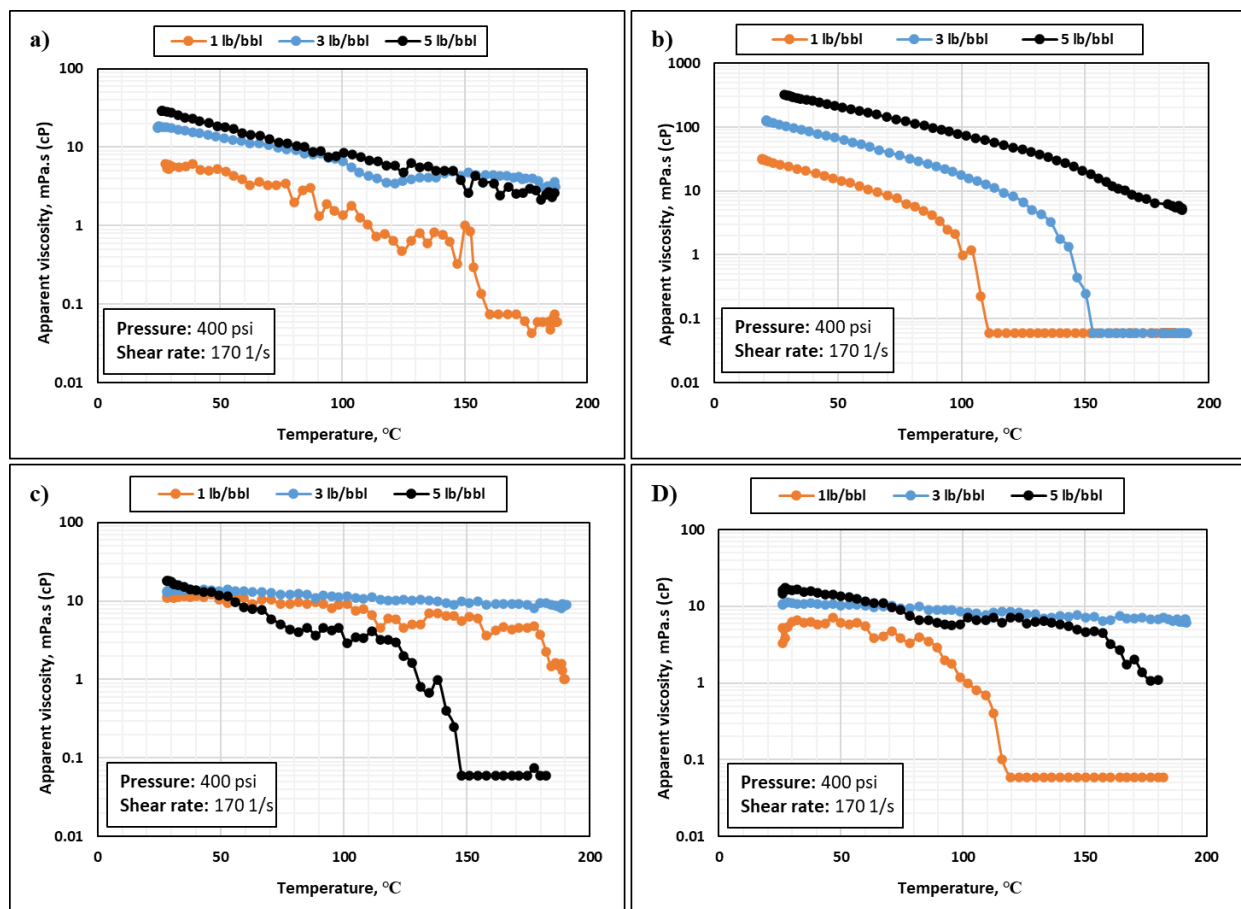


Figure 5.6: Effect of filtration control additives' concentration on fluid viscosity with temperature: a) PAC-L, b) PAC-R, c) POLYAC PLUS, and d) THERMA-CHEK.

5.1.3 Effect of Shear Rate

The synthetic hectorite clay (THERMA-VIS) was the best additive to maintain the mud rheological properties at high temperatures due to its high thermal stability; therefore, it was selected for further analysis to study the effect of shear rate on fluid samples. The optimum concentration of THERMA-VIS (3.0 lb/bbl) was used in this screening. The rheological behavior was studied by measuring the apparent viscosity at a wide range of shear rate (0.01-510 1/s) and temperature (37-150°C/100-300°F). As shown in Figure 5.7, fluid samples with THERMA-VIS behaved as non-Newtonian fluids with a high shear-thinning behavior (Skelland, 1967; Mezger, 2006). Their viscosity decreased with the shear rate. The level of shear-thinning can be assessed

using the fluid behavior index (n). The flow curves of the fluids are fitted to the Power-law model with a correlation coefficient (R^2) ranging between 0.85-0.93. The fluid behavior index obtained from the curve fitting ranges from 0.1 to 0.2 for all temperatures. The consistency index (K) increased with temperature due to the activation of THERMA-VIS while maintaining the same shear-thinning behavior. This high shear-thinning behavior of drilling fluid is favorable in drilling operations as it would reduce the sensitivity of frictional pressure loss to the change in flow rate.

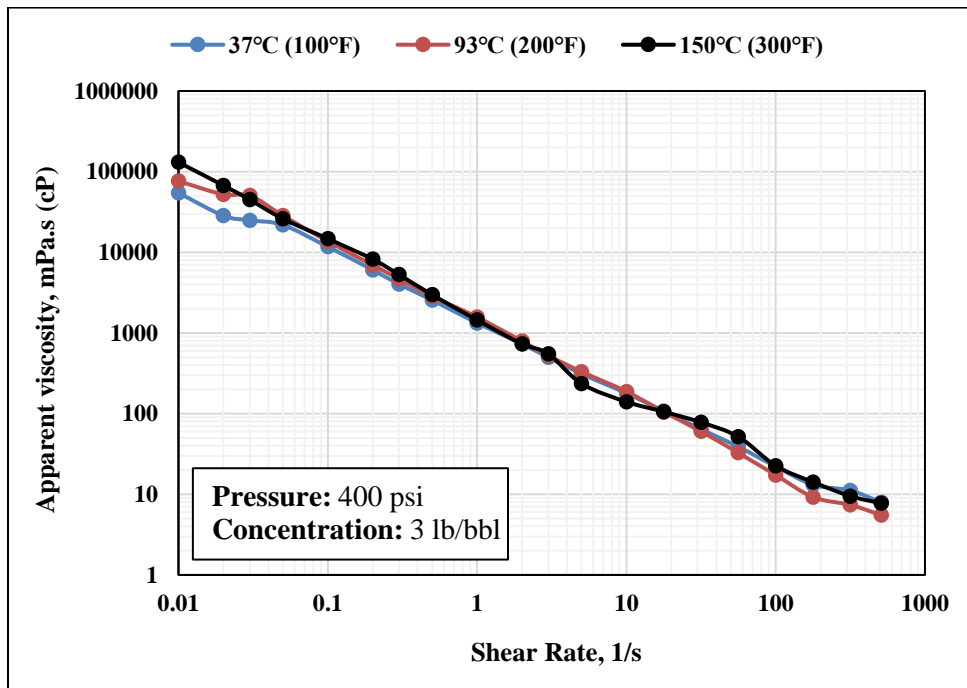


Figure 5.7: Effect of shear rate on THERMA-VIS viscosity at different temperatures.

5.1.4 Effect of Time

The thermal stability of THERMA-VIS-based fluid was also studied with time to ensure the thermal stability of the mud during extended exposure to high temperatures in drilling operations. The optimum concentration of THERMA-VIS (3.0 lb/bbl) was used in this experiment. The temperature was increased gradually from room temperature to 177°C (350°F) and kept at that high temperature for more than two hours. As shown in Figure 5.8, the viscosity increased gradually, and THERMA-VIS activated at around 150°C (300°F). Then, the apparent viscosity

remained almost constant throughout the experiments. This stable performance with time and temperature makes THERMA-VIS a suitable viscosifier for geothermal drilling applications. It maintains the mud's rheological properties and ensures more efficient and successful drilling operations.

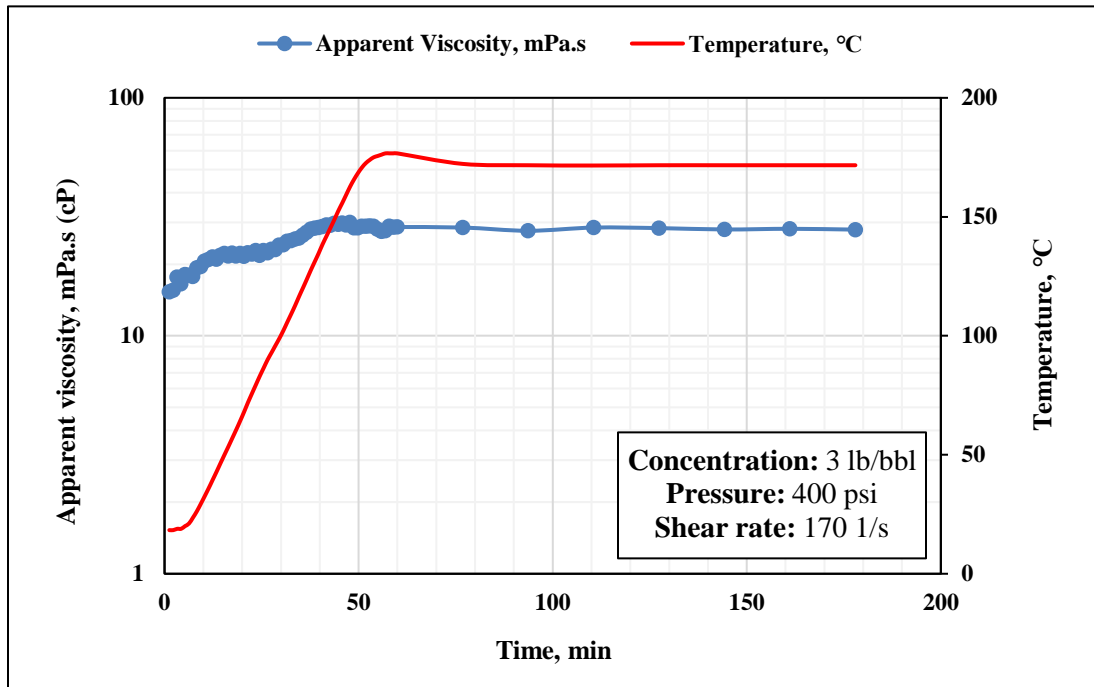


Figure 5.8: Thermal stability of THERMA-VIS with time.

The following sections evaluate the performance of shape memory polymer as a lost circulation material for geothermal drilling applications. The optimized base fluid formulation was used for these experiments. SMP performance was compared with other conventional LCMs, such as cedar fiber, calcium carbonate, and walnut, in terms of settling behavior, flow characteristics, and sealing efficiency.

5.2 Shape Memory Polymer Activation

The shape memory polymer was used in this study as a smart lost circulation material programmed to activate at a high temperature (above 149°C). The activation process was studied by visualizing

the annular flow through two viewports with the aid of a high-speed camera. The experiments were performed at 21°C and 160°C to detect the change in SMP particles with temperature. In this experiment, SMP was added to the base fluid in 1.0 wt.% to easily detect the change in SMP particles. The captured videos were processed and analyzed using frame-by-frame image processing techniques by commercial image processing software.

Figure 5.9 shows the activation process of SMP particles with temperature. Initially, SMP particles have an irregular shape with a particle size ranging from 840 to 2360 μm (0.84-2.36 mm). At low temperature (21°C), most SMP particles ranged from 1 to 2 mm (Figure 5.9a), while a significant increase in the SMP particle size was observed at high temperature (160°C). The SMP particle size reached 3-5 mm with some small particles (Figure 5.9b). The activation of thermoset shape memory polymers was addressed in previous studies by visualizing the change in particle size before and after heating (Mansour et al., 2018, 2019), infrared laser light (Leng et al., 2010), or by tracking the change in energy (stresses and strains) during the programming and activation processes (Fan and Li, 2018; Li and Xu, 2011). However, the increase in particle size observed in this study confirmed the thermally induced activation of the shape memory polymer at high temperatures within the mud system, considering the effect of other mud additives and mud circulation. This particular reason makes the results of this study more representative of actual field operations, while previous studies considered only the temperature effect in the absence of other factors.

Based on these observations, the shape memory polymer can be programmed to activate at a specific temperature after reaching the targeted formation to seal large fractures with minimal risk of plugging downhole tools. As reported in previous studies, these size variations would be more efficient in bridging and sealing fractures (Alsaba, 2015; Alsaba et al., 2017; Ezeakacha et

al., 2017a; Magzoub et al., 2020; Whitfill, 2008). Large particles are required to form the bridge on the fracture, while small particles create the seal matrix and plug the space between large particles and the fracture wall (Magzoub et al., 2021).

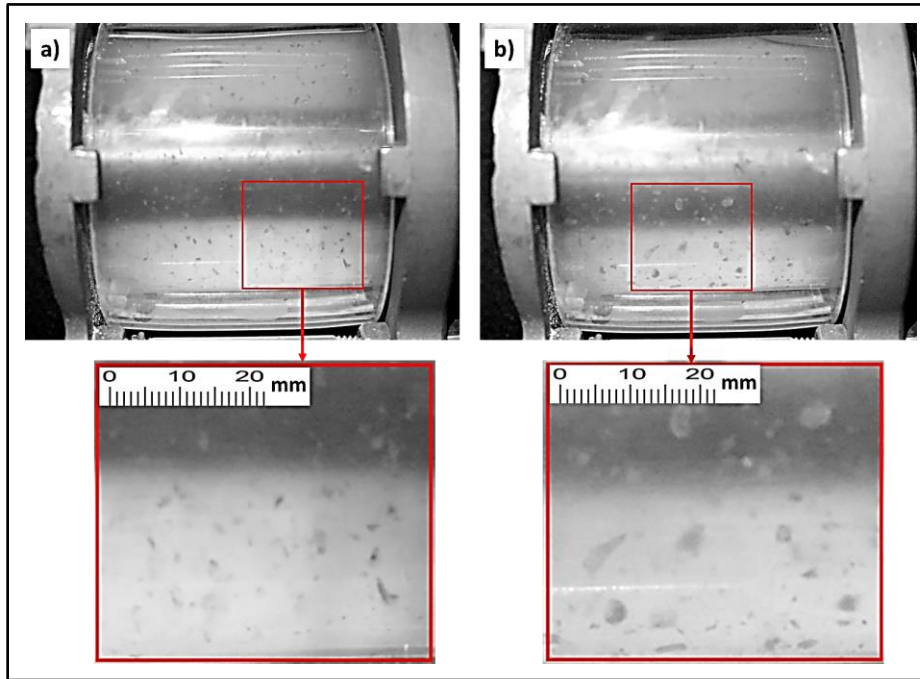


Figure 5.9: Effect of temperature on SMP particles: a) 21°C, and b) 160°C. An apparent increase in particle size was seen at 160°C.

5.3 Rheology Experiments and Wellbore Hydraulics Analyses

5.3.1 Effect of Temperature on the Base Fluid Rheology

First, the rheological properties of the base fluid were measured at different temperatures (21, 93, and 160°C) to study its performance and then investigate the effect of SMP on its rheological behavior. Following the procedure illustrated in steps i to vii in Section 4.4.4, the flow curve of the base fluid at different temperatures was construed in Figure 5.10a. It was observed from the flow curve that the base fluid is a non-Newtonian fluid with shear-thinning behavior at all temperatures. The thinning degree varied with temperature because the viscosifier (synthetic hectorite clay) was engineered to activate and build viscosity with high shear-thinning behavior at

high temperatures (Baroid, 2012; Mohamed et al., 2021b). The power-law model can describe the base fluid behavior with a correlation parameter (R^2) of 0.88-0.93. The power-law model is simple and suitable for describing shear-thinning fluids (Mohamed et al., 2021a; Wu, 2016). Casson and Herschel–Bulkley models were also considered in the rheological analysis. The Casson model yielded a correlation parameter of around 0.86, slightly lower than the power-law model. Because the base drilling fluid exhibited a low yield stress (τ_0) value of about 0.18 Pa, no significant change in the rheological behavior of the drilling fluid was observed. A slight improvement in the flow curve was noticed with an R^2 of 0.882-0.931. Therefore, power-law and Herschel–Bulkley models can describe the drilling fluid well.

As shown in Figure 5.10a, the degree of thinning increases with temperature, which can be proven by the flow index values (n). The base fluid showed a flow index of 0.454, 0.168, and 0.101 at 21°C, 93°C, and 160°C, respectively. However, higher viscosities were observed at high temperatures due to the thermally induced activation of the synthetic hectorite clay, improving the mud capacity for carrying/suspending the LCM and drilled cuttings (Baroid, 2012; Mohamed et al., 2021b). The drop in the apparent viscosity with the increase in shear rate also confirmed the high shear-thinning behavior of the base fluid, Figure 5.10b. This high shear-thinning performance is favorable in drilling operations because it makes the frictional pressure drops less sensitive to the change in flow rate. Therefore, no additional frictional pressure drops would result during mud circulation through bit nozzles and tubular systems.

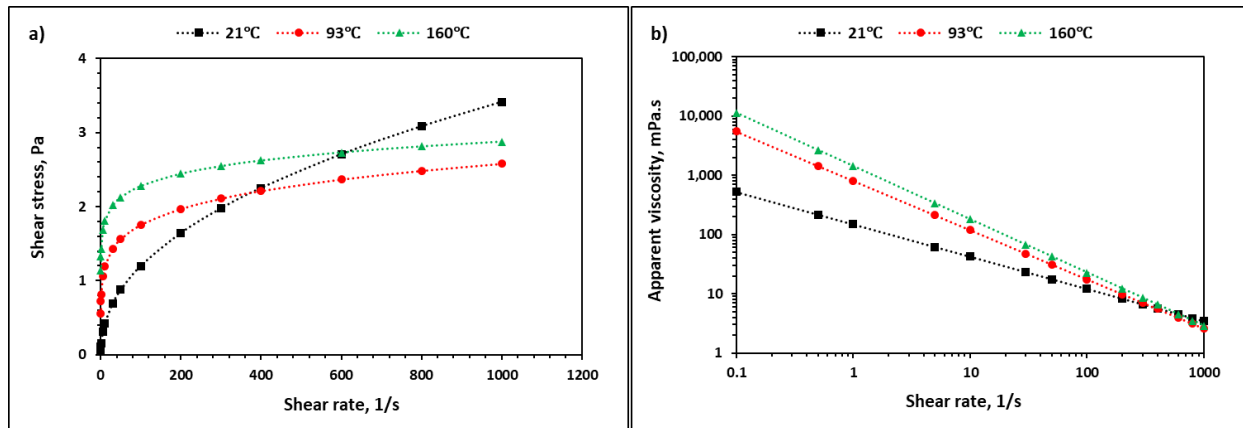


Figure 5. 10: Effect of temperature on the base fluid's performance: a) flow curve, and b) apparent viscosity.

5.3.2 Effect of Lost Circulation Materials (LCMs) on Fluid Rheology

The lost circulation materials were added to the base fluid in two concentrations, 1.0 and 3.0 wt.%. The rheology data were analyzed for each fluid sample using the procedure discussed in Section 4.4.4. τ_w and $\dot{\gamma}_{nom}$ data of all mud samples yielded a straight line on a logarithmic scale with an R-squared ranging between 0.8-0.98. Therefore, all LCM mud samples can be described by the Power-law or Herschel–Bulkley models. K and n were obtained from the curve fitting and used to construct the flow curves at 160°C (320°F). Similar to the base fluid, a high shear-thinning behavior ($n < 1$) was observed with all LCMs at both concentrations (Figures 5.11a & 5.11b). At 1.0 wt.% concentration, the flow index (n) varied in a range of 0.025-0.261, while the base fluid had a flow index of 0.101. At 3.0 wt.%, a slight increase in the flow index was observed for most lost circulation materials. The flow index (n) values ranged from 0.061 to 0.282. Figure 5.12 exhibits the effect of shear rate on the apparent viscosity of all mud samples at the two different LCM concentrations, 1.0 and 3.0 wt.%. The apparent viscosity was calculated from the pipe viscometer data measured at 160°C (320 °F). The viscosity profile confirmed the shear-thinning behavior of all LCM mud samples, where the apparent viscosity decreased with the shear rate. Cedar fiber and walnut showed lower viscosity values than the base fluid and other LCMs,

resulting in less frictional pressure drops. The fiber impact on frictional pressure losses was also observed in previous studies by Ahmed and Takach, 2009 and Elgaddafi et al., 2012.

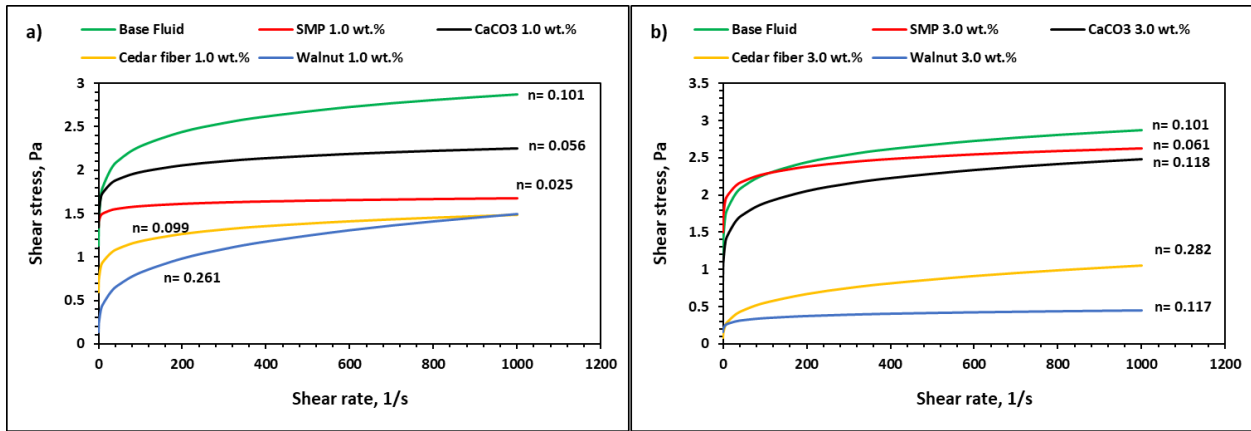


Figure 5. 11: Effect of LCM concentration on the base fluid's flow curve at 160°C: a) 1.0 wt.%, and b) 3.0 wt.%.

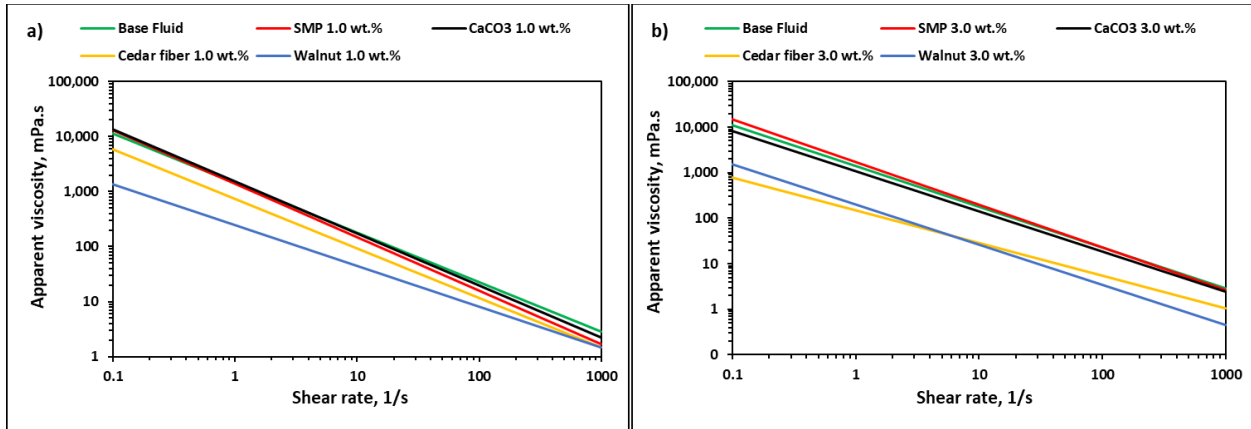


Figure 5. 12: Effect of LCM concentration on the base fluid's viscosity at 160°C: a) 1.0 wt.%, and b) 3.0 wt.%.

5.3.3 Effect of Lost Circulation Materials (LCMs) on Wellbore Hydraulics

Figure 5.13 shows the raw data of pressure drop and flow rate obtained for all LCM mud samples using the pipe viscometer readings at 160°C (320 °F). The data in Figure 5.13a shows that all LCMs at 1.0 wt.% concentration reduced the frictional pressure drops across the pipe, and this effect is more significant in the laminar flow regime. Cedar fiber and walnut showed the lowest frictional pressure drops among other LCMs. Conversely, at 3.0 wt.% concentrations, some LCMs (SMP and calcium carbonate) showed no significant change in the pressure drops of the base fluid.

At the same time, cedar fiber and walnut yielded significantly less frictional pressure drops than the base fluid and other LCMs (Figure 5.13b). The Fanning friction factor is presented in Figure 5.14 as a function of the generalized Reynolds number. The flow regime changed from laminar to turbulent when the generalized Reynolds number reached around 3,700. A slight reduction in the frictional pressure drops was observed with 3.0 wt.% in the turbulent flow regime. This reduction can help avoid the increase in ECD that may complicate the lost circulation treatment and cause additional losses if it exceeds the fracture pressure of the drilled formation (Caenn et al., 2017; Mohamed et al., 2021c).

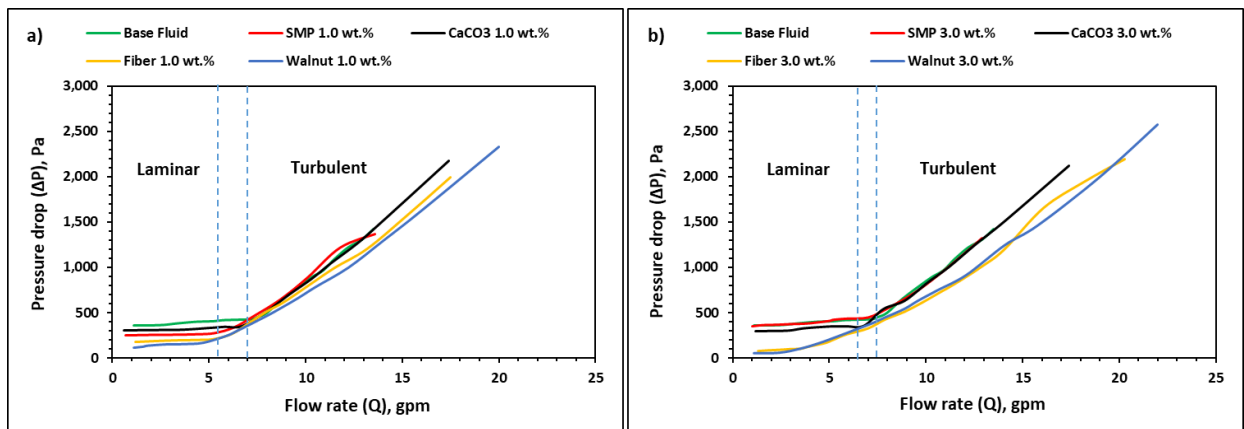


Figure 5.13: Raw data of ΔP and Q for LCM muds at 160°C: a) 1.0 wt.%, and b) 3.0 wt.%.

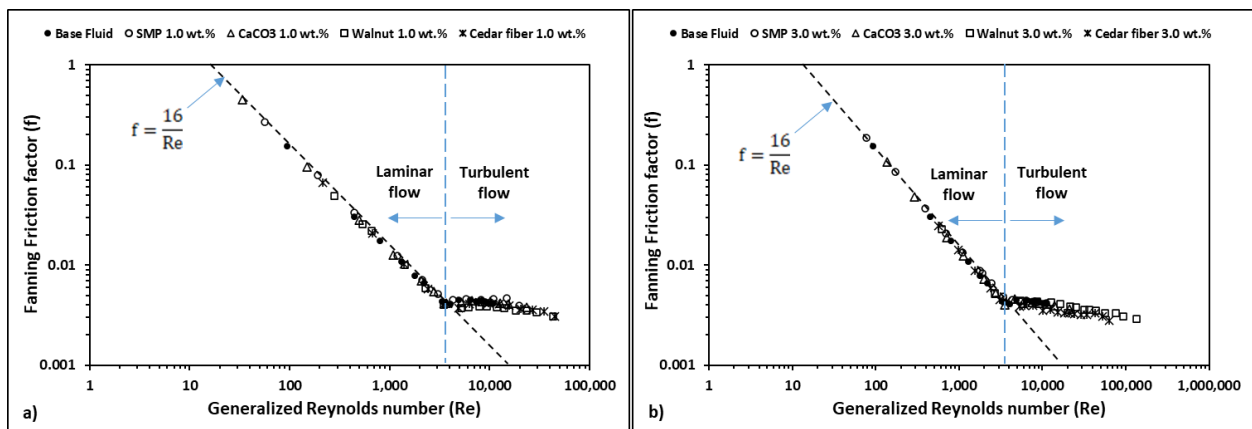


Figure 5.14: Fanning friction factor data of LCM muds at 160°C: a) 1.0 wt.%, and b) 3.0 wt.%.

5.4 Settling Behavior of Lost Circulation Materials

This section discusses the findings of LCM transportation in the annulus at high temperatures and under a broad range of experimental parameters. LCM transportation plays a significant role in sealing efficiency and drilling operations. Good LCM suspension within the mud system ensures better sealing efficiency and prevents other drilling issues such as pipe sticking and hole cleaning. The experiments were conducted using the flow loop setup. LCMs were tested at two concentrations (1.0 wt.% and 3.0 wt.%). The LCM performance was evaluated by changing the concentration, annular velocity (flow rate), inclination angle, and pipe rotational speed. The range of experimental parameters was discussed in Section 4.4.5.2. The visualization data was processed and analyzed to detect solid particles settlement and identify the optimum parameters for better LCM dispersion. The effect of these parameters on LCM transportation is discussed in detail in the subsequent sections.

5.4.1 Effect of LCM Concentration and Annular Velocity

Figure 5.15 compares the LCM settling performance at two concentrations (1.0 wt.% and 3.0 wt.%) and different annular velocities (16.33-163 ft/min). These experiments were conducted at 160°C and at a horizontal angle without pipe rotation. These conditions represent the worst-case scenario to evaluate the effect of LCM concentration and annular velocity and eliminate the impact of other parameters. At 1.0 wt.%, it was observed that at a low annular velocity (flow rate), the walnut particles tend to settle down and form a stationary or moving bed with a bed height of around 40-50% of the annular space, as shown in Figure 5.15a. Increasing the annular velocity (flow rate) improved the particles' suspension and reduced the bed height. The increased annular velocity dispersed the particles and improved mud carrying capacity (Werner, 2018). A high annular velocity of around 81 ft/min was required to erode the formed bed completely and ensure good walnut transportation. However, field operations cannot achieve this high velocity in the

annulus. Therefore, low sealing efficiency would result when walnut is used as LCM, and other drilling issues may result, such as pipe sticking and increased equivalent circulating density (ECD). These drilling issues complicate the lost circulation treatment and may cause additional mud losses in the formation. Conversely, cedar fiber and shape memory polymer showed excellent performance at 1.0 wt.%. LCM particles were fully suspended at all circulation rates, and no bed was developed throughout the experiment.

In contrast, particle transportation was more challenging when the walnut concentration was increased to 3.0 wt.%. Walnut particles started to accumulate immediately in the lower section of the annulus, forming a stationary bed that was challenging to remove. Increasing the flow rate helped erode the formed beds and slightly reduced their heights. With a circulation rate of up to 10 gpm (81 ft/min), the solids accumulation at the lower section was inevitable. A circulation rate of 20 gpm (163 ft/min) was required to remove the accumulated solids completely. However, this high circulation rate is not attainable in field operations. Cedar fiber and SMP also showed a better suspension than walnut. Cedar fiber required a circulation rate of 10 gpm (81 ft/min) to entirely suspend the solid particles, while increasing the circulation rate to only 5 gpm (40 ft/min) was adequate to suspend the SMP particles efficiently.

Thus, the lost circulation materials have different performances due to the difference in densities, shapes, particle sizes, and interactions between solid particles and fluid. However, reducing material concentration and increasing circulation rate improve the carrying capacity and particle suspension. Optimizing these parameters would ensure better sealing efficiency and successful drilling operations.

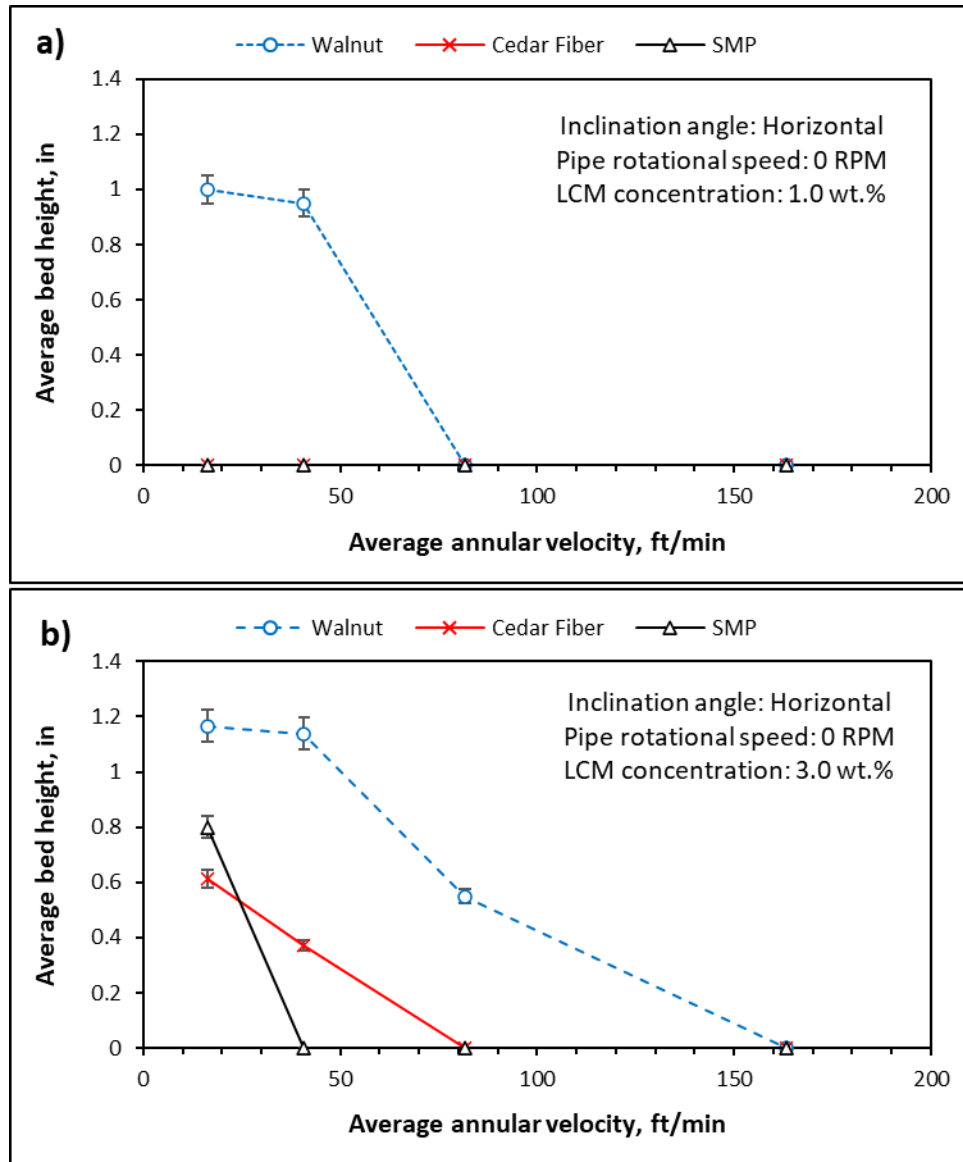


Figure 5.15: Effect of annular velocity on LCM transportation at 160°C: a) 1.0 wt.%, and b) 3.0 wt.%.

5.4.2 Effect of Pipe Rotational Speed

The impact of pipe rotation on LCM dispersion was also studied using the flow loop setup. Figure 5.16 compares the settling performance of different LCMs under various rotational speeds. The rotational speed varied from 0 to 150 RPM, and accumulated solids were captured in all conditions. Lost circulation materials were added to the base mud with a concentration of 3.0 wt.%. Walnut particles showed a poor suspension profile, and solid particles accumulated in the lower section of

the annulus to cover more than 50% of the annular space. The pipe rotation was inefficient in removing the accumulated solids. Increasing the pipe rotational speed up to 150 RPM failed to erode the formed bed significantly. Therefore, poor sealing efficiency would result because low LCM concentration would get to the fracture while most LCM particles would accumulate in the annulus. Moreover, the deposited solids reduce the area open to the flow and cause an increase in the annular velocity. This increase will consequently increase the frictional pressure drops and ECD. More fractures and mud losses may result if the ECD exceeds the fracture gradient of the drilled formations. Geothermal formations are more prone to such issues because most geothermal formations are weak and have a narrow mud window.

On the other hand, muds containing cedar fiber and SMP showed better LCM suspension with much less accumulated solids without pipe rotation. When the pipe rotational speed was increased, a significant improvement in the solid suspension capacity was observed. Pipe rotation agitated the mud and reduced the accumulated solids in the annulus. Shape memory polymer showed superior performance compared to other LCMs. A rotational speed of only 75 RPM was adequate to erode the formed bed entirely and carry the SMP particles, while cedar fiber required a rotational speed of 150 RPM.

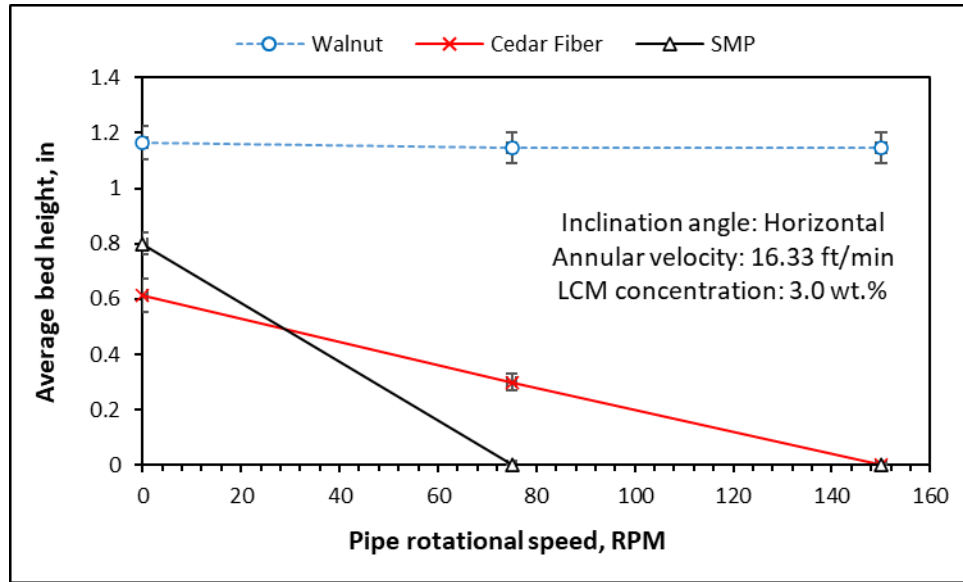


Figure 5. 16: Effect of pipe rotational speed on LCM transportation at 160°C.

5.4.3 Effect of Inclination Angel

LCM settling behavior was also studied at various inclination angles (45°-90° from vertical). The experiments were conducted at 3.0 wt.% LCM concentration, low annular velocity (16.3 ft/min), and without pipe rotation (0 RPM). As shown in Figure 5.17, walnut particles also showed the highest bed heights compared to other LCMs, while SMP showed the best suspension performance. Overall, the base mud showed a better carrying capacity in inclined wells than in horizontal wells. As the inclination angle from vertical increased, the tendency of solid particles to settle down increased, and accumulated solids concentration increased. The settling behavior was worse in horizontal sections than in inclined sections because the vertical component of fluid velocity diminished as the inclination angle increased. The vertical velocity component reached zero in horizontal wells, which is insufficient to carry all LCM particles. Thus, solid particles tend to settle down easily with the limited hydrodynamic force that opposes the gravitational force and prevents deposition (Czuprat et al., 2020). On the other hand, the vertical component of velocity

increases in inclined wells and acts against the gravity effect, reducing the solid accumulation (Ahmed and Takach, 2009; George et al., 2012).

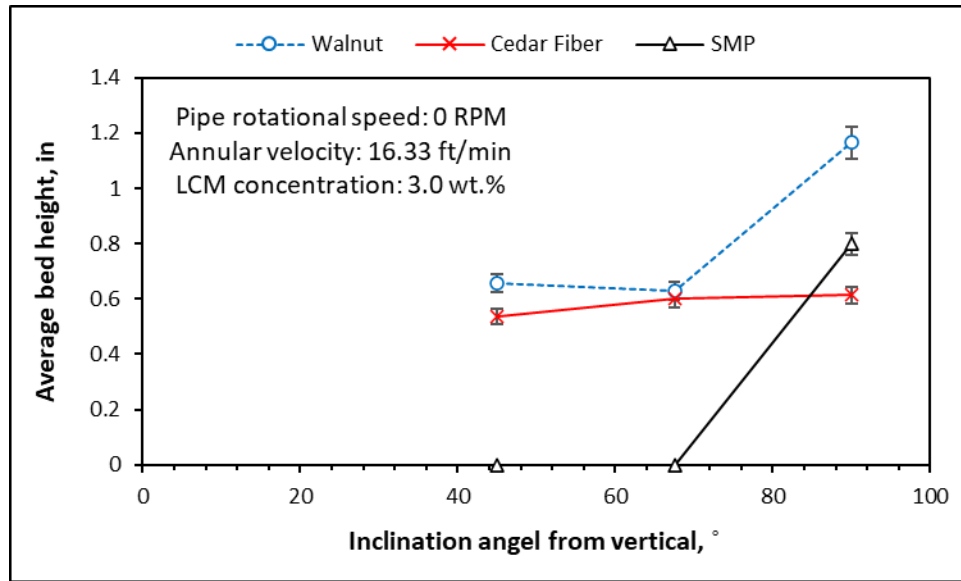


Figure 5. 17: Effect of inclination angel on LCM transportation at 160°C.

The settling behavior is a complex phenomenon, and many parameters should be considered to understand it well, including solid particles' shape, size, and density. Overall, shape memory polymer outperformed other lost circulation materials in terms of transportation. Figure 5.18 summarizes the effect of test parameters on the SMP dispersion to determine the optimum conditions for SMP transport at the two concentrations. Depending on well inclination and concentration, circulation rate and pipe rotational speed need to be optimized to improve the SMP transportation, thus the sealing efficiency and lost circulation treatment.

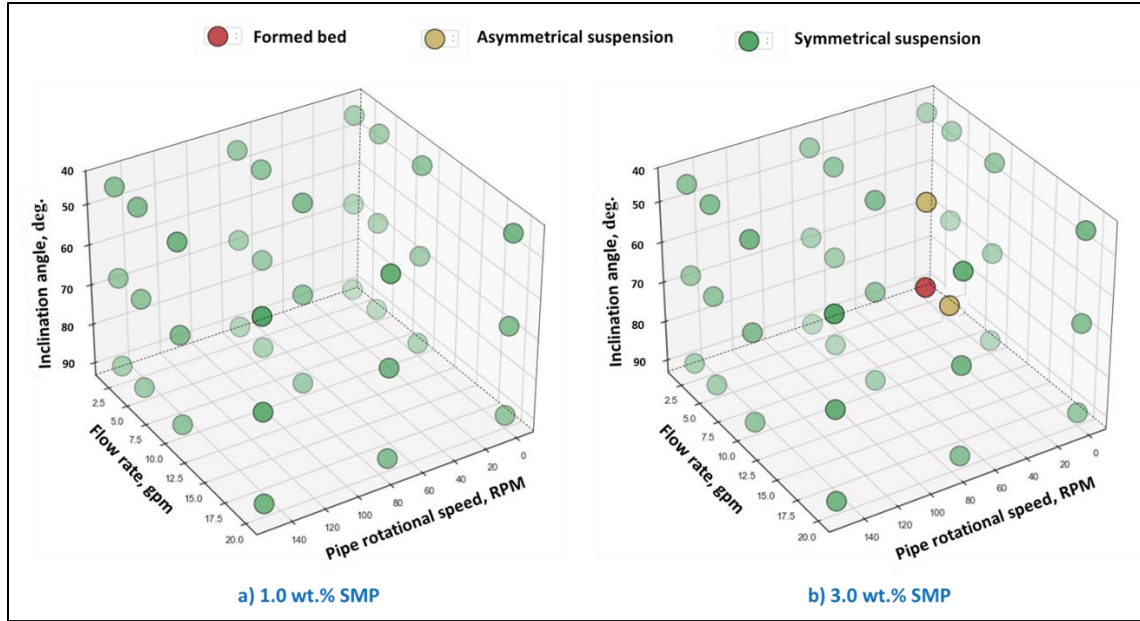


Figure 5. 18: Summary of the effect of the operational parameters on SMP transportation at 160°C.

5.5 Fracture Sealing Experiments

This section of the results discusses the findings of fracture sealing experiments with shape memory polymer and other conventional LCMs. Three different fractured discs were used in these experiments; 2000 μm , 3000 μm , and complex fracture. All LCMs were added with a concentration of 1.0 wt.% after reaching the testing temperature, 160°C (320°F). The performance of each LCM is discussed in detail in the subsequent sections.

5.5.1 Calcium Carbonate

The differential pressure data from the main test sections were used to evaluate the LCM sealing efficiency. Generally, the increase in differential pressure as the experiment progresses indicates that the LCM particles seal the fracture, partially or entirely. The higher the differential pressure, the higher the sealing efficiency. Figure 5.19 shows the change in differential pressure across the fracture throughout the experiments with calcium carbonate. The differential pressure across the fractures did not increase significantly, indicating that calcium carbonate was ineffective in sealing all the fracture sizes. Although some spikes in the pressure were observed with calcium carbonate

due to the particles bridging, the bridging was not strong enough to seal the fracture (Figure 5.20). The fracture reopened as the pressure built up, resulting in immediate drops in the differential pressure. It can also be seen that the calcium carbonate performed slightly better in the 2000-micron fracture than in the 3000-micron and complex fractures, as higher spikes were detected with the 2000-micron fracture. This poor performance observed with calcium carbonate was attributed to its fine and uniform particles. A broad range of particle sizes is always required for better sealing efficiency.

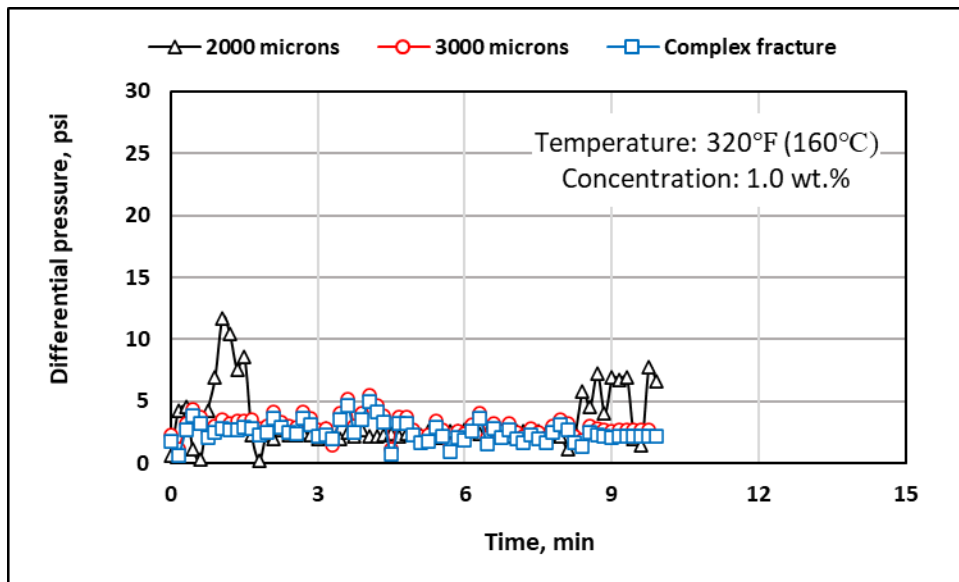


Figure 5.19: Sealing performance of calcium carbonate at different fracture sizes.

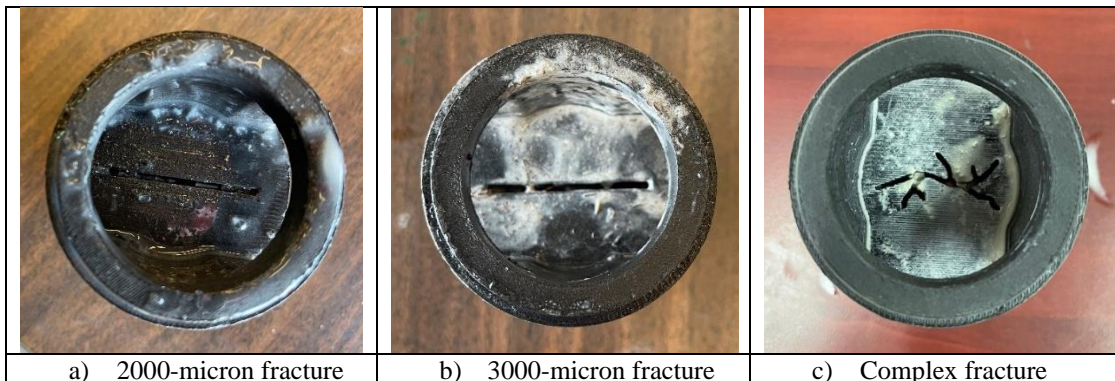


Figure 5.20: Fractured discs after the experiments with calcium carbonate.

5.5.2 Walnut

Figure 5.21 compares the performance of walnut particles in the three fractured discs. Walnut particles showed a good plugging performance in the 2000-micron fracture, where the differential pressure increased after 2 min, reaching up to 25 psi. In contrast, walnut particles failed to seal the 3000-micron and complex fractures. The differential pressure slightly increased to around 12 psi and remained constant until the end of the experiments. This low differential pressure confirmed that the walnut particles partially plugged the fractures without forming a solid bridge on the fracture opening. Fluid filtrate flow was also observed until the end of the experiments. This performance was mainly due to the uniform shape of walnut particles and no variation in their sizes. Figure 5.22 shows the formed bridge after the experiments with all fractured discs.

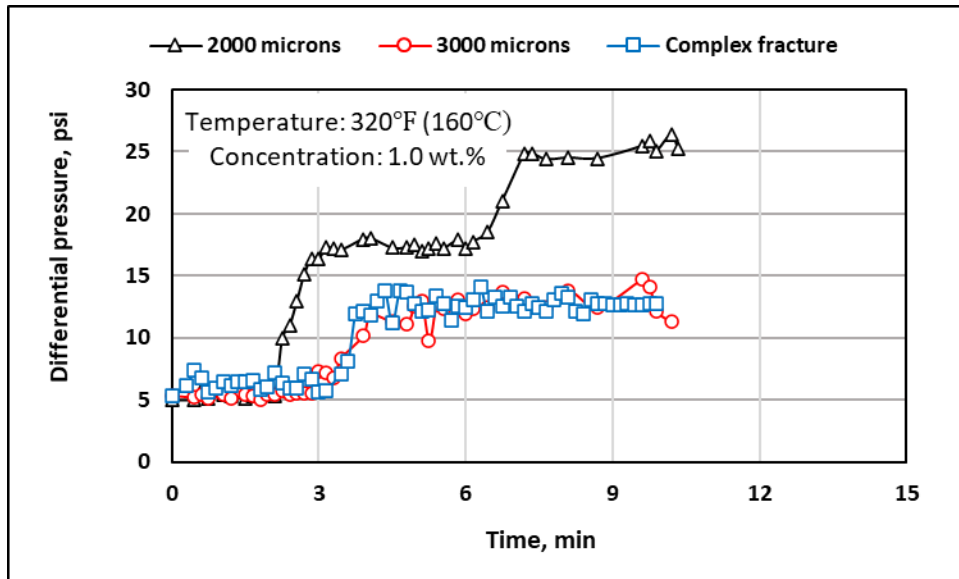


Figure 5.21: Sealing performance of walnut at different fracture sizes.

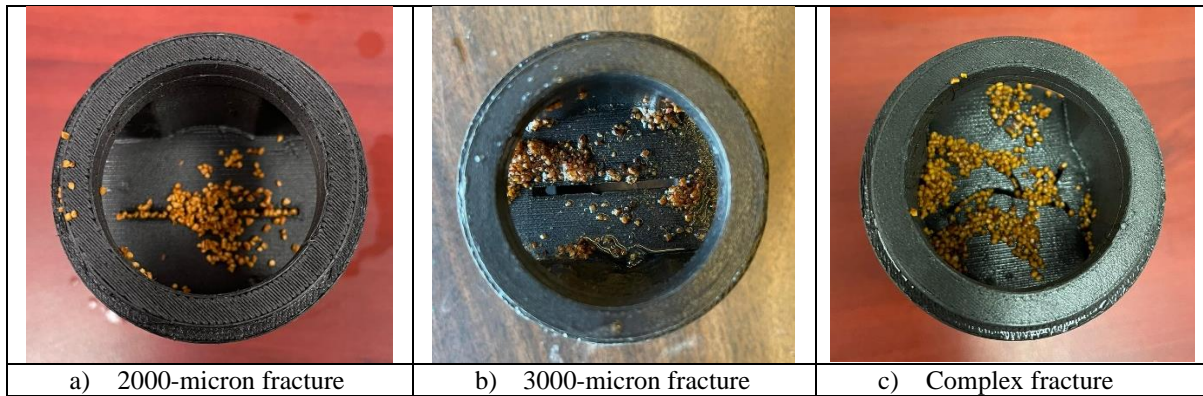


Figure 5.22: Fractured discs after the experiments with walnut.

5.5.3 Cedar Fiber

Cedar fiber performed better than calcium carbonate, where the differential pressure increased with time, confirming the plugging process. In all fractures, the pressure started to increase after around 3 min. Better performance of cedar fiber was observed in the 2000-micron fracture, and the differential pressure increased up to 22 psi compared to 17 psi in the 3000-micron fracture. Conversely, sudden drops and spikes in the differential pressure in the complex fracture were observed (Figure 5.23). These sudden changes are attributed to the bridging not being strong enough to hold the pressure. However, in all fractures, cedar fiber did not plug the fracture completely; as a result, filtrate flow was observed until the end of the experiments, indicating the fractures' partial plugging and the formation of a permeable bridge as shown in Figure 5.24. Blending fiber with other LCMs or introducing smaller particles are required to seal the pore space between fiber particles and improve the cedar fiber performance.

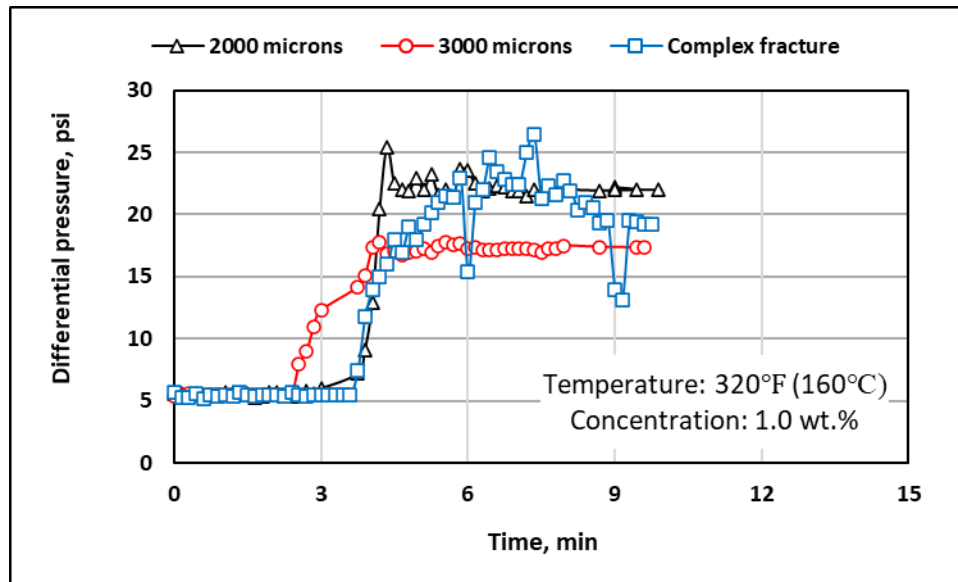


Figure 5.23: Sealing performance of cedar fiber at different fracture sizes.

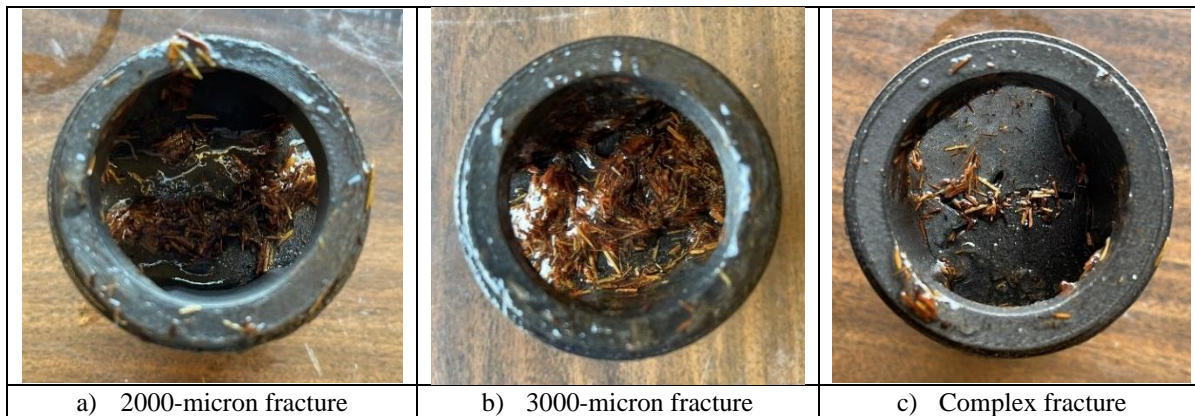


Figure 5.24: Fractured discs after the experiments with cedar fiber.

5.5.4 Shape Memory Polymer

As shown in Figure 5.25, SMP outperformed all other LCMs with a higher sealing pressure, and the fractures started to seal in a shorter time (around 1.5 min). SMP showed almost the same performance with the 2000-micron and 3000-micron fractured disc with slightly lower pressure for the 3000-micron fracture. Similarly, SMP was effective in sealing the complex fracture with a slight delay; the fracture started to seal after 3 min to reach a differential pressure of 27 psi at the end of the experiments. The longer it takes to seal the fracture, the more fluid will be lost to the formation; therefore, more cost for the lost fluid and more damage to the producing formation

(Adebayo and Bageri, 2020; Marx and Rahman, 2007). The captured videos and flowmeter readings showed that the filtrate flow stopped entirely after the fractures were sealed. The flow rate dropped down to zero, indicating the high sealing efficiency with SMP. Figure 5.26 clearly shows the seal created on the fractured discs by SMP particles. The excellent sealing performance of SMP with large and complex fractures can be attributed to the increase in particle size due to the thermal activation of SMP. Moreover, the wide range of SMP particle sizes improved the sealing efficiency. The large particles create the bridge on the fracture mouth, while the small particles plug the pore space between large particles and the fracture wall (Magzoub 2021).

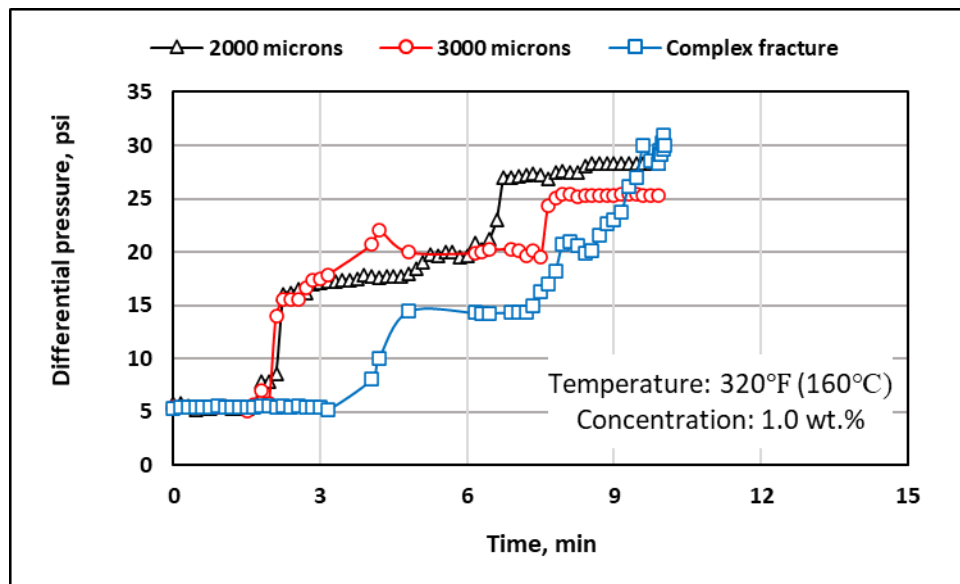


Figure 5.25: Sealing performance of shape memory polymer at different fracture sizes.

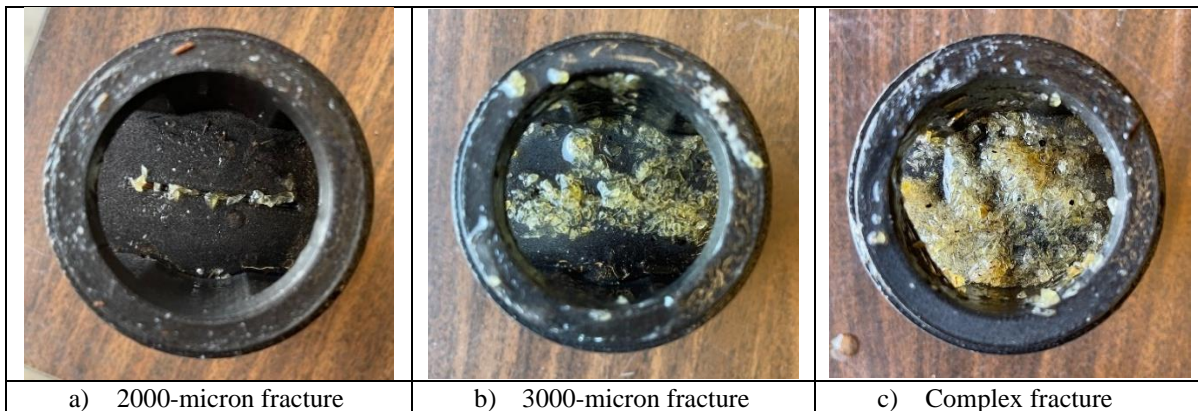


Figure 5.26: Fractured discs after the experiments with shape memory polymer.

5.5.5 Blend of Shape Memory Polymer and Cedar Fiber

To improve the performance of cedar fiber, it was mixed with SMP in a 25% to 75% ratio. The SMP and cedar fiber blend was tested on the 3000-micron and complex fractures. The SMP-fiber combination showed the best sealing integrity and efficiency (Figure 5.27). The differential pressure started to shoot up after around 2 min to reach the maximum differential pressure detected with the differential pressure transmitter, 30 psi. The maximum differential pressure was maintained with both fractures until they were plugged entirely, and the flow rate dropped to zero. This phenomenal performance is attributed to the complementary effects of the LCMs. The variety in sizes and irregular shape of SMP and long and thin particles of cedar fiber helped plug the fracture by forming a robust bridge of LCMs inside the fracture (Figure 5.28). Therefore, cedar fiber and SMP blends can potentially seal large and complex fractures in high-temperature and geothermal formations. However, more experimental studies are required to optimize the ratio of SMP to cedar fiber depending on the fracture size and shape to ensure optimal results in the field operations. These results also confirmed the findings of the previous study by Magzoub et al. (2021a, 2021b).

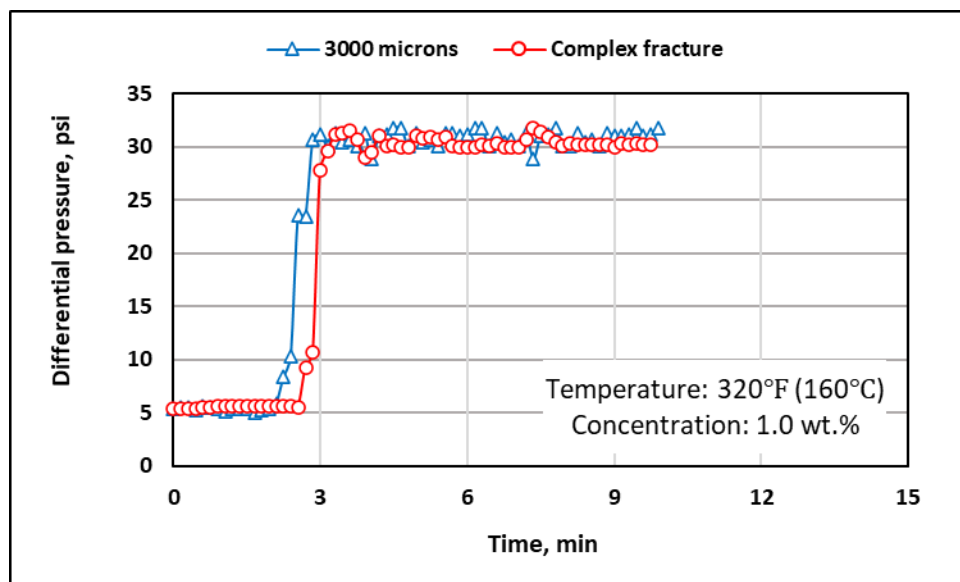


Figure 5.27: Sealing performance of SMP-fiber blend at different fracture sizes.

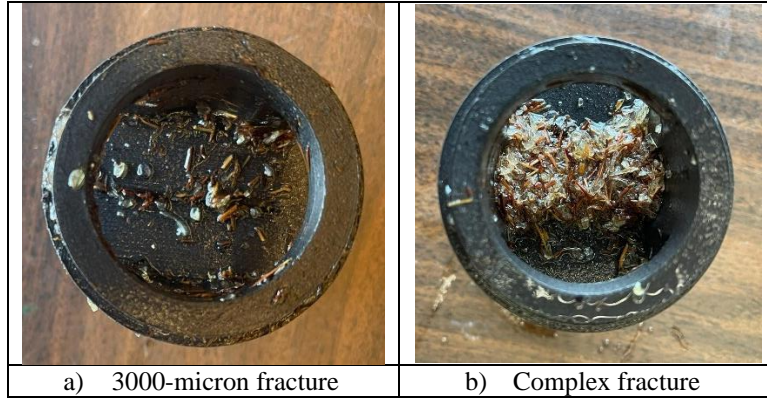


Figure 5.28: Fractured discs after the experiments with SMP-fiber blend.

Chapter 6: Computational Fluid Dynamics (CFD) Simulation Study

This chapter discusses the CFD model developed to simulate the annular flow of SMP-based mud and predict the settling behavior of SMP particles at high temperatures and under different experimental parameters. The method and assumptions made to develop the model are first discussed. Then, the findings from the CFD study are presented to assess the impact of experimental parameters on SMP transportation, and the prediction accuracy of the developed model is discussed.

6.1 Model Development and Assumptions

The experimental setup tested different lost circulation materials under high temperatures and various conditions by changing the concentration, annular velocity, inclination angle, and pipe rotational speed. Although the experimental setup was built on a large scale, the dimensions are still different from actual drilling operations. Additionally, this type of experiment is time-consuming and limited and requires large quantities of materials. Therefore, a simulation study was integrated with the experimental work to upscale the results and extend the findings to a broader range of operating parameters. The simulation study is a multiphase flow fluid dynamics study that aims to simulate and investigate the SMP dispersion and transportation by the drilling mud in the annulus under a broader range of operational parameters. Computational fluid dynamics (CFD) concepts were utilized to develop the model using Ansys Fluent software.

Several models describe multiphase flow phenomena, such as the Volume of Fluid model (VOF), the mixture model, and the Eulerian model. Each model is appropriate for a specific multiphase system and determining the best model to describe the multiphase system is the first step toward accurate predictions. The VOF model is suitable for stratified or free-surface flows, where the interface between phases is of interest. The VOF model solves a single set of momentum

equations shared by the fluids. On the other hand, the mixture and Eulerian models describe flows in which the phases mix or separate and when the dispersed-phase volume fraction exceeds 10%. The Eulerian model is the most complex because it solves many sets of momentum and continuity equations for each phase. The Eulerian model deals with each phase as an independent phase because the volume of each phase cannot be occupied by another phase. Then, the results are coupled through the pressure and interface exchange coefficients.

This study used the Eulerian model to simulate the multiphase flow of the solid phase (SMP) and the fluid phase (base mud). The Eulerian model was used because it is the most suitable model for granular flow. Additionally, based on the experimental results, the volume fractions of the dispersed phase (SMP) exceed 10% in some cases; thus, other models, such as the VOF model, are limited and would not yield accurate predictions. After selecting the multiphase model, the data were split into two sets depending on the flow regime. The few turbulent flow data points were excluded from the analysis because the drilling fluid flow in the annulus falls typically within the laminar flow region.

First, the analysis was performed on an annular section that matches the exact dimensions of the experimental setup. The geometry was created on Ansys SpaceClaim software and converted to ANSYS Meshing Software to generate the mesh. A mesh was generated on the geometry, and a sensitivity analysis was performed to optimize the mesh and ensure solution convergence. The mesh sensitivity analysis considered the mesh orthogonal quality, aspect ratio, skewness, and model prediction accuracy. After running the model, the experimental results were used to evaluate the CFD simulation model, validate the modeling results, and calculate the model prediction accuracy. The bed height data calculated from the experimental results were converted to volume fractions to be easier for comparison. After the model was validated, the model was run using a

larger scale and a wider range of parameters to predict the SMP performance under various operating conditions. Upscaling the results could be used as a robust tool to optimize the SMP dispersion in each well geometry, dimensions, and inclination to ensure efficient lost circulation treatment in field operations. Figure 6.1 describes the steps of conducting the CFD study.

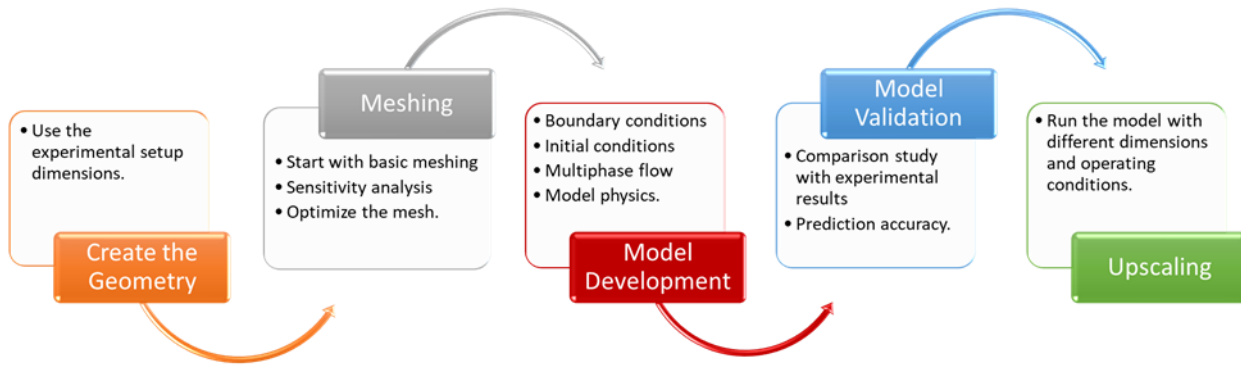


Figure 6.1: Workflow of the CFD simulation study.

The following assumptions were made to develop the CFD model, and some of these assumptions were validated with the experimental results:

- The SMP flow in the annulus is a viscous flow within the laminar flow regime
- The flow is transient
- Base fluid and SMP particles are incompressible (Pressure-based solver)
- SMP particles activate as soon as they get to the formation; thus, the SMP particles in the annulus are already activated and have the particle size obtained from the experimental results.
- The SMP particles have a uniform and spherical shape
- At the inlet, the SMP particles flow with the same annular velocity as the base fluid
- There is no backpressure at the outlet of the test section
- No slip at the inner and outer wall for both liquid and solid particles

- The deposited bed observed from the view ports is uniform and has the same height along the test section.

6.2 Geometry and Mesh Independence Study

A structural mesh was used in this study because it yields high accuracy of predictions. For validation, the geometry used in this study matches the experimental setup dimensions. The geometry was divided into several sections to generate the structural mesh easily. Figure 6.2 shows an example of the mesh used in this study. The structural mesh consists of uniform grids across the annular section because all annular section is of interest. After building the geometry and developing the model, a sensitivity analysis was performed to optimize the mesh size and ensure a converged and accurate solution independent of the mesh size. First, the model convergence was determined by monitoring the solution residuals of each phase's momentum, pressure, and velocity. To ensure accurate results, the convergence state was set when all residuals were equal to or less than $1e-5$. Figure 6.3 shows an example of converged (6.3a) and diverged (6.3b) solutions.

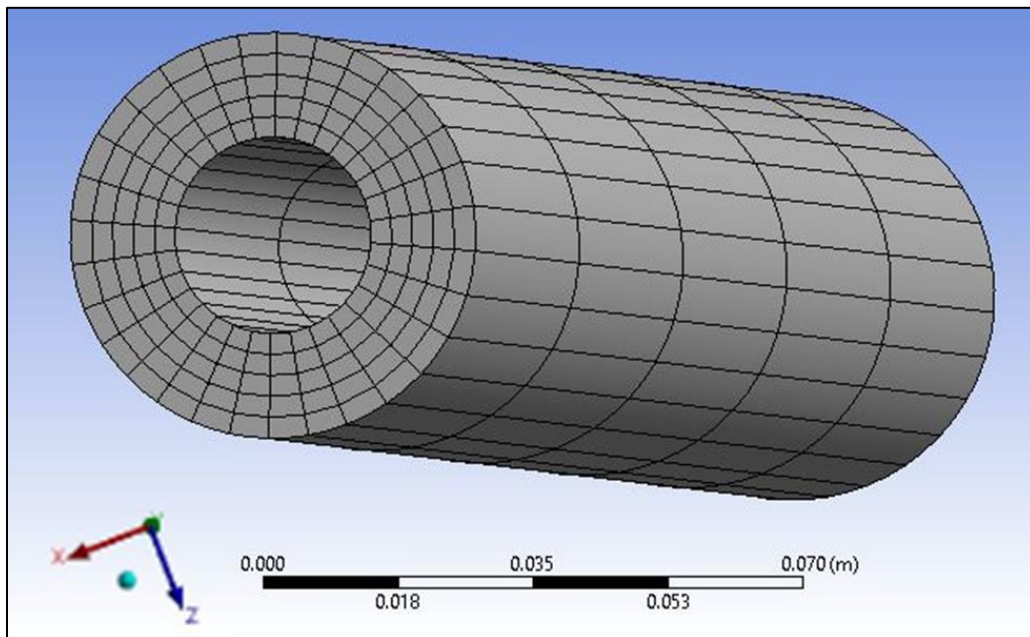


Figure 6.2: Quadratic structural mesh used in this study (Average orthogonal quality: 0.996).

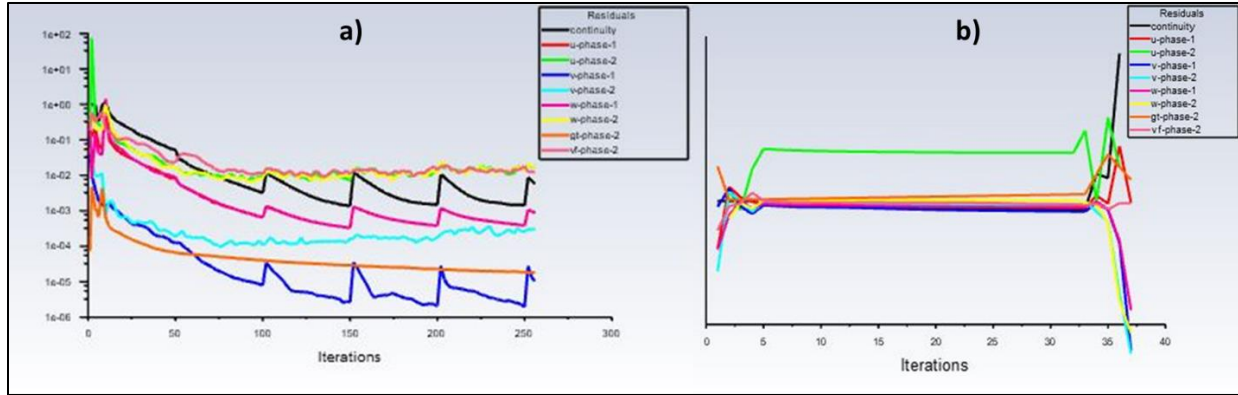


Figure 6.3: Example of a) converged solution (residual $\leq 1e-05$) and b) diverged solution (residual $\gg 1e-05$).

The mesh-independence study was conducted to investigate the sensitivity of the model results to the mesh size. Four different mesh sizes were evaluated in this study. Table 6.1 shows the specifications of each mesh size. The results revealed that the SMP volume fraction is independent of the mesh size above 72,000 elements. The mesh with 72,000 elements was selected as the optimum mesh size. Finer mesh sizes would require more computational time without any significant improvement in the model accuracy. The optimized mesh had an average orthogonal quality of 0.9986, an aspect ratio of 300.7, and an average skewness of 3.3546e-002.

Table 6.1: Specifications of the different mesh sizes tested in this study

No	Elements	Nodes	Average Skewness	Average orthogonal quality	SMP vol. %
1	250	1320	0.20023	0.95072	15.21
2	16,000	68,880	5.0214e-002	0.997	9.01
3	72,000	300,720	3.3546e-002	0.99864	7.13
4	90,000	374,520	3.3545e-002	0.99864	7.1

6.3 Model Performance and Accuracy

In this section, the model was run at different conditions to evaluate the effect of various operational parameters on SMP transportation in the annulus at 160°C (320°F). These operating parameters are annular velocity, pipe rotational speed, and inclination angle. The range of experimental parameters used in this section matches the experimental data to validate the model.

3.0 wt.% concentration of SMP was used because it gave various results and a wide range of volume fractions and bed height to validate the model. While 1.0 wt.% concentration showed good dispersion, no bed was observed in all testing conditions.

The experimental data was converted from bed height to volume fraction to validate the model and quantify the prediction accuracy. Figures 6.4 compares the experimental data with those predicted with the developed CFD model at different annular velocities, pipe rotational speeds, and inclination angles, respectively. The data was captured at the viewport location of the experimental setup because the experimental setup only allows detecting the bed height in that particular location. The figures show that the CFD model yielded a good match with the localized experimental data obtained from the viewport with an average absolute percentage error (AAPE) ranging between 5-12%.

After validating the model with localized experimental data, the model was used to determine the solid particle distribution along the annular section and fill the experimental gap. Figure 6.5 shows the effect of annular velocity (mud circulation rate) on the SMP transportation and volume fraction distribution across the main test section. This data was generated using the developed CFD model. As shown in the figure, the SMP particles accumulate at a low circulation rate, forming a solid bed. The volume fraction distribution shown in Figure 6.5a was obtained at the exact location of the viewport to compare the modeling data with the experimental data. Due to the gravity effect, the solid particles' concentration increased with the Z direction. As the circulation rate (annular velocity) increased, the SMP particles' dispersion improved and fluid flow helped erode the deposited bed. This performance was also observed with the experimental data. A minimum annular velocity of 0.2 m/s was required to maintain an excellent solid dispersion and ensure most SMP particles could get to the fracture and stop the mud losses.

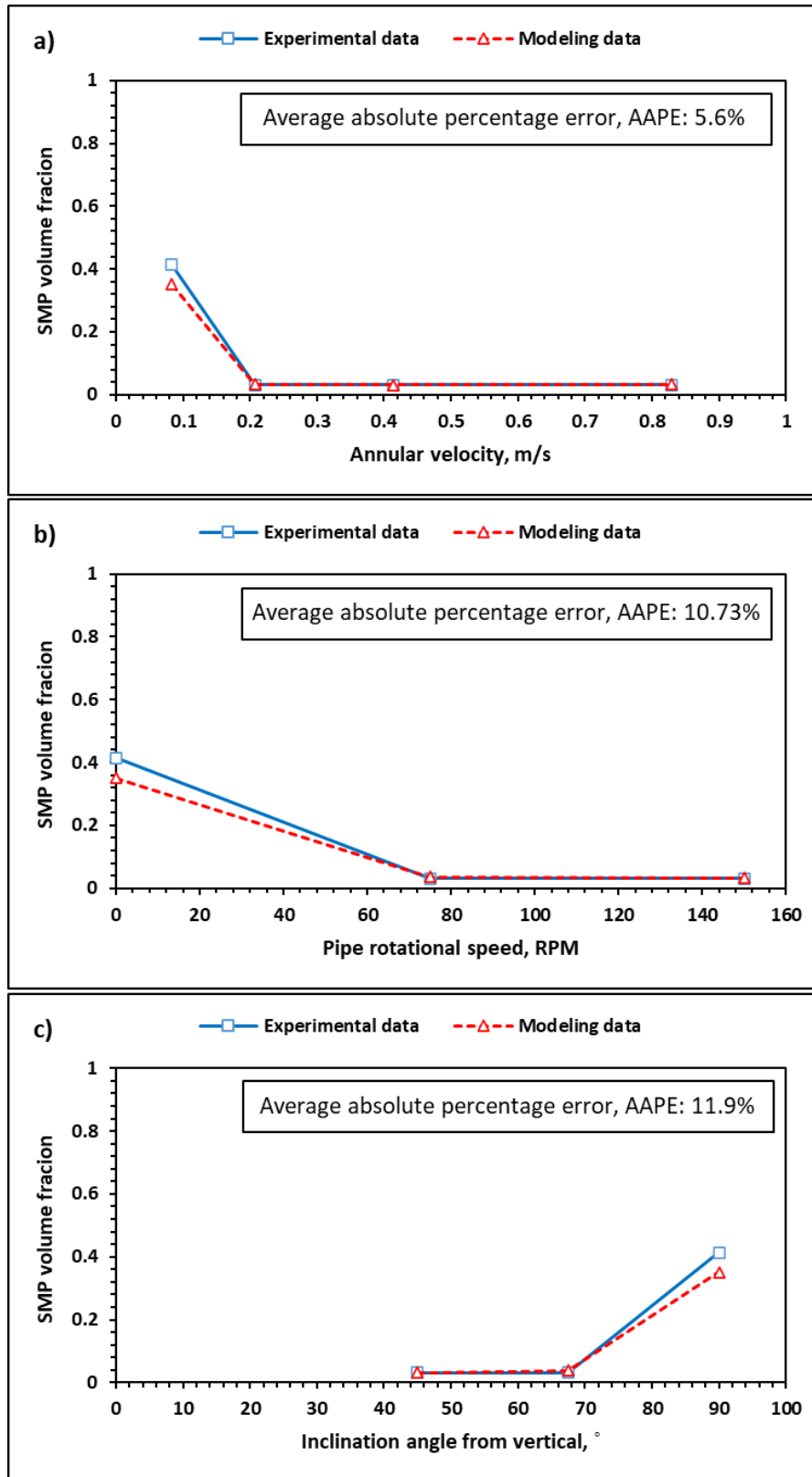


Figure 6.4: Modeling vs. experimental data at the viewport location under different: a) annular velocities, b) pipe rotational speeds and c) inclination angles.

However, Figure 6.5b illustrates the SMP volume fraction distribution along the annular section. It can be seen that the deposited bed did not have a uniform height in all locations. Therefore, the experimental setup has some limitations that it cannot give a complete insight into the solid particle distribution along the annular section because the visualization data were only obtained from the viewport location. Due to the temperature, pressure, and safety limitations, the annular section cannot be transparent in all locations. Thus, coupling the experimental and modeling data would give a better and more comprehensive view of the SMP transportation in the annulus.

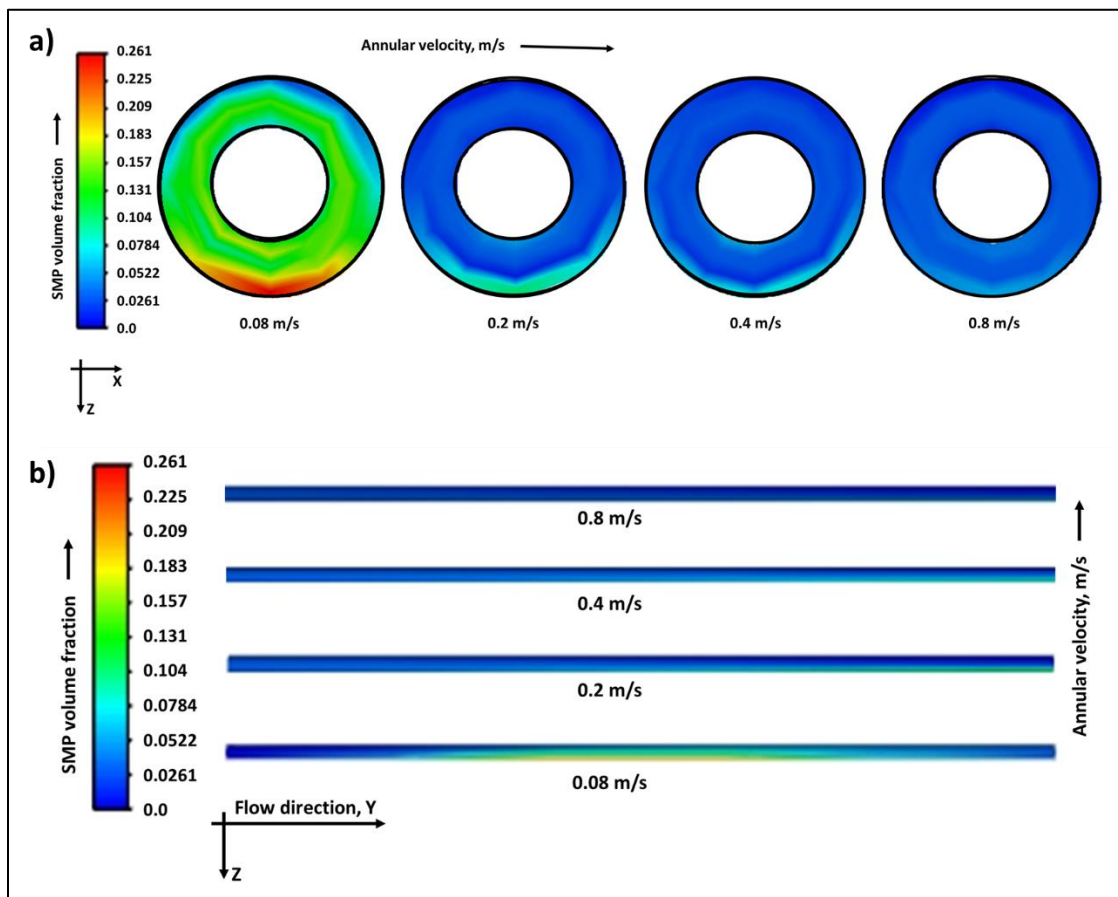


Figure 6.5: Effect of annular velocity on SMP transportation at 160°C (3.0 wt.%).

Figure 6.6 illustrates the impact of pipe rotation on SMP dispersion at high temperatures. The modeling data was also found in a good match with the experimental results. The SMP

transportation was significantly improved when using the drill pipe rotation. A rotational speed of 75 RPM was adequate to disperse SMP particles and erode the bed formed at 0 RPM rotational speed.

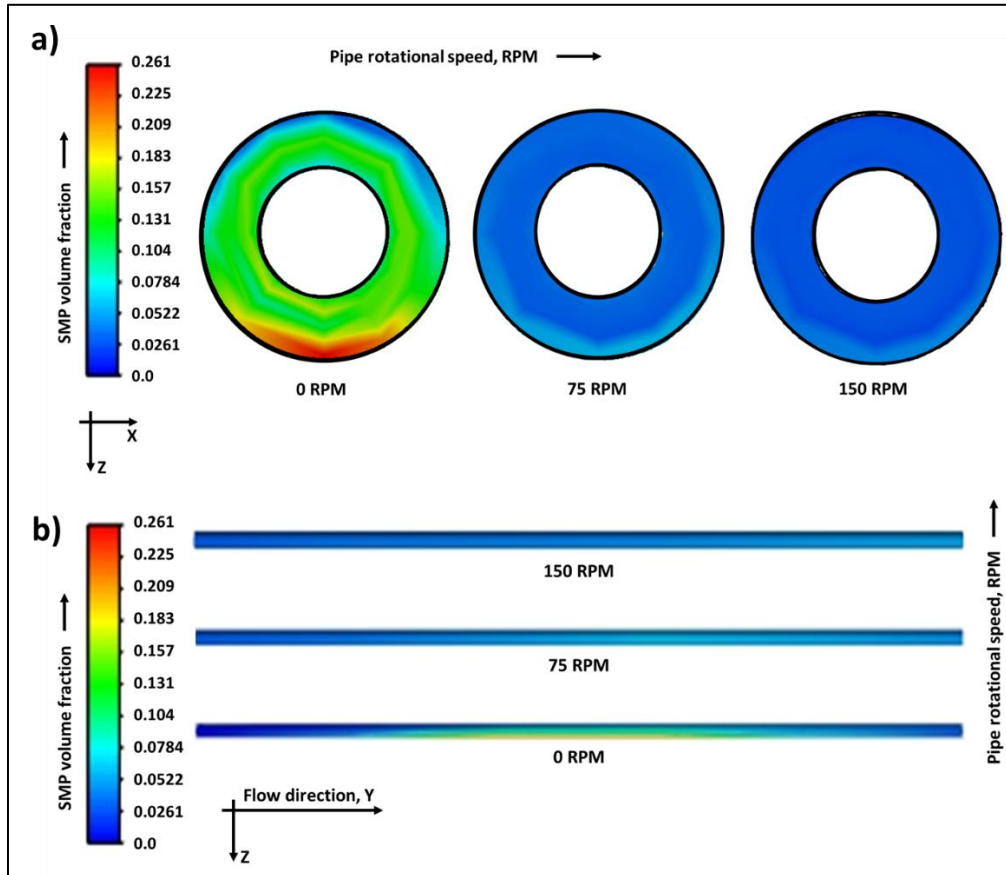


Figure 6.6: Effect of drill pipe rotation on SMP transportation at 160°C (3.0 wt.%).

In contrast, the CFD model showed interesting findings with the inclination angle, Figure 6.7. Figure 6.7a shows the localized SMP particles' distribution in the annular cross-section at the exact location of the viewport. These results indicated that as the inclination angle from vertical decreased, the SMP suspension improved, and no bed formed at both 45° and 67.5° from vertical. These findings were also observed with the experimental data. However, looking into the full SMP distribution along the experimental section (Figure 6.7b) highlights the limitation of the experimental setup. A solid bed was formed at a 67.5° inclination angle far from the viewport

location that the experiments could not detect. Thus, relying on experimental data only to predict the SMP settling behavior would give misleading results. The model was run for enough time until the results were stable to ensure that the bed height and location detection are accurate and based on solid predictions.

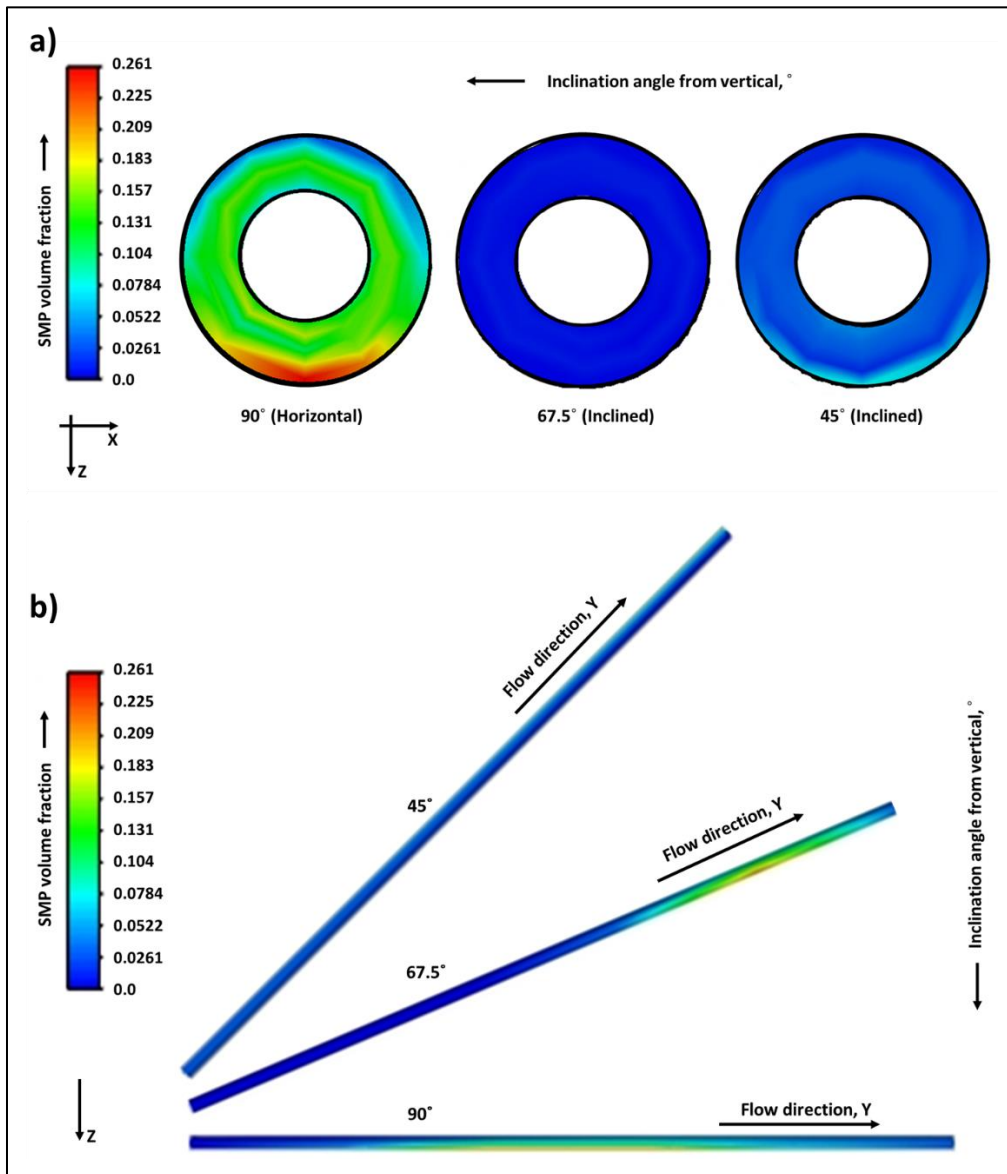


Figure 6.7: Effect of inclination angle on SMP transportation at 160°C (3.0 wt.%).

Therefore, assuming a uniform bed height across the annular section to extrapolate the experimental data obtained from the viewport would not be valid and thorough modeling

investigation should be conducted to fill in the experimental gap. Figure 6.8 shows the huge error that might result in bed height prediction when assuming a uniform bed height along the annulus. The AAPE increased from 5-12% to 22-70%. This high error is not because of the prediction accuracy of the CFD model but rather because the assumption of a uniform bed was invalid. Therefore, the CFD validation with the localized bed height was successful with an acceptable error (5-12%), and coupling the experimental and modeling data would give accurate SMP settling behavior predictions. These predictions can be upscaled to field dimensions using the validated CFD model to optimize the SMP transportation and ensure successful lost circulation treatments.

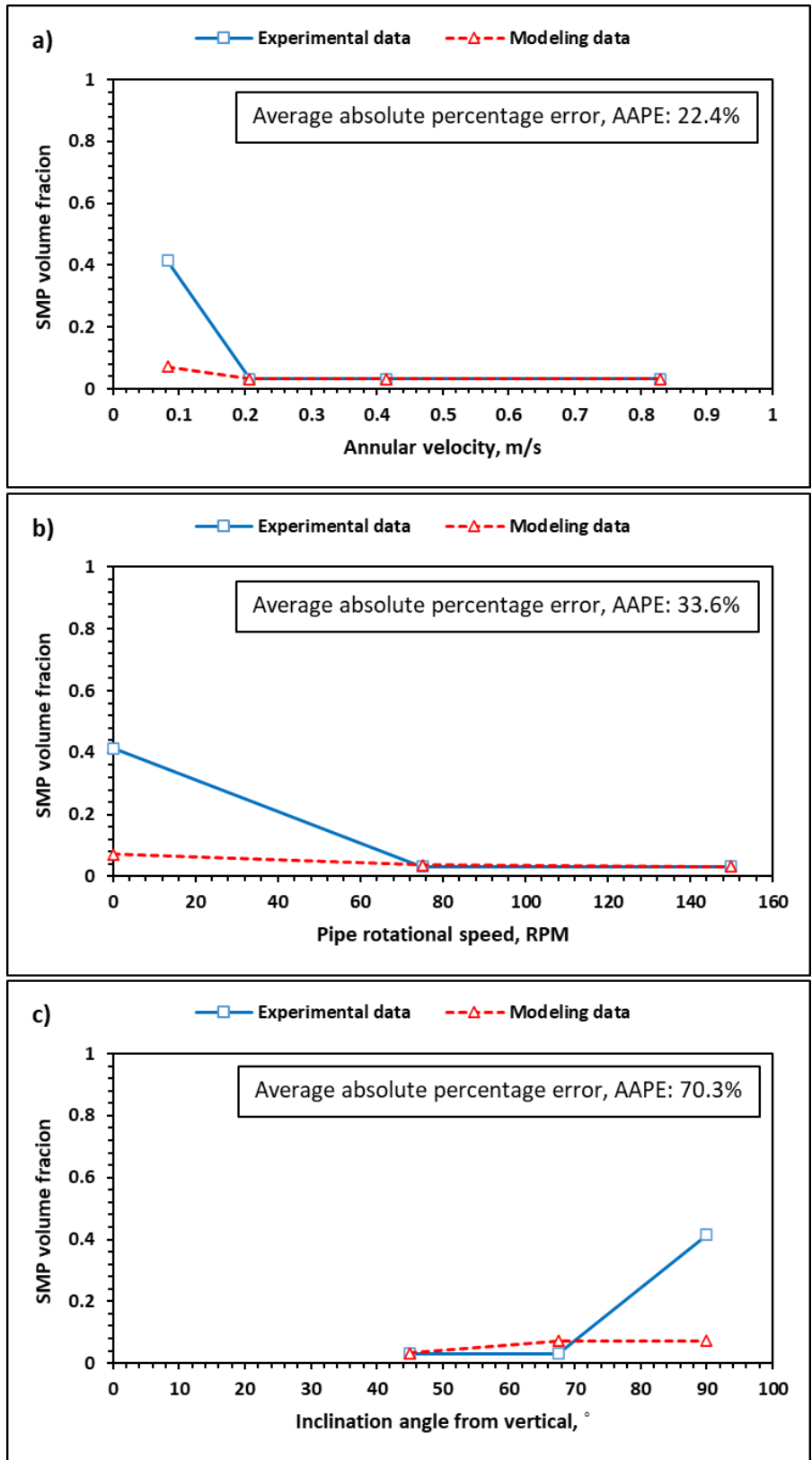


Figure 6.8: Modeling data vs. extrapolated experimental data under different: a) annular velocities, b) pipe rotational speeds and c) inclination angles.

Chapter 7: Environmental and Economic Feasibility Analyses of Different LCM

7.1 Environmental Analysis

As discussed in previous chapters, selecting the optimal LCM and optimizing the mud formulations are vital in lost circulation treatment. The LCM type, shape, particle size distribution, physical and chemical properties, and concentration are crucial and significant factors that should be considered in the selection criterion. However, in field operations, other aspects need to be considered in lost circulation treatment, such as availability, economics, and environmental impact of LCMs (Al-Hameedi et al., 2020). The optimum LCM should have a high success rate in field operations, economical price, and minimal effect on the health and environment. Thus, researchers and engineers continuously look for better mud formulations that combine all these aspects.

As discussed in Chapter 4, many conventional and unconventional solutions have been introduced to solve the lost circulation problems. These solutions include adding natural or synthesized, organic or inorganic, solid or gel, and inert or reactive materials to the drilling fluid formulations to plug the fractured formations and stop the losses. These materials' health and environmental impact are mainly due to manufacturing, handling, and waste disposal.

The environmental impact of waste disposal varies with the amount of disposed waste, type of disposed waste (oil-based or water-based), and the nature of the disposal area (offshore or onshore). Several waste disposal methods are controlled and monitored by the regulatory health and environment organizations. These methods include: 1) traditional solid control, 2) injection into safe formations, 3) fluid ejection, 4) separation into clean solids and clean liquids, 5) distillation and fixation, 6) incineration, 7) solids encapsulation, 8) microorganisms processing and 9) removal to off-location disposal sites (Nesbitt and Sanders, 1981).

Measuring the degree of toxicity is the standard technique to assess the environmental impact of drilling fluids (Onwukwe and Nwakaudu, 2012). Toxicity tests investigate the effects of substances on living organisms under controlled lab conditions in the short and long terms. There are different ways to conduct these tests, either animal-based or nonanimal-based (Theodorakis, 2005). The drilling fluid's environmental impact on marine life is evaluated by performing the shrimp bioassay test. Shrimps are placed inside a treatment tank full of seawater with different concentrations of mud waste. Daily observations such as irritability, erratic movement, broken appendages, and mortality are recorded. The mortality rate of shrimp is recorded when exposed to drilling mud sediments in seawater.

This work evaluates an unconventional smart material to treat lost circulation events in geothermal formations. This smart material is a thermoset shape memory polymer (SMP) with a temporarily deformed shape and is activated with formation temperature. Once activates, SMP particle size increases and restores its original shape and size. The SMP performance was compared to some conventional LCMs commonly used in lost circulation treatments. These conventional materials are calcium carbonate, cedar fiber, and walnut. This section will discuss the health and environmental impacts of these conventional and unconventional materials.

7.1.1 Calcium Carbonate (CaCO₃)

Calcium carbonate is a noncombustible odorless material commonly used as bridging and lost circulation material with drilling fluid. It occurs naturally in different forms but commercially in aragonite (2.83 g/cc) and calcite (2.71 g/cc) forms. Calcium carbonate is insoluble in water and alcohol; however, it dissolves in acids and generates carbon dioxide. Irritations are the main environmental and health issues of calcium carbonate. According to the US Department of Health and Human Services (HHS), moderate-to-severe irritation would result when the tissues of animals

are exposed to calcium carbonate. Calcium carbonate dust also impacts the human eye, nose, and skin. Calcium carbonate dust causes eye redness and pain, moderate skin irritation, sneezing, coughing, and nasal irritations (HHS, 1995).

The primary source of exposure to calcium carbonate is through direct contact or inhalation during the mixing and preparation of drilling muds. According to the Occupational Safety and Health Administration (OSHA), 15 mg/m³ of air and 5 mg/m³ respirable fraction as an 8-hr time-weighted average is the allowable exposure limit to calcium carbonate. Exposure to higher concentrations is considered hazardous, and immediate medical attention should be taken. According to the US Environmental Protection Agency (EPA), calcium carbonate is not subject to the emergency planning requirements, and there is no reportable quantity for disposing of calcium carbonate. Moreover, according to the resource conservation and recovery act, calcium carbonate is not listed as hazardous waste (HHS, 1995).

However, general safety precautions and regulations must be considered when dealing with calcium carbonate. Calcium carbonate should be stored in a dry and well-ventilated area away from acids, heat, hydrogen, mercury, and ammonium salts. Proper protective clothing and equipment are required to handle calcium carbonate to avoid health issues.

7.1.2 Cedar Fiber

Cedar fiber is produced as a by-product of the essential cedar oil extraction and cedarwood manufacturing. The remaining fiber has been primarily used in the oil industry as lost circulation material. Due to its drag reduction property, fiber is also used in the sweep drilling fluids to aid the hole cleaning process in oil and gas wells drilling (George et al., 2012). Like other natural substances, cedar fiber has minimal impacts on health and the environment. Cedar fiber is non-toxic, biodegradable, and environmentally friendly. Manufacturing fiber produces much fewer

toxins and greenhouse gasses than other human-made materials. However, the only concern with using cedar fiber in lost circulation treatment is that the fine powder produced with fiber particles may cause eye and respiratory irritation to the rig crew. Therefore, safe handling with proper protective equipment is recommended when mixing and preparing the LCM pill.

7.1.3 Walnut

Walnut is one of the primary sources of nut-based LCMs that can be mixed with drilling fluid to treat mud losses. Walnut has higher compressive strength compared to Pecan. It can be used in different concentrations and sizes and can be mixed with other materials to provide variety in shapes and sizes to ensure a better sealing efficiency. The walnut particle size and concentration are selected depending on the loss severity and formation type.

Walnut shell is a natural organic material and is not subject to Toxic Substance Control Act (TSCA) requirements; therefore, it is non-hazardous to humans and animals. However, the black walnut trees produce juglone in all their parts. This chemical is toxic to some plants and inhibits the growth of juglone-sensitive plants nearby. Because roots can release juglone, toxicity may occur for many years after tree removal. Brown walnut also produces juglone but in much lower concentrations; thus, it does not impact juglone-sensitive plants.

Like other mud additives, walnut should be handled appropriately to avoid health issues. The generated dust may cause eye irritation and respiratory tract irritation if inhaled. Therefore, proper eye and respiratory protection are required when dealing with walnut to avoid direct contact. It should be stored in an open, ventilated area away from heat and flames.

7.1.4 Shape Memory Polymer (SMP)

SMP is a smart polymer that can be programmed to a temporarily deformed shape and return to its original form under certain conditions using external stimuli. SMP can be triggered by different

mechanisms in the activation process, such as pH change, light, temperature, magnetic field, and electric field. SMP has been widely used in many applications such as textiles, aerospace, biomedical devices, energy, and other engineering applications (Meng and Li, 2013). However, the application of shape memory polymer in drilling operations to cure mud losses has been introduced recently (Mansour et al., 2017).

Different structures and materials have been used to develop SMPs in laboratories and on large scales, such as polyurethane, aliphatic polyurethane, UV curable polyurethane, epoxy-based SMP, and polystyrene-based (Meng and Li, 2013). All these materials are used widely in daily life products and are harmless. Polyurethane is safe, biodegradable, and environmentally friendly and is used in almost every product. It is used in building insulation, furniture, coatings, automotive, clothing, and other applications. It is chemically inert (Dernehl, 1966), and according to OSHA, there is no exposure limit or carcinogenicity hazards. However, polyurethane is combustible and produces toxic gases when exposed to flames; thus, it must be treated with flame retardants in case of fire (McKenna and Hull, 2016).

Polystyrene is a synthetic aromatic hydrocarbon polymer that can be foamed or solid. It is one of the commonly used plastics; several million tonnes are produced yearly. According to ASTM standards, polystyrene is non-biodegradable. It accumulates as environmental litter, especially along shores and waterways (Kwon et al., 2014). Biodegradation of waste polystyrene takes centuries (Bandyopadhyay and Basak, 2013), and it impacts the health of birds or marine animals when significant quantities are swallowed (Hofer et al., 2008). However, according to the American Chemistry Council (ACC) and Hong Kong Food and Environmental Hygiene Department, polystyrene is safe for food service products (ACC, 2010). Therefore, polystyrene's primary health and environmental impact is the waste disposal that would impact the bird and

marine life. Incineration is an effective method for polystyrene waste disposal. Only around 1% of the starting volume will remain when modern facilities are used for incineration.

However, the SMP used in this study is a thermoset epoxy-based SMP. This type of SMPs is well known for its thermal stability, chemical resistance, and high mechanical properties (Mather et al., 2009). SMP was prepared by mixing a commercial epoxy resin (EPON 826) with an isophorone diamine (IPD) crosslinker, with a ratio of 100 g to 23.2 g, in a mechanical blender. After achieving the thermoset network, the SMP was programmed by heating at 320°F and applying mechanical load; then, the programmed SMP was crushed into small particles to use as LCM. Therefore, to assess the environmental impact of SMP, we should refer to its main components; epoxy resin and IPD.

Epoxy resins are widely used in paints, metal coatings, adhesives, electronics, electrical insulators, plastics, and other purposes. Epoxy resin's health and environmental issues are mainly associated with its handling and manufacturing. Respiratory problems, allergic reactions, and contact dermatitis are the primary health risks of epoxy resins. These risks are due to some of the hardeners used in resin manufacturing, not the resins themselves. For instance, aromatic amine hardeners are corrosive, toxic, or carcinogenic; thus, their use is now restricted. However, other safe hardeners exist, such as aliphatic or cyclo aliphatic amines. Solid resins are non-hazardous substances and safer than uncured (liquid) resins. Uncured epoxy resins are toxic to aquatic life and cause eye and skin irritation and allergic reactions (Spee et al., 2006). Allergic reactions may occur after several days of exposure in the form of dermatitis. The sensitization risk is more evident in low molecular weight epoxy resins (Tavakoli, 2003).

On the other hand, isophorone diamine (IPD) is classified as hazardous according to the 2012 OSHA Hazard Communication Standard (29 CFR 1910.1200). It causes skin burns, allergic

skin reactions, and eye damage. It is also considered harmful to aquatic organisms with long-lasting impacts. Therefore, like other chemicals, proper protective equipment should be worn when handling IPD. IPD should be stored in a cool, dry, and ventilated area in locked containers.

Therefore, SMP's primary health and environmental impact are associated with manufacturing and handling its main components. As reported in previous studies, SMP is biodegradable and non-toxic to aquatic life (Mansour et al., 2017). Moreover, various materials can be utilized to develop safe and eco-friendly types of SMP with good mechanical and chemical properties to cure mud losses in drilled formations with different downhole conditions.

7.2 Economic Feasibility Analysis

Lost circulation is considered one of the challenging events faced during drilling operations (Alkinani et al., 2019). It introduces many issues to the drilling fluid and increases the drilling time and cost. Huge revenues are spent on treating lost circulation events due to the high price of lost drilling fluids and the prolonged drilling time to treat the mud losses. For instance, curing mud loss events in the Gulf of Mexico was responsible for more than 10% of the non-productive time (NPT) between 1993 and 2003. Around 10-20% of the geothermal well cost in the United States is spent on lost circulation treatment (Lavrov, 2016). Therefore, considering the cost of lost circulation is vital to minimize the drilling cost and increase the economic feasibility of geothermal projects. The drilling mud and LCM price vary depending on the drill mud system and LCM type. For instance, according to US Environmental Protection Agency (EPA) reports, one barrel of water-based mud, oil based-mud, and synthetic-based mud costs around \$45, \$75, and \$200, respectively.

This research evaluates four types of conventional and unconventional LCMs in treating lost circulation events in geothermal formations. These LCMs are calcium carbonate, cedar fiber, walnut, and shape memory polymer. The economic feasibility study compares the cost of four

LCM formulations per barrel. In this study, all LCM pills use water as base fluid and 3.0 lb/bbl of synthetic hectorite clay to maintain the viscosity of the LCM pill. Then, different concentrations of the lost circulation materials are added to the formulation based on their recommended concentration to treat severe mud losses. Therefore, the LCM type is the only factor that affects the pill cost. The recommended concentrations are based on laboratory and field studies. Table 7.1 shows the cost and recommended concentrations of the four LCMs used in this study. SMP is one of the recent advances in lost circulation treatment. Previous studies evaluated the SMP performance in laboratory scale and no field trial or mass production took place. Therefore, no price estimation is available in the literature for SMP as lost circulation material. However, shape memory polymers are well known for their low cost in different applications and uses. In this study, SMP cost was roughly estimated using the available SMP-based products made from the same manufacturing materials. Currently, the SMP price ranges between 0.85 to 1.05 \$/lb. Prices of other LCMs are averaged from various suppliers in the geothermal industry.

Table 7.1: Price and recommended concentrations of different LCMs for severe mud losses

LCM type	Concentration (lb/bbl)	Price (\$/lb)
Calcium carbonate	55	0.2
Cedar fiber	10-30	0.4
Walnut	5-25	0.5
SMP	10-22	0.85-1.05

Figure 7.1 compares the cost of SMP with other conventional LCMs (calcium carbonate, cedar fiber, and walnut). All LCMs are added in their recommended concentrations. LCMs cost varies slightly with the LCM type, which ranges between 11 and 12.5 \$/bbl. Although calcium carbonate is very cheap compared to other LCMs, its total cost was close to other LCMs because higher concentrations are required in the lost circulation pill. Cedar fiber and walnut come in second place, costing 12 and 12.5 \$/bbl, respectively.

In contrast, SMP showed the highest cost among other LCMs ranging between 18.7 and 23.1 \$/bbl (average of 20.9 \$/bbl). However, SMP is a new lost circulation product, and there is no commercial production for field applications. The price of SMP used in this study is based on the cost of other SMP-based products made from the same manufacturing materials but at a smaller production rate and small-scale manufacturing. Therefore, despite the relatively close cost of SMP to other LCMs, its price is expected to reduce with the mass production for such applications, especially with the high sealing efficiency observed in all previous studies. While, using conventional LCMs may require more than one field trial to treat losses which increases the total treatment cost, making it less feasible than efficient LCMs like shape memory polymer. Moreover, blending SMP with other conventional LCMs can reduce the cost further and increase the sealing efficiency, as observed with cedar fiber. Mixing SMP with cedar fiber (75% to 25%) reduced the average LCM cost from 20.9 to 18.7 \$/bbl, while it showed better sealing performance than SMP alone. Therefore, optimizing the SMP-fiber blend ratio would also help reduce the cost of lost circulation treatment with better results in field operations.

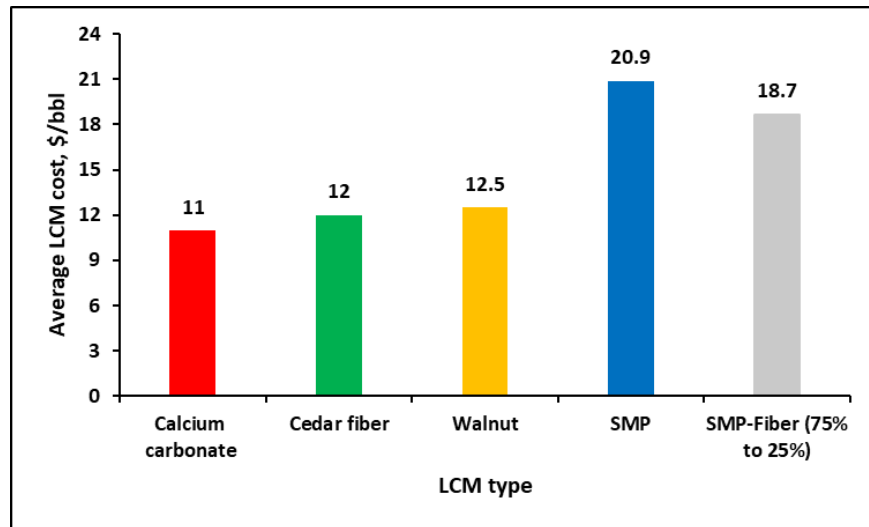


Figure 7.1: Cost of shape memory polymer compared to conventional LCMs.

Chapter 8: Summary, Conclusions, and Recommendations

8.1 Summary

This dissertation discussed the lost circulation issue encountered while drilling geothermal wells. The weak nature of geothermal formations and the existence of large and complex fractures increased the urge for efficient lost circulation materials (LCMs) and methods to mitigate the lost circulation events and the associated challenges. This study evaluated a smart lost circulation material on a large scale and at high-temperature conditions to treat mud losses in geothermal formations. The experimental evaluation was performed using a novel flow loop, considering a broad range of experimental parameters affecting lost circulation treatment and drilling operations. The performance of the smart polymer was evaluated by studying the activation, rheology, wellbore hydraulics, transportation, and fracture sealing efficiency. This smart LCM was also compared with other conventional LCMs such as calcium carbonate, cedar fiber, and walnut. The work also included economic feasibility and environmental analysis of the different lost circulation materials. A computational fluid dynamics study was conducted and validated with the experimental results to upscale the experimental data and predict the settling performance of the smart LCM under a broader range of operational parameters. This computational study is a robust tool to help optimize the lost circulation treatment and ensure successful field implementation.

8.2 Conclusions

The smart material has a great potential to treat lost circulation in geothermal wells where most conventional LCMs fail or cause other complications. Based on the obtained results, the following conclusions can be drawn:

1. The smart polymer activates at the designed downhole temperature (above 150°C), increasing its particle size by 80-100%. This activation feature gives the shape memory

polymer the potential to seal large and complex fractures with minimal risk of plugging downhole tools.

2. The base fluid used in this study is non-Newtonian fluid with high shear-thinning behavior that is favorable in drilling operations.
3. The smart LCM increased the shear-thinning behavior by decreasing the flow index (n) of the base fluid to 0.0247-0.0605. SMP showed minimal impact on fluid viscosity and frictional pressure losses, giving a wide range of concentrations to optimize the lost circulation treatment.
4. The settling performance of lost circulation materials varies in the same conditions depending on the shape, density, particle size, and interactions with drilling fluid.
5. The new LCM has superior transportation performance compared to the other conventional materials. Accumulated solids with a bed height of 40-50% of the annular section were observed only at a horizontal inclination, high concentration (3.0 wt.%), and at a very low circulation rate (2 gpm) without pipe rotation (0 RPM).
6. Pipe rotation and circulation rate effectively dispersed LCM particles and eroded the formed bed. Optimizing these operational parameters is essential for better LCM dispersion and thus better sealing efficiency.
7. Maintaining a pipe rotational speed of 75 RPM or an annular velocity of 40 ft/min was adequate to ensure excellent transportation of the smart polymer (3.0 wt.%) at all testing conditions with no solid particles accumulating in the test section. At the same time, pipe rotation and increasing circulation rate were unnecessary with low SMP concentration (1.0 wt.%).

8. High rotational speeds (150 RPM) and annular velocity (above 80 ft/min) were required to disperse cedar fiber and walnut particles and remove the deposited bed.
9. The inclination angle was found very significant in carrying and transporting all LCMs. LCMs showed better dispersion in inclined sections than in horizontal sections. As the inclination angle from vertical decreased, solid deposition became less likely. This performance was because the vertical velocity component increases with the inclination angle decrease, reducing the gravity effect.
10. Lost circulation materials performed differently in various fracture sizes and complexities. Calcium carbonate was ineffective in sealing large and complex fractures in geothermal wells due to their fine uniform particles. It failed to form a sealing bridge on all tested fracture sizes, and high fluid filtrate resulted.
11. Walnut and cedar fiber work better than calcium carbonate in sealing large fractures, and they can seal the fractures partially. A wider range of particle sizes is required to improve their sealing performance.
12. Shape memory polymer outperformed the conventional LCMs in sealing large and complex fractures. The different fractures were plugged entirely, and filtrate flow stopped in around 2 minutes with higher differential pressure than other LCMs.
13. Blending shape memory polymer and cedar fiber (75% to 25%) yielded the highest sealing efficiency (differential pressure). It improved the performance of both cedar fiber and SMP, which can also help reduce the cost of lost circulation treatment. This performance is mainly due to the variety in particle sizes and shapes that can form a more robust bridge on the fracture.

14. A CFD model was developed to study and predict the settling performance of the smart material under different operational parameters. The CFD model matched the localized bed height observed in the viewports with an error of less than 10%. The error increased to more than 20% because of the limitations of the experimental setup that cannot give complete insight into the bed distribution along the test section.
15. Combining the CFD model and experimental data provided a better understanding of the smart LCM's settling behavior. The CFD model can generate a good distribution of the particles' volume fraction that the experimental setup can not visualize.
16. LCMs cost varies slightly with the LCM type, which ranges between 11 and 14.3 \$/bbl. Although calcium carbonate is very cheap compared to other LCMs, its total cost was close to other LCMs because higher concentrations are required in the lost circulation pill. Cedar fiber and walnut come second, costing 12 and 12.5 \$/bbl, respectively.
17. SMP cost was roughly estimated and compared with other LCMs used in the industry. SMP showed great potential to be used in the industry with feasible prices. However, SMP is a new lost circulation product, and there is no commercial production for field applications. The actual cost estimation of SMP-based lost circulation pills is still in the research and development phase.

8.3 Recommendations

Based on the results, findings, and conclusions obtained from this study, recommendations for future research work in this area include but are not limited to the following:

1. Experimental evaluation can be extended to higher temperatures to assess the performance of the smart LCMs in harsher conditions of geothermal formations such as supercritical and magmatic formations. Compatibility with brine and other drilling systems, such as oil-

based muds (OBM) and synthetic-based muds (SBM) can also be evaluated to extend the application of shape memory polymer to high-pressure, high-temperature oil and gas wells.

2. Extending the testing conditions of fracture sealing experiments can give more insights into the smart LCM performance with larger and more complex fractures, including a broader range of inclination angles and pipe rotation. Moreover, the experimental evaluation can also be extended to investigate different treatment methods by considering flow stop and circulation to allow more time for SMP particle placement/activation and to investigate the backflow and formation damage during the production stage.
3. The experimental study was limited with the fracture length and size, and it did not account for the drill pipe eccentricity in the evaluation. Therefore, extending the experimental study to evaluate how the shape memory polymer would perform in larger fracture sizes also considering the fracture length in the study. Moreover, testing the LCM transportation in case of eccentric drill pipe is promising to cover all scenarios might be encountered in actual field operations.
4. The blend of SMP and cedar fiber showed excellent sealing performance. Therefore, more studies are required to optimize the blend ratio and include drilled cuttings with SMP to reduce the treatment cost further.
5. Cleaning SMP-based LCM after drilling operations was not investigated in previous studies. Therefore, evaluating the formation damage and developing an effective cleaning formulation/method can be a potential area for improving the SMP performance as lost circulation material.
6. To ensure successful lost circulation treatment, a careful design of the activation process and operational parameters is required in actual drilling operations.

7. The computation model is essential to optimize the lost circulation treatment in different formations and well conditions before field implementation.

Nomenclature

Acronyms

AAPE	average absolute percentage error, %
ACC	American chemistry council
CFD	computational fluid dynamics
CLG	closed-loop geothermal system
CwD	casing while drilling
DAQ	data acquisition
DCM	drilling choke manifold
ECD	equivalent circulating density
EDS	energy-dispersive X-ray spectroscopy
EPA	environmental protection agency
ft/min	feet per minute
gpm	gallons per minute
HEC	hydroxyethyl cellulose
HHS	US Department of Health and Human Services
HPHT	high-pressure high-temperature
IPD	isophorone diamine
IPT	ideal packing theory
lb	pound
lb/bbl	pound per barrel
LCM	lost circulation materials
LPLT	low pressure low temperature

LwD	logging while drilling
MPD	managed pressure drilling
MwD	measure while drilling
NPs	nanoparticles
NPT	non-productive time
OBM	oil-based mud
OSHA	occupational Safety and Health Administration
PAC-L	low-viscosity polyanionic cellulose
PAC-R	regular-viscosity polyanionic cellulose
PPA	permeability plugging apparatus
ppg	pound per gallon
RDC	rotating control device
ROP	rate of penetration
rpm	rotation per minute
SBM	synthetic-based mud
SEM	scanning electron microscopy
SMP	shape memory polymer
TSCA	toxic substance control act
UBD	underbalanced drilling
VFDs	variable frequency drives
VOF	volume of Fluid model
WBM	water-based mud
XC	Xanthan gum

Symbols

D	viscometer diameter
d	particle diameter
DP, ΔP	differential pressure
f	Fanning friction factor
K	consistency
L	viscometer length
n	flow index
Pa	pascal
Q	flow rate
Re	Reynold's number

Greek Symbols

μ_a	apparent viscosity (cp)
τ_w	wall shear stress (Pa)
$\dot{\gamma}_{nom}$	nominal Newtonian wall shear rate (1/s)
τ	shear stress (Pa)
$\dot{\gamma}$	shear rate (1/s)

References

- ACC. 2010. Q & A on the Safety of Polystyrene Foodservice Products. <https://web.archive.org/web/20110824143749/http://plasticfoodservicefacts.com/main/Safety/Californias-Proposition-65/Q-A-on-the-Safety-of-Polystyrene-Foodservice-Products.GMEditor.html>
- Adebayo, A.R., Bageri, B.S. 2020. A simple NMR methodology for evaluating filter cake properties and drilling fluid-induced formation damage. *Journal of Petroleum Exploration Production Technology* **10**: 1643–1655. <https://doi.org/10.1007/s13202-019-00786-3>
- Ahmed, R.M., Takach, N.E. 2009. Fiber sweeps for hole cleaning. *SPE Drilling Completion* **24**: 564–573. <https://doi.org/10.2118/113746-PA>
- Akhtarmanesh, S., Al-Saba, M., Cedola, A.E. et al. 2016. Barite nano-micro particles with LCM seals fractured form better in weighted water based drilling fluid. Presented at the 50th US Rock Mechanics/Geomechanics Symposium, Houston, Texas, USA.
- Al-Hameedi, A.T.T., Alkinani, H.H., Dunn-Norman, S. et al. 2020. Experimental investigation of environmentally friendly drilling fluid additives (mandarin peels powder) to substitute the conventional chemicals used in water-based drilling fluid. *Journal of Petroleum Exploration Production Technology* **10**: 407–417. <https://doi.org/10.1007/s13202-019-0725-7>
- Al Maskary, S., Halim, A.A., Al Menhali, S. 2014. Curing Losses While Drilling & Cementing. Presented at the 30th Abu Dhabi International Petroleum Exhibition Conference, Abu Dhabi, UAE. <https://doi.org/10.2118/171910-MS>
- AlAwad, M.N.J., Fattah, K.A., AlGobany, A.A. 2018. Innovative wellbore strengthening using crushed date palm seeds and shredded waste car tyres. Presented at the 10th Asian Rock Mechanics Symposium, ARMS 2018, Singapore.

- Alderman, N.J., Pugh, S.J. 2004. Non-Newtonian fluids: tube viscometry – worked example (No. 04005), the ESDU Series on Internal Flow. London, United Kingdom.
- Alkinani, H.H., Al-Hameedi, A.T.T., Dunn-Norman, S. et al. 2019. State-of-the-art review of lost circulation materials and treatments - Part I: General trends and uses. Presented at the Abu Dhabi International Petroleum Exhibition and Conference, Abu Dhabi, UAE. <https://doi.org/10.2118/197393-ms>
- Alsaba, M. 2015. Investigation of lost circulation materials impact on fracture gradient. PhD Dissertation. Missouri University of Science and Technology.
- Alsaba, M., Al Dushaishi, M.F., Nygaard, R. et al. 2017. Updated criterion to select particle size distribution of lost circulation materials for an effective fracture sealing. *Journal of Petroleum Science and Engineering* **149**: 641–648. <https://doi.org/10.1016/j.petrol.2016.10.027>
- Alsaba, M., Nygaard, R., Saasen, A. et al. 2014. Laboratory evaluation of sealing wide fractures using conventional lost circulation materials. Presented at the SPE Annual Technical Conference & Exhibition, Amsterdam, The Netherlands. <https://doi.org/10.2118/170576-ms>
- Amani, M., Al-Jubouri, M. 2012a. An experimental investigation of the effects of ultra-high pressure and temperature on the rheological properties of water-based drilling fluids. Presented at the SPE/APPEA International Conference on Health, Safety and Environment in Oil and Gas Exploration and Production. Perth, Australia. <https://doi.org/10.2118/157219-MS>
- Amani, M., Al-Jubouri, M. 2012b. The effect of HP and HT on water based DF. *Energy Science Technology* **4**: 27–33. <https://doi.org/10.3968/j.est.1923847920120401.256>
- Amanullah, M., Arfaj, M.K. 2018. Date palm tree-based fibrous LCM “ARC eco-fiber” -A better

- alternative to equivalent imported products. Presented at the Annual Technical Symposium and Exhibition, Dammam, Saudi Arabia. <https://doi.org/10.2118/192160-ms>
- Andaverde, J.A., Wong-Loya, J.A., Vargas-Tabares, Y. et al. 2019. A practical method for determining the rheology of drilling fluid. *Journal of Petroleum Science and Engineering* **180**: 150–158. <https://doi.org/10.1016/j.petrol.2019.05.039>
- Avci, E., Mert, B.A. 2019. The Rheology and Performance of Geothermal Spring Water-Based Drilling Fluids. *Geofluids* **2019**, 8. <https://doi.org/10.1155/2019/3786293>
- Bageri, B.S., Benaafi, M., Mahmoud, M. et al. 2019. Effect of Arenite, Calcareous, Argillaceous, and Ferruginous Sandstone Cuttings on Filter Cake and Drilling Fluid Properties in Horizontal Wells. *Geofluids* **2019**: 10. <https://doi.org/10.1155/2019/1956715>
- Bandyopadhyay, A., Basak, G.C. 2013. Studies on photocatalytic degradation of polystyrene. *Materials Science and Technology* **23** (3): 307–314. <https://doi.org/10.1179/174328407X158640>
- Baroid, 2012. Product Data Sheets.
- Baujard, C., Hehn, R., Genter, A. et al. 2017. Rate of penetration of geothermal wells: a key challenge in hard rocks. Presented at the 42nd Workshop on Geothermal Reservoir Engineering, Stanford, California, USA.
- Bavadiya, V., Srivastava, S., Salehi, S. et al. 2019. Geothermal Drilling Training and Certification: Should It Be Different?. Presented at the 44th Workshop on Geothermal Reservoir Engineering, Stanford, California, USA.
- Bavadiya, V.A., Alsaihati, Z., Ahmed, R. et al. 2017. Experimental investigation of the effects of rotational speed and weight on bit on drillstring vibrations, torque and rate of penetration. Presented at the SPE Abu Dhabi International Petroleum Exhibition and Conference, Abu

- Dhabi, UAE. <https://doi.org/10.2118/188427-ms>
- Bourgoyne, A., Millheim, K., Chenevert, M. 1984. Applied Drilling Engineering. Society of Petroleum Engineers. ISBN: 978-1-55563-001-0.
- Brege, J., Christian, C., Quintero, L. et al. 2010. Improving Wellbore Strengthening Techniques by Altering the Wettability of Non-Aqueous Fluid Lost to Drilling Induced Fractures. Presented at the AADE Fluids Conference and Exhibition, Houston, Texas, USA.
- Busahmin, B., Saeid, N.H., Hasan, U.H.B.H. et al. 2017. Analysis of Hole Cleaning for a Vertical Well. *Open Access Library Journal* **04**: 1–10. <https://doi.org/10.4236/oalib.1103579>
- Caenn, R., Darley, H.C.H., Gray, G.R. 2017. Composition and Properties of Drilling and Completion Fluids: Seventh Edition, Elsevier. <https://doi.org/10.1016/C2015-0-04159-4>
- Calçada, L.A., Scheid, C.M., de Araújo, C.A.O. et al. 2011. Analysis of Dynamic and Static Filtration and Determination of Mud Cake Parameters. *Brazilian Journal of Petroleum and Gas* **5**: 159–170. <https://doi.org/10.5419/bjpg2011-0016>
- Capuano, L.E. 2016. Geothermal Power Generation: Developments and Innovation, CH5 Geothermal well drilling, Elsevier. <https://doi.org/10.1016/B978-0-08-100337-4.00005-X>
- Chemwotei, S.C. 2011. Geothermal drilling fluids, Kenya Electricity Generating Company Ltd. – KenGen.
- Cheraghian, G. 2021. Nanoparticles in drilling fluid: A review of the state-of-the-art. *Journal of Materials Research and Technology* **13**: 737-753.
<https://doi.org/10.1016/j.jmrt.2021.04.089>
- Chilingarian, G.V., Vorabutr, P. 1983. Drilling and drilling fluids, Elsevier, New York, United States.
- Cole, P., Young, K., Doke, C. et al. 2017. Geothermal Drilling: A Baseline Study of Nonproductive

- Time Related to Lost Circulation. Presented at the 42nd Workshop on Geothermal Reservoir Engineering, Stanford, California.
- Czuprat, O., Faugstad, A.M., Byrski, P. et al. 2020. Hole cleaning efficiency of sweeping pills in horizontal wells - Facts or philosophy? Presented at the SPE Annual Technical Conference and Exhibition, Virtual. . <https://doi.org/10.2118/201634-ms>
- De Angelis, R., Holdeman, M., Pidcock, G. et al. 2011. Challenges of drilling in the Chilean altiplano. Presented at the SPE/IADC Drilling Conference and Exhibition. Amsterdam, The Netherlands. <https://doi.org/10.2118/140051-MS>
- Dernehl, C.U. 1966. Health hazards associated with polyurethane foams. *Journal of Occupational Medicine* **8** (2): 59-62.
- Elgaddafi, R., Ahmed, R., George, M. et al. 2012. Settling behavior of spherical particles in fiber-containing drilling fluids. *Journal of Petroleum Science and Engineering* **84–85**: 20–28. <https://doi.org/10.1016/j.petrol.2012.01.020>
- Ezeakacha, C.P., Salehi, S., Bi, H. 2017. How does Rock Type and Lithology Affect Drilling Fluid’s Filtration and Plastering? Presented at the AADE National Technical Conference and Exhibition, Houston, Texas, USA.
- Ezeakacha, C.P., Salehi, S., Hayatdavoudi, A. 2017. Experimental Study of Drilling Fluid’s Filtration and Mud Cake Evolution in Sandstone Formations. *Journal of Energy Resources Technology* **139** (2): 02291. <https://doi.org/10.1115/1.4035425>
- Falcone, G., Teodoriu, C. 2008. Oil and gas expertise for geothermal exploitation - The need for technology transfer. Presented at the 2008 SPE Europec/EAGE Annual Conference and Exhibition, Rome, Italy. <https://doi.org/10.2118/113852-MS>
- Fan, J., Li, G. 2018. High enthalpy storage thermoset network with giant stress and energy output

in rubbery state. *Nature Communications* **9**: 642 (2018). <https://doi.org/10.1038/s41467-018-03094-2>

Finger, J., Blankenship, D. 2010. Handbook of Best Practices for Geothermal Drilling, Sandia Report.

George, M., Ahmed, R., Growcock, F. 2012. Stability and Flow Behavior of Fiber-Containing Drilling Sweeps. *Rheology*: 205-238. <https://doi.org/10.5772/35736>

Ghalambor, A., Salehi, S., Shahri, M.P. et al. 2014. Integrated workflow for lost circulation prediction. Presented at the SPE European Formation Damage Conference, Lafayette, Louisiana, USA. <https://doi.org/10.2118/168123-ms>

Hamza, A., Shamlooh, M., Hussein, I.A. et al. 2019. Polymeric formulations used for loss circulation materials and wellbore strengthening applications in oil and gas wells: A review. *Journal of Petroleum Science and Engineering* **180**: 197–214. <https://doi.org/10.1016/j.petrol.2019.05.022>

HHS. 1995. Occupational Safety and Health Guideline for Calcium Carbonate.

Hofer, T.N., Abessa, D.M.S., Aguiar, V.M.C et al. 2008. Marine pollution: new research. Nova Science Pub Inc. ISBN: 1604562420

Hossain, M.E., Al-Majed, A.A. 2015. Fundamentals of Sustainable Drilling Engineering. Scrivener Publishing LLC, Beverly, MA, USA.

Huang, W.M., Yang, B., An, L. et al. 2005. Water-driven programmable polyurethane shape memory polymer: Demonstration and mechanism. *Applied Physics Letters* **86**: 1–3. <https://doi.org/10.1063/1.1880448>

Huque, M.M., Imtiaz, S., Rahman, A. et al. 2020. Kick detection and remedial action in managed pressure drilling: a review. *SN Applied Sciences* **2**: 1178. <https://doi.org/10.1007/s42452->

- Javeri, S.M., Haindade, Z.W., Jere, C.B. 2011. Mitigating loss circulation and differential sticking problems using silicon nanoparticles. Presented at the SPE/IADC Middle East Drilling Technology Conference and Exhibition, Muscat, Oman. <https://doi.org/10.2118/145840-ms>
- Karimi, M., Moellendick, E., Holt, C. 2011. Plastering Effect of Casing Drilling; A Qualitative Analysis of Pipe Size Contribution. Presented at the SPE Annual Technical Conference and Exhibition, Denver, Colorado, USA. <https://doi.org/10.2118/147102-MS>
- Kiran, R., Salehi, S. 2020. Assessing the Relation between Petrophysical and Operational Parameters in Geothermal Wells: A Machine Learning Approach. Presented at the 45th Workshop on Geothermal Reservoir Engineering, Stanford, California, USA.
- Kruszewski, M., Wittig, V. 2018. Review of failure modes in supercritical geothermal drilling projects. *Geothermal Energy* **6**: 1–29. <https://doi.org/10.1186/s40517-018-0113-4>
- Kuang, X., Shi, Q., Zhou, Y. et al. 2018. Dissolution of epoxy thermosets: Via mild alcoholysis: The mechanism and kinetics study. *RSC Advances* **8**: 1493–1502. <https://doi.org/10.1039/c7ra12787a>
- Kulkarni, S.D., Savari, S., Maghrabi, S. et al. 2013. Normal stress rheology of drilling fluids and potential in lost circulation control. Presented at the North Africa Technical Conference and Exhibition, Cairo, Egypt. <https://doi.org/10.2118/164617-ms>
- Kwon, B.G., Saido, K., Koizumi, K. et al. 2014. Regional distribution of styrene analogues generated from polystyrene degradation along the coastlines of the North-East Pacific Ocean and Hawaii. *Environmental Pollution* **188**: 45–49. <https://doi.org/10.1016/J.ENVPOL.2014.01.019>
- Lakhera, N., Laursen, C.M., Safranski, D.L. et al. 2012. Biodegradable thermoset shape-memory

- polymer developed from poly(β -amino ester) networks. *Journal of Polymer Science Part B Polymer Physics* **50**: 777–789. <https://doi.org/10.1002/polb.23059>
- Lavrov, A. 2016. Lost circulation: Mechanisms and solutions. Gulf Professional Publishing, Oxford, UK. <https://doi.org/10.1016/C2015-0-00926-1>
- Lee, L., Taleghani, A.D. 2020. The effect particle size distribution of granular LCM on fracture sealing capability. Presented at the SPE Annual Technical Conference and Exhibition, Virtual. <https://doi.org/10.2118/201668-ms>
- Leng, J., Zhang, D., Liu, Y., Yu, K., Lan, X. 2010. Study on the activation of styrene-based shape memory polymer by medium-infrared laser light. *Applied Physics Letter* **96**: 2008–2011. <https://doi.org/10.1063/1.3353970>
- Li, G., Xu, W. 2011. Thermomechanical behavior of thermoset shape memory polymer programmed by cold-compression: Testing and constitutive modeling. *Journal of the Mechanics and Physics of Solids* **59**: 1231–1250. <https://doi.org/10.1016/j.jmps.2011.03.001>
- Liu, Y., Lv, H., Lan, X. et al. 2009. Review of electro-active shape-memory polymer composite. *Composites Science and Technology* **69** (13): 2064–2068. <https://doi.org/10.1016/j.compscitech.2008.08.016>
- Loeppke, G.E., Glowka, D.A., Wright, E.K. 1990. Design and evaluation of lost-circulation materials for severe environments. *Journal of Petroleum Technology* **42**: 328–337. <https://doi.org/10.2118/18022-PA>
- Luzardo, J., Oliveira, E.P., Derks, P.W.J. et al. 2015. Alternative lost circulation material for depleted reservoirs. Presented at the Offshore Technology Conference, Rio de Janeiro, Brazil. <https://doi.org/10.4043/26188-ms>
- Magzoub, M. 2021. Development of Polymer Gel Systems for Lost Circulation Treatment and

Wellbore Strengthening. PhD Dissertation, University Of Oklahoma.

- Magzoub, M., Anyaezu, T., Salehi, S. et al. 2021a. Evaluating sealability of blended smart polymer and fiber additive for geothermal drilling with the effect of fracture opening size. *Journal of Petroleum Science and Engineering* **206**: 108998. <https://doi.org/10.1016/J.PETROL.2021.108998>
- Magzoub, M., Salehi, S., Li, G. et al. 2021b. Loss circulation prevention in geothermal drilling by shape memory polymer. *Geothermics* **89**: 101943. <https://doi.org/10.1016/j.geothermics.2020.101943>
- Magzoub, M., Salehi, S., Hussein, I. et al. 2021. Development of a Polyacrylamide-Based Mud Formulation for Loss Circulation Treatments. *Journal of Energy Resources Technology* **143**: 1–8. <https://doi.org/10.1115/1.4048682>
- Magzoub, M.I., Salehi, S., Hussein, I.A. et al. 2021. Investigation of Filter Cake Evolution in Carbonate Formation Using Polymer-Based Drilling Fluid. *ACS Omega* **6**: 6231–6239. <https://doi.org/10.1021/acsomega.0c05802>
- Magzoub, M.I., Salehi, S., Hussein, I.A. et al. 2020. Loss circulation in drilling and well construction: The significance of applications of crosslinked polymers in wellbore strengthening: A review. *Journal of Petroleum Science and Engineering* **185**: 106653. <https://doi.org/10.1016/j.petrol.2019.106653>
- Mahmoud, O., Nasr-El-Din, H.A., Vryzas, Z. et al. 2018. Effect of ferric oxide nanoparticles on the properties of filter cake formed by calcium bentonite-based drilling muds. *SPE Drilling and Completion* **33**: 363–376. <https://doi.org/10.2118/184572-PA>
- Mansour, A., Ezeakacha, C., Taleghani, A.D. et al. 2017. Smart Lost circulation materials for productive zones. Presented at the SPE Annual Technical Conference and Exhibition, San

- Antonio, Texas, USA. <https://doi.org/10.2118/187099-ms>
- Mansour, A.K., Taleghani, A.D., Li, G. 2017. Smart Expandable LCMs - A Theoretical and Experimental Study. Presented at the AADE National Technical Conference and Exhibition, Houston, Texas, USA.
- Mansour, A.K., Taleghani, A.D., Li, G. 2017. Smart Lost Circulation Materials for Wellbore Strengthening. Presented at the 51st U.S. Rock Mechanics/Geomechanics Symposium, San Francisco, California, USA.
- Mansure, A.J. 2002. Polyurethane Grouting Geothermal Lost Circulation Zones. Presented at the Drilling Conference, Dallas, Texas, USA. <https://doi.org/10.2118/74556-ms>
- Marx, C., Rahman, S.S. 2007. Evaluation of Formation Damage Caused by Drilling Fluids, Specifically in Pressure-Reduced Formations. *Journal of Petroleum Technology* **39**: 1449–1452. <https://doi.org/10.2118/12494-pa>
- Mather, P.T., Luo, X., Rousseau, I.A. 2009. Shape memory polymer research. *Annual Review of Materials Research* **39**: 445–471. <https://doi.org/10.1146/annurev-matsci-082908-145419>
- McKenna, S.T., Hull, T.R. 2016. The fire toxicity of polyurethane foams. *Fire Science Reviews* **5**: 1–27. <https://doi.org/10.1186/S40038-016-0012-3>
- Meng, H., Li, G. 2013. A review of stimuli-responsive shape memory polymer composites. *Polymer* **54** (9): 2199–2221. <https://doi.org/10.1016/j.polymer.2013.02.023>
- Miyazaki, K., Ohno, T., Karasawa, H. et al. 2019. Performance of polycrystalline diamond compact bit based on laboratory tests assuming geothermal well drilling. *Geothermics* **80**: 185–194. <https://doi.org/10.1016/j.geothermics.2019.03.006>
- Mohamed, A., Elkatatny, S., Al-Majed, A. 2020. Removal of calcium carbonate water-based filter cake using a green biodegradable acid. *Sustainability* **12**: 994.

<https://doi.org/10.3390/su12030994>

- Mohamed, A., Elkatatny, S., Basfar, S. 2019. One-stage calcium carbonate oil-based filter cake removal using a new biodegradable acid system. Presented at the SPE Kuwait Oil and Gas Show and Conference, Mishref, Kuwait. <https://doi.org/10.2118/198045-ms>
- Mohamed, A., Salehi, S., Ahmed, R. 2021a. Significance and complications of drilling fluid rheology in geothermal drilling: A review. *Geothermics* **93**: 102066. <https://doi.org/10.1016/j.geothermics.2021.102066>
- Mohamed, A., Salehi, S., Ahmed, R. 2021b. Rheological Properties of Drilling Fluids Containing Special Additives for Geothermal Drilling Applications. Presented at the 46th Workshop on Geothermal Reservoir Engineering. Stanford, California, USA.
- Mohamed, A., Salehi, S., Ahmed, R. et al. 2021b. Experimental study on rheological and settling properties of shape memory polymer for fracture sealing in geothermal formations. *Journal of Petroleum Science and Engineering* **208**: 109535. <https://doi.org/10.1016/J.PETROL.2021.109535>
- Murray, D., Sanders, M.W., Houston, K. et al. 2013. Case study - ECD management strategy solves lost circulation issues on complex salt diapirs/paleocene reservoir. Presented at the SPE Annual Technical Conference and Exhibition, New Orleans, Louisiana, USA. <https://doi.org/https://doi.org/10.2118/166134-MS>
- Nasiri, A., Ghaffarkhah, A., Dijvejin, Z.A. et al. 2018. Bridging performance of new eco-friendly lost circulation materials. *Petroleum Exploration and Development* **45** (6): 1154–1165. [https://doi.org/10.1016/S1876-3804\(18\)30119-8](https://doi.org/10.1016/S1876-3804(18)30119-8)
- Nesbitt, L.E., Sanders, J.A. 1981. Drilling Fluid Disposal. *Journal of Petroleum Technology* **33**: 2377–2381. <https://doi.org/10.2118/10098-PA>

- Onwukwe, S.I., Nwakaudu, M.S. 2012. Drilling Wastes Generation and Management Approach. *International Journal of Environmental Science and Development* **3** (3): 252–257. <https://doi.org/10.7763/IJESD.2012.V3.226>
- Patel, D., Thakar, V., Pandian, S. et al. 2019. A review on casing while drilling technology for oil and gas production with well control model and economical analysis. *Petroleum* **5**: 1–12. <https://doi.org/10.1016/j.petlm.2018.12.003>
- Petty, S., Bour, D.L., Livesay, B.J. et al. 2009. Synergies and opportunities between EGS development and oilfield drilling operations and producers. Presented at the SPE Western Regional Meeting, San Jose, California, USA. <https://doi.org/10.2118/121165-ms>
- Rahmanifard, H., Rasouli, A.R., Mayahi, N. et al. 2014. Best Practice in Managing Lost Circulation Challenges During Drilling and Cementing Operations in Azar Oil. Presented at the 2nd International Conference of Oil, Gas And Petrochemical, Tehran, Iran.
- Randeberg, E., Ford, E., Nygaard, G. et al. 2012. Potentials for Cost Reduction for Geothermal Well Construction in View of Various Drilling Technologies and Automation Opportunities. Presented at the 36th Workshop on Geothermal Reservoir Engineering, Stanford, California, USA.
- Ravi, K., Savery, M., Reddy, B.R. et al. 2006. Cementing technology for low fracture gradient and controlling loss circulation. Presented at the SPE/IADC Indian Drilling Technology Conference and Exhibition, Mumbai, India. <https://doi.org/10.2523/102074-ms>
- Reinsch, T., Regensburg, S., Feldbusch, E. et al. 2015. Reverse cleanout in a geothermal well: Analysis of a failed coiled-tubing operation. *SPE Production Operations* **30**: 312–320. <https://doi.org/10.2118/174080-PA>
- Rohani, M.R. 2012. Managed-pressure drilling: Techniques and options for improving operational

- safety and efficiency. *Petroleum and Coal* **54**: 24–33.
- Rosenberg, S.M., Gala, D.M. 2012. Use of Liner Drilling Technology as a Mitigation to Loss Intervals and Hole Instability: A Case Study in Mississippi Canyon. Presented at the IADC/SPE Drilling Conference and Exhibition, San Diego, California, USA. <https://doi.org/10.2118/151181-MS>
- Salehi, S., Nygaard, R. 2011. Evaluation of new drilling approach for widening operational window: Implications for wellbore strengthening. Presented at the SPE Production and Operations Symposium, Oklahoma City, Oklahoma, USA. <https://doi.org/10.2118/140753-ms>
- Sauki, A., Hasan, N.I., Naimi, F.B.M. et al. 2017. Development of environmental friendly lost circulation material from banana peel. *AIP Conference Proceedings* **1901**: 130016. <https://doi.org/doi.org/10.1063/1.5010576>
- Shadravan, A., Amani, M. 2012. HPHT 101-What Petroleum Engineers and Geoscientists Should Know About High Pressure High Temperature Wells Environment. *Energy Science and Technology* **4** (2): 36–60. <https://doi.org/10.3968/j.est.1923847920120402.635>
- Skelland, A.H.P. 1967. *Non-Newtonian Flow and Heat Transfer*. John Wiley & Sons, Inc., New York, USA. <https://doi.org/10.1002/app.1967.070110920>
- Spee, T., Van Duivenbooden, C., Terwoert, J. 2006. Epoxy resins in the construction industry *Annals of the New York Academy of Sciences*. John Wiley & Sons, Ltd, 429–438. <https://doi.org/10.1196/annals.1371.010>
- Sun, Y., Huang, H. 2015. Effect of rheology on drilling mud loss in a natural fracture. Presented at the 49th US Rock Mechanics/Geomechanics Symposium, San Francisco, California, USA.
- Tare, U.A., Whitfill, D.L., Mody, F.K. 2001. *Drilling Fluid Losses and Gains: Case Histories and*

- Practical Solutions. Presented at the SPE Annual Technical Conference and Exhibition, New Orleans, Louisiana, USA. <https://doi.org/10.2118/71368-ms>
- Tavakoli, S. 2003. An assessment of skin sensitisation by the use of epoxy resin in the construction industry, HSE Books. ISBN: 9780717626755
- Teodoriu, C. 2015. Why and when does casing fail in geothermal wells: a Surprising Question? Presented at the Proceedings World Geothermal Congress, Melbourne, Australia.
- Teodoriu, C., Yi, M.C., Salehi, S. 2019. A Novel Experimental Investigation of Cement. *Energies* **12** (18): 3426. <https://doi.org/10.3390/en12183426>
- Theodorakis, C. 2005. Encyclopedia of Toxicology: Environmental Toxicology, 210–212, Elsevier. <https://doi.org/10.1016/B0-12-369400-0/00374-4>
- U.S. Department of Energy. 2019. GEO Vision: Harnessing the Heat Beneath Our Feet. DOE/EE-1306. U.S. Department of Energy, Washington, USA.: <https://www.energy.gov/eere/geothermal/geovision>.
- Van Horn, A., Amaya, A., Higgins, B. et al. 2020. New Opportunities and Applications for Closed-Loop Geothermal Energy Systems. *GRC Transactions* **44**: 1123–1143.
- Vivas, C., Salehi, S., Tuttle, J.D. et al. 2020. Challenges and Opportunities of Geothermal Drilling for Renewable Energy Generation. *Geothermal Resources Council Transactions* **44**: 904–918.
- Vollmar, D., Wittig, V., Bracke, R. 2013. Geothermal Drilling Best Practices: The Geothermal translation of conventional drilling recommendations - main potential challenges. IGA Academy Report 0104-2013.
- Wagle, V., Kalgaonkar, R., Al-Yami, A.S. 2018. Nanoparticle-based chemical treatment for preventing loss circulation. Presented at the SPE Kingdom of Saudi Arabia Annual Technical

- Symposium and Exhibition, Dammam, Saudi Arabia. <https://doi.org/10.2118/192309-ms>
- Wastu, A.R.R., Hamid, A., Samsol, S. 2019. The effect of drilling mud on hole cleaning in oil and gas industry. *Journal of Physics: Conference Series* **1402** (2): 022054. <https://doi.org/10.1088/1742-6596/1402/2/022054>
- Werner, B. 2018. The Influence of Drilling Fluid Rheology on Cuttings Bed Behavior. Norwegian University of Science and Technology. <https://doi.org/10.13140/RG.2.2.19105.30566>
- Whitfill, D. 2008. Lost circulation material selection, particle size distribution and fracture modeling with fracture simulation software. Presented at the IADC/SPE Asia Pacific Drilling Technology Conference, Jakarta, Indonesia. <https://doi.org/10.2118/115039-ms>
- Wight, N.M., Bennett, N.S. 2015. Geothermal energy from abandoned oil and gas wells using water in combination with a closed wellbore. *Applied Thermal Engineering* **89**: 908–915. <https://doi.org/10.1016/j.applthermaleng.2015.06.030>
- Wilson, A. 2014. ECD-Management Strategy Solves Lost Circulation Issues. *Journal of Petroleum Technology* **66**: 77–80. <https://doi.org/10.2118/0214-0077-jpt>
- Wu, Y. 2016. Immiscible Displacement of Non-Newtonian Fluids, in: *Multiphase Fluid Flow in Porous and Fractured Reservoirs*: 127–166, Elsevier. <https://doi.org/10.1016/b978-0-12-803848-2.00007-6>
- Wu, Y., Patel, H.R., Salehi, S. 2020. Thermal Considerations of Cement Integrity in Geothermal Wells. Presented at the 45th Workshop on Geothermal Reservoir Engineering, Stanford, California, USA.
- Zhang, J.J. 2019. Applied Petroleum Geomechanics: Fracture gradient prediction and wellbore strengthening, **Ch 9**: 337–374. <https://doi.org/10.1016/b978-0-12-814814-3.00009-5>
- Zilch, H.E., Otto, M.J., Pye, D.S. 1991. Evolution of geothermal drilling fluid in the Imperial

Valley. Presented at the Western Regional Meeting, Long Beach, California, USA.
<https://doi.org/10.2118/21786-MS>.